



Assessing the potential for macroalgae aquaculture in coastal and estuarine areas

Francisco Cunha e Costa Santos Reis

Thesis to obtain the Master of Science Degree in

Environmental Engineering

Supervisors: Prof. Ramiro Joaquim de Jesus Neves

Dr. Ana Sofia de Carvalho Saraiva

Examination Committee

Chairperson: Prof. Ana Fonseca Galvão

Supervisor: Prof. Ramiro Joaquim de Jesus Neves

Members of the Committee: Dr. Irene Isabel da Cruz Martins

December 2021

Acknowledgements

I would first like to thank my supervisors Professor Ramiro Neves and Dr. Sofia Saraiva, for their patience, enthusiasm, and for their suggestions on how to approach my obstacles during this thesis.

I would like to thank Professor Marcos Mateus for his advice and for his help in reviewing my work.

I would also like to thank my friends at MARETEC, for their company, support and friendly work environment from the first day I started, through these last seven months.

I would like to thank my family, for their continuous support in achieving my goals.

At last, but not least, I would like to thank the friends I made at IST, who made these last five years of my life less obscure.

Abstract

Kelp aquaculture is a fast-developing biomass producing sector for food, pharmaceutical and cosmetics production, while providing ecosystem services like carbon sequestration, fish habitats and pollution remediation.

This modelling study aimed to identify the best places to install *Saccharina latissima* aquaculture inside and in the vicinity of the Tagus River estuary, in Lisbon, Portugal and at what time of the year should algae be planted to maximize their yield. For these purposes, numerical tests were performed to understand the effects of temperature, salinity, nutrients, light availability, and water velocity on algae yield. The model was tested in three numerical mesocosms, a closed system with no water motion, a river segment and in a schematic estuary. After these tests, macroalgae growth was tested with data provided by an operational model of the Tagus estuary and adjacent platform. Results show that the best location to practice aquaculture of *S. latissima* is inside the Tagus estuary right in the central part, where the best compromise between nutrients, light and salinity is found. The best time of the year to plant is by the beginning of November and harvesting can be done in May of the following year. The model is generic and can be used to simulate other species providing the appropriate parameters. To finalize the decision process of placing *S. latissima*, these growth results should be crossed with the estuary usage data as well as requesting permission from the local government to find the best possible available area.

Keywords: macroalgae; aquaculture; environmental modelling, *Saccharina latissima*; Tagus River; estuary.

Resumo

A aquacultura de algas é um sector em rápido desenvolvimento de produção de biomassa que pode ser utilizada na produção de bens alimentares, produtos farmacêuticos e cosméticos, providenciando ao mesmo tempo serviços de ecossistema como o sequestro de carbono, habitats para peixes e remediação de poluição marinha.

O objetivo deste estudo de modelação foi identificar qual o melhor sítio para instalar a espécie *Saccharina latissima* na região do estuário do Tejo, Lisboa, Portugal e qual a melhor altura do ano para as cultivar, maximizando o rendimento. Para atingir estes objetivos, foram realizados vários testes numéricos para compreender o efeito da temperatura, salinidade, disponibilidade de nutrientes, luz e velocidades da corrente no crescimento das algas. O modelo foi testado em três mesocosmos numéricos, um tanque sem hidrodinâmica, um tanque que simulou um trecho de um rio e um pequeno estuário esquemático. De seguida, simulou-se o crescimento destas algas com dados de um modelo operacional do estuário do Tejo. Os resultados mostram que o melhor local para praticar aquacultura de *S. latissima* é na parte central do estuário, onde o melhor balanço entre nutrientes, luz e salinidade se verifica, e que a melhor altura do ano para se plantarem as algas foi em Novembro, extraindo-as depois até Maio do ano seguinte. Para finalizar a decisão de onde as colocar, será necessário conciliar os resultados do crescimento de algas deste estudo com estudos da disponibilidade e utilização atuais do estuário, bem como autorizações do governo local para encontrar o melhor sítio permitido.

Palavras-chave: macroalgas; aquacultura; modelação ambiental; *Saccharina latissima*; Rio Tejo; estuário.

Table of Abbreviations

Abbreviation	Explanation
<i>S. latissima</i>	<i>Saccharina latissima</i>
FAO	Food and Agriculture Organization
PON	Particulate Organic Nitrogen
POP	Particulate Organic Phosphorus
DONnr	Dissolved Non-refractory Organic Nitrogen
DONr	Dissolved Refractory Organic Nitrogen
DOPnr	Dissolved Non-refractory Organic Phosphorus
DOPr	Dissolved Refractory Organic Phosphorus

Table of contents

Acknowledgements	ii
Abstract	iii
Resumo	iv
Table of Abbreviations	v
Table of Figures	vii
Index of Tables	ix
1 – Introduction	1
2 - State-of-the-art	2
2.1 - Saccharina latissima	2
2.2 - Kelp Aquaculture	2
2.3 - Brown seaweeds	3
2.4 - Estuarine physics and biogeochemistry	4
3 - Methodology	9
3.1 - A Macroalgae Model	10
3.2 – Governing Equations	11
3.3 - Mesocosms, a simpler approach to study ecosystems	19
4 – Results and Discussion	21
4.1 - First Mesocosm - Sensibility Analysis on a nutrient limited environment	21
4.1.1 - Setup and components of the simulations	21
4.1.2 – Simulations	22
4.1.3 - Final remarks	36
4.2 - Second Mesocosm – The influence of nutrient availability	37
4.2.1 – Setup and conditions of the simulations	37
4.2.2 – Simulations	38
4.2.3 - Final remarks	47
4.3 - Third Mesocosm – Schematic Estuary	47
4.3.1 - Estuary characteristics	48
4.3.2 – Simulation	49
4.3.3 – Final remarks	56
4.4 – Saccharina latissima in the Tagus Estuary	57
4.4.1 – Contextualization	57
4.4.2 – Setup and simulation conditions	57
4.4.3 – Simulations	61
4.4.4 – Analysis	63
5 - Conclusions	71
References	72

Table of Figures

Figure 1 - <i>Saccharina latissima</i> . Source: NOAA Fisheries. https://www.fisheries.noaa.gov/species/sugar-kelp	2
Figure 2 - Influence of the moon's gravitational pull on tides. Source: National Ocean Service NOAA. https://oceanservice.noaa.gov/education/tutorial_tides/tides03_gravity.html	5
Figure 3 - Conceptual model of macroalgae biomass and nutrient flows. Black lines represent nutrient and carbon fluxes, red lines represent oxygen fluxes.	11
Figure 4 - a) Nitrogen limiting factor (left) and b) Phosphorus limiting factor (right) in function of nitrogen and phosphorus concentrations, respectively, with $K_x^N = 0.065$ mgN/L and $K_x^P = 0.001$ mgP/L	13
Figure 5 - Temperature limitation factor in function of the temperature (°C) for $T_{opt_{min}} = 10^\circ\text{C}$; $T_{opt_{max}} = 15^\circ\text{C}$; $T_{min} = 0^\circ\text{C}$ and $T_{max} = 20^\circ\text{C}$, with $K_1 = 0.05$, $K_2=K_3=0.98$ and $K_4 = 0.02$	14
Figure 6 - Salinity limitation factor in function of salinity (psu) with $S_{min} = 0$, $S_{max} = 50$, $S_{opt} = 25$ and $S_c = 5$ psu.....	15
Figure 7 - Light limitation factor in function of the solar irradiance at the top of the water column, for $k = 0.08$ m ⁻¹ and $z = 2$ meters.....	16
Figure 8 - Light extinction in function of depth, for different light extinction coefficients	17
Figure 9 - a) Nitrate and inorganic phosphorus; b) Nitrite and ammonia; c) PON and POP and d) Dissolved oxygen concentrations in the system along the simulation period for the control scenario.	24
Figure 10 - a) Nitrate and inorganic phosphorus; b) Nitrite and ammonia; c) PON and POP; d) Dissolved oxygen and e) Phytoplankton concentrations in the system along the simulation period for the nutrients and phytoplankton scenario.....	25
Figure 11 - a) Nitrate and inorganic phosphorus; b) Nitrite and ammonia; c) PON and POP; d) Dissolved oxygen concentrations and e) macroalgae density in the system along the simulation period for the nutrients and macroalgae scenario.....	27
Figure 12 - a) Macroalgae density and b) nitrate and inorganic phosphorus concentrations for the increased nitrate test.	28
Figure 13 - a) Macroalgae density and b) nitrate and inorganic phosphorus concentrations for the lower phosphate test.	29
Figure 14 - a) Macroalgae density and b) nitrate and inorganic phosphorus concentrations for the higher phosphate test	29
Figure 15 - a) Nitrate, b) inorganic phosphorus and c) macroalgae concentrations at 2, 5, 10 and 20 meters.....	31
Figure 16 - a) Nitrate, b) inorganic phosphorus, c) macroalgae and d) phytoplankton concentrations at 2, 5, 10 and 20 meters in the first mesocosm experiment.	32
Figure 17 - Macroalgae concentration at a) 0, 5 and 40°C and b) 8, 10, 13, 15, 20 and 25°C.	34
Figure 18 - Macroalgae concentration at a) 0 and 3 psu and b) 5, 15, 25, 35, 40 and 45 psu.....	36
Figure 19 - Second mesocosm tank.	38
Figure 20 - Control property evolution for the river mesocosm without the presence of phytoplankton or macroalgae. a) Nitrate and inorganic phosphorus; b) Nitrite and ammonia; c) PON and POP and d) Dissolved oxygen concentrations.....	40
Figure 21 - a) Nitrate and inorganic phosphorus; b) Nitrite and ammonia; c) PON and POP; d) Dissolved oxygen and e) Phytoplankton concentrations in the system along the simulation period for the nutrients and phytoplankton scenario in the second mesocosm.	41
Figure 22 - a) Nitrate and inorganic phosphorus; b) Nitrite and ammonia; c) PON and POP; d) Dissolved oxygen and e) macroalgae concentrations in the system along the simulation period for the nutrients and macroalgae scenario in the second mesocosm.....	43
Figure 23 - Macroalgae concentration evolution at depth 2, 5 10 and 20m in the second mesocosm experiment.	44
Figure 24 – Macroalgae and phytoplankton concentration evolution at depths 2, 5 10 and 20m in the second mesocosm experiment.	45
Figure 25 - Macroalgae evolution at temperatures a) 0, 5, 8, 10 and 13°C and temperatures b)15, 20, 25 and 40°C in the second mesocosm experiments.	46
Figure 26 - Macroalgae evolution in salinities 0, 3, 5, 15, 25, 35, 40 and 45 psu in the salinity experiment of the second mesocosm.	47
Figure 27 - Bathymetry of the schematic estuary.	48
Figure 28 - a) Macroalgae, b) Nitrate, c) Phytoplankton and d) salinity concentration distribution maps at the beginning of the schematic estuary simulation (01/01 – 06h00).....	50
Figure 29 - a) Macroalgae, b) Nitrate, c) phytoplankton and d) salinity concentration distribution maps at the instant before flowrate increases in the schematic estuary simulation (30/06 – 18h00).....	51
Figure 30 - Macroalgae concentration distribution map 6 hours after the flow increased.....	52

Figure 31 - Instantaneous phytoplankton evolution a) 6 hours, b) 18 hours and c) 30 hours after the flow increase (ebb tides only).	52
Figure 32 – Instantaneous nitrate evolution a) 6 hours, b) 18 hours and c) 30 hours after the flow increase (ebb tides only).	53
Figure 33 - Instantaneous salinity evolution a) 6 hours, b) 18 hours and c) 30 hours after the flow increase (ebb tides only).	53
Figure 34 - a) Macroalgae, b) Nitrate, c) phytoplankton and d) salinity concentration distribution maps at (12/09 – 12h00). in the schematic estuary simulation	54
Figure 35 - a) nitrate concentration at 30/12 – 12h00 in flow tide and b) at 18h00 in ebb tide. c) salinity at 30/12 – 12h00 in flow tide and d) at 18h00 in ebb tide.....	55
Figure 36 – Macroalgae distribution at the end of the simulation - 30/12 - 18h00 (ebb tide).	56
Figure 37 - Map of the Tagus Estuary in Lisbon, Portugal overlaid with the bathymetry and location of the points where macroalgae were simulated.	58
Figure 38 – <i>S. latissima</i> biomass per meter of line in sites a) 1 to 5; b) 6 to 9; c) 10 to 15 and d) 16 to 21 at a one-meter depth.....	61
Figure 39 - <i>S. latissima</i> biomass per meter of line in sites a) 1 to 5; b) 6 to 9; c) 10 to 15 and d) 16 to 21 at a five-meter depth.....	62
Figure 40 - <i>S. latissima</i> biomass per meter of line in sites a) 11 to 15 and b) 6 to 9 at a ten-meter depth.	62
Figure 41 – Nitrate concentrations inside a) and outside b) of the estuary and phosphorus concentrations inside c) and outside d) of the estuary.....	63
Figure 42 – Temperature variation in the selected sites a) 3; b) 9; c) 12; d) 15; e) 17 and f) 18, during a year of simulation.	65
Figure 43 - Salinity variation in the selected sites a) 3; b) 9; c) 12; d) 15; e) 17 and f) 18, during a year of simulation.....	66
Figure 44 - Nutrient variation in the selected sites a) 3; b) 9; c) 12; d) 15; e) 17 and f) 18, during a year of simulation.	67
Figure 45 - Phytoplankton variation in the selected sites a) 3; b) 9; c) 12; d) 15; e) 17 and f) 18, during a year of simulation.	68
Figure 46 - Cohesive sediments variation in the selected sites a) 3; b) 9; c) 12; d) 15; e) 17 and f) 18, during a year of simulation.....	69
Figure 47 - a) <i>S. latissima</i> biomass, b) nitrate and inorganic phosphorus concentrations and c) salinity over the course of May 2017 to May 2020.	70

Index of Tables

Table 1 - Laminaria/Saccharina cultivation production, 2019. Source: FAO (2021b).....	4
Table 2 - Macroalgae parameters assumed in the tests (from [1] Default program values http://wiki.mohid.com/index.php?title=Mohid_Bibliography/ and [2] This study.)	20
Table 3 - Water properties and their default values on the tank.	23
Table 4 - Initial concentrations of phytoplankton and zooplankton.	24
Table 5 - Initial macroalgae concentration value.	26
Table 6 - Initial nitrate concentration for the increased nitrate test.	28
Table 7 - Initial nutrient concentrations for the lower inorganic phosphorus test.	28
Table 8 - Initial phosphorus concentration for the higher phosphorus test.	29
Table 9 - Macroalgae initial concentration for all depths.	30
Table 10 - Macroalgae, phytoplankton and zooplankton concentrations for this experiment.	32
Table 11 - Macroalgae initial concentration.	34
Table 12 - Macroalgae initial concentration.	35
Table 13 - Measurements and flowrates for the tanks of the second mesocosm.	38
Table 14 – Inflow water characteristics. property concentration values inside the saltwater river mesocosm and of the discharges entering it.	39
Table 15 - Phyto and zooplankton concentrations added to the control scenario.	40
Table 16 - Macroalgae initial concentration added to the control scenario.....	42
Table 17 - Macroalgae initial concentration in the light and depth test of the second mesocosm experiment.	44
Table 18 - Macroalgae, phytoplankton and zooplankton initial concentrations in the light and depth test of the second mesocosm experiment.	44
Table 19 - Macroalgae initial concentration in the temperature experiment of the second mesocosm.	45
Table 20 - Macroalgae initial concentration in the salinity experiment of the second mesocosm.	46
Table 21 - <i>River discharge flows along the simulation</i>	48
Table 22 - <i>Estuary initial property values and river discharge characteristics</i>	48
Table 23 - Parameters for <i>Saccharina latissima</i> , adapted from Broch and Slagstad (2012).	59
Table 24 - Phytoplankton and cohesive sediments specific light extinction coefficients for the Tagus simulations.	60
Table 25 – Sites grouped by <i>S. latissima</i> growth and respective representative station.	64

1 – Introduction

The objective of this study is to evaluate the potential growth of a brown macroalgae species named *Saccharina latissima* in the estuary of one of the greatest rivers in Portugal (either by length or drainage area), the Tagus River (*Rio Tejo*). The assumption is that the algae are fixed in longlines submerged at a specific depth. This work aims to answer the following questions:

- Where is the best location for *Saccharina latissima* to grow in the Tagus Estuary?
- When is the best time of the year to place them, in order to maximize growth?

This study starts with the hypothesis that inside the estuary *S. latissima* will have a greater availability of nutrients than in the ocean, and thus, macroalgae will grow better. The nutrients are washed from the Tagus watershed and provide a steady inflow of nutrients for the algae to grow. The river's freshwater mixes with the Atlantic Ocean saltwater, creating a mixing zone inside the estuary which might create favorable conditions for *S. latissima* proliferation. Inside the estuary, the ideal location to place the algae is where the best compromise of ideal conditions of temperature, light, salinity, and nutrients is achieved.

Before studying the behavior of *S. latissima* in the Tagus Estuary, three mesocosms with different conditions were constructed to verify if MOHID Water Modeling system was responding accordingly with the parameters used and to test the behavior of macroalgae against nutrient availability, depth, light availability, temperature and salinity variations.

The first mesocosm served to test how macroalgae responded to parameter variations on a simple, closed, nutrient limited system.

The second mesocosm simulated a segment of a river with the water flow providing an unlimited supply of nutrients for macroalgae to grow, and once again test the how they respond to the variation of temperature, salinity, depth and light without being inhibited by nutrient shortage.

The third mesocosm mimics a small estuary with irregular bathymetry, where two rivers discharge freshwater at a variable flowrate, to study macroalgae resilience against physical stresses caused by water velocity, as well as different gradients of nutrients, salinity, phytoplankton concentrations and light conditions.

Lastly, after verifying the functionalities of the model and analysing how macroalgae are affected by their growth limiting factors, the growth of *S. latissima* was evaluated in sites inside and in the outside surroundings of the Tagus Estuary, determining where and when does this species grow best as well as explaining the reasons for it.

2 - State-of-the-art

2.1 - *Saccharina latissima*

Saccharina latissima, also known as *Laminaria saccharina* or more commonly as sugar kelp is a species of large brown algae commonly found in Northern Atlantic coasts of Europe and America, in the northern Pacific coasts of America and Japan. It usually lives in low depths (less than 30 meters) in sublittoral zones attached to stable solid substrates and sometimes unstable substrates like rocks and boulders. Its morphology consists of a long yellowish-brown undivided blade with a wrinkled surface and frilly margins, a stipe that can reach 50 cm, a small branching holdfast that attaches to substrates and no midrib. When fully grown, it can achieve 4 m in length, live between two to four years and grow quickly from winter to April (White and Marshall, 2007). After harvesting, these algae have several uses in the industry. They produce alginic acid that can be used to make gels, stabilizers in food, pharmaceuticals, and cosmetics (McHugh, 2003). When dried, it forms a sweet white powder on the frond named mannitol, that can be used as a sweetener or in medication, hence the name sugar kelp. Figure 1 displays a unit of *S. latissima*.



Figure 1 - *Saccharina latissima*. Source: NOAA Fisheries. <https://www.fisheries.noaa.gov/species/sugar-kelp>

2.2 - Kelp Aquaculture

For centuries, seaweed has been used as a food source for coastal communities. It provided and still provides the communities with proteins, low fat and carbohydrates and a rich mixture of macronutrients and micronutrients (FAO, 2021a).

Nowadays, hunger is a global issue that mainly affects the great majority of the population of developing countries and a part of the population in developed countries. Kelp aquaculture has been pointed as a key solution due to its rapidly expanding practice that, if explored responsibly might in time, prevent these global deaths from malnourishment epidemic.

“By farming just two per cent of the ocean, we could provide enough protein to feed a world population of 12 billion people. Seaweed is extremely protein rich, low in fat, low in carbohydrates, and rich in vitamins, zinc and iron”

– Vincent Doumeizel, UN News (2020) - <https://news.un.org/en/story/2020/11/1077212>.

Other than having a good nutritional value and providing food security, kelp aquaculture provides several environmental benefits, such as pollution remediation, carbon sequestration and biofuel production (Brummet et al. 2016). By 2014, 124 million tons were used globally as a fertilizer of which about half was not taken by plants and 15% - 30 % ended up in coastal waters (FAO (2015) and Lassaletta et al. (2014)). Carbon dioxide in the atmosphere is causing ocean acidification to increase, lowering the oceans pH, and damaging marine life (Ciais et al. 2013). Seaweed production could absorb many of these excess nutrients while producing biomass, which also removes carbon from the water through its use in photosynthesis. Reaching a global level of 500 million tons of seaweed production would assimilate 10 million tons of nitrogen from seawater, equalling some 30% of the nitrogen estimated to enter the ocean and absorb 135 million tons of carbon, about 3.2% of the carbon added annually to seawater from greenhouse gas emissions (Brummet et al. 2016).

2.3 - Brown seaweeds

Brown algae are marine multicellular algae of the class *Phaeophyceae*. Among them, kelps are the largest and most complex brown algae, being the only algae to have internal tissue differentiation into conducting tissue. Most brown algae have an alternation of haploid and diploid generations.

Brown macroalgae live attached to fixed substrates, like the seabed or in continental shelves. They remain in place for the continuity of their lifespan or until removed by high shear stress caused by the passing water. Once removed from the surface where they were previously attached, they stop being biologically functional and remain in the water columns as biomass.

World cultivation of brown seaweeds increased from 13000 tonnes in 1950 to 16.4 million tonnes in 2019 and in that same year, brown seaweeds accounted for 47.3% of world cultivation in terms of tonnage and 52 % in terms of value (FAO, 2021a). Cultivation of brown seaweeds has concentrated on two cold-water genera, *Laminaria/Saccharina* (kelp) and *Undaria* (wakame). Table 1 displays the cultivation of the *Laminaria/Saccharina* genera in 2019:

Table 1 - Laminaria/Saccharina cultivation production, 2019. Source: FAO (2021b)

Country	Laminaria/Saccharina cultivation	
	Tonnes (wet weight)	Share of the world (%)
World	12273748	100
China	10978362	89.45
Republic of Korea	662557	5.4
Democratic people's Republic of Korea	699999	4.89
Japan	32600	0.27
Faroe Island	156	0
Norway	73	0
Spain	0.14	0

As of 2019, brown algae aquaculture is focused mainly on eastern Asia, with China, South Korea, North Korea, and Japan producing nearly 100% of kelps.

2.4 - Estuarine physics and biogeochemistry

Tides

Tides are the periodical variation of the ocean water level. They are waves with a very long period that move through the oceans as a consequence of the gravitational pull of the sun and the moon. When the tide rises, the water level goes up and moves against the shores, while when the tide falls, the water level goes down and water recedes. When the water level reaches its highest and lowest point, it's designated as high and low tide respectively. The difference between high and low tide corresponds to the tidal range.

With the rising and falling of the tide, there is an associated horizontal movement of water. When the tide rises, there's a motion of water in the direction of the shore, called flood current. The movement in the opposite direction that occurs while the tide falls is named the ebb current. These movements are driving forces for water mixing.

Tides have two main constituents, the forces exerted by the moon and the sun, which depend on the position of the sun and the moon in relation to the Earth. The strongest component is the force of the moon. While the sun has several times the mass of the moon and gravitational force is directly proportional to the masses of the objects, it is also inversely proportional to the square of the distance (as stated by the Universal Gravitation Law). Since the moon is much closer to the Earth than the sun, the gravitational pull of the moon in the oceans is stronger than the suns.

The moon component is called the principal lunar semi-diurnal or the M2 tidal constituent and its responsible for two the occurrence of two high tides and low tides per each lunar day, which is about 24 hours and 50 minutes.

When the moon completes one revolution around the Earth, it produces two high and two low tides. The first one due to the gravitational pull of the moon and the second due to the inertial pull, contrary to gravity, when the moon is exactly on the opposite side of the globe (Figure 2).

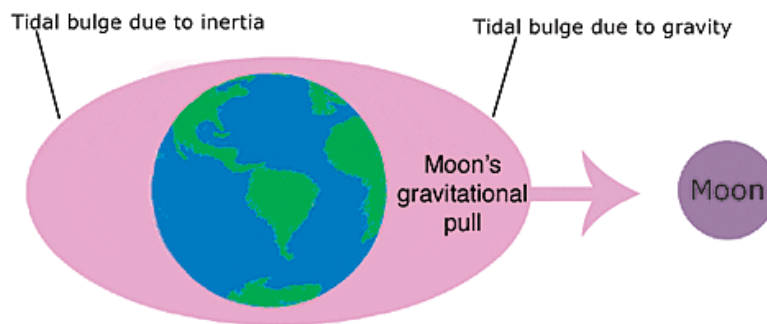


Figure 2 - Influence of the moon's gravitational pull on tides. Source: National Ocean Service NOAA.

https://oceanservice.noaa.gov/education/tutorial_tides/tides03_gravity.html

The solar component, called the S2 tidal constituent, lower in intensity than the M2 constituent, exhibits similar bulges that shift places with Earth's own rotation and rotation around the sun.

Solar Irradiance

Light, or incident solar radiation is the electromagnetic radiation emitted by the sun. It's used by primary producers like terrestrial plants, microalgae, macroalgae and other plant-like organisms during photosynthesis along with nutrients, where it is essential in the conversion of CO₂ into carbohydrates. That chemical energy, through cellular respiration, is then used by the organism's cells to maintain metabolic functions. The solar irradiation that illuminates a given place depends mainly on the time of the year (proximity of the Earth to the sun), hemisphere of the place and cloud cover (Solar Energy Technologies Office: <https://www.energy.gov/eere/solar/solar-radiation-basics>).

The chlorophyll present in plant cells captures de energy within the light to produce glucose to be later used as an energy source for its metabolic activities through respiration. In this specific case, it affects the growth of macroalgae and phytoplankton suspended in the water column.

The light availability in the water column decreases in function of the depth and depends on several elements. The first one is the incident radiation at the surface level, the extinction of light in the water due

to its optical properties and the photosynthetic response to light, by the primary producers. The behaviour of the irradiance in the water can be described here by the Lambert-Beer law:

$$I(z) = I_0 e^{-kz} \quad (1)$$

Where:

$I(z)$ is the irradiance ($W.m^{-2}$) at depth z (m); I_0 is the irradiance at the surface ($W.m^{-2}$) and k is the light extinction coefficient (m^{-1}).

Light can be divided here into two components, shortwave solar radiation, which consists of about 40 to 60% of the total radiation at the top of the of the water body (I_0) and longwave solar radiation that makes up the rest of the total irradiance. And so:

$$I_0 = Sw_0 + Lw_0 \quad (2)$$

For this thesis and in all its experiments, it's acknowledged that shortwave and longwave radiations make up 60% and 40% (MOHID Light Extinction Manual: http://wiki.mohid.com/index.php?title=Mohid_Bibliography) of the radiation at the top of the water-air surface, respectively.

$$\begin{cases} Sw_0 = 0.6 * I_0 \\ Lw_0 = 0.4 * I_0 \end{cases} \quad (3)$$

I_0 , Sw_0 and Lw_0 ($W.m^{-2}$) are total irradiance at the top of the water body, shortwave and longwave irradiance, in this respective order.

The shortwave component consists of radiation with wavelengths in the near infrared (NIR), visible, to near ultraviolet (NUV) in the electromagnetic spectrum. It is the part of the solar radiation that photosynthetic organisms employ in their autotrophic activities. It's a penetrative radiation that distributes heat across a significant portion of the water column.

Longwave radiation is light in the infrared spectrum. It's the portion that's not used by primary producers and doesn't penetrate too far into the water, but it affects the temperature of the water. It can be divided into upward and downward longwave radiations. Downward longwave radiation is the longwave radiation that reaches the sea from the atmosphere. Upward longwave radiation is the radiation flux that is emitted by the surface of the water back to the atmosphere.

Splitting the Lambert-Beer equation (Equation 1) into its two components, results:

$$\begin{cases} Sw_z = Sw_0 * e^{-k_s * z} \\ Lw_z = Lw_0 * e^{-k_l * z} \end{cases} \quad (4)$$

Where k_s and k_l (m^{-1}) are the shortwave and longwave light extinction coefficients. Since this report aims to study the growth of macroalgae in a marine or estuarine environment, it will specially focus on the shortwave component.

Nutrient dynamics in the ocean

Nutrients are chemical elements or compounds required for the survival, development, and reproduction of living organisms. The most important for plant and algae growth are nitrogen, phosphorous and silica for diatoms. These organisms uptake nutrients for maintenance, growth, and reproduction. They are present in the water column and sediments in several different forms and their concentration is influenced by several properties.

Nitrogen is essential to all life because it's one of the main components of proteins, and for photosynthetic organisms, it's an important constituent of chlorophyll, making itself indispensable for photosynthesis.

As for phosphorus, another chemical element essential to all life, it provides structure to the DNA and RNA and it's crucial in the transmission of chemical energy by the ATP molecule, being a constituent in other cellular structures, among other functions (Paytan and McLaughlin, 2006).

In the ocean, there is a close resemblance between the molar carbon to nitrogen to phosphorus ratio of phytoplankton composition and the average ratio of those nutrients in the ocean, which was identified by and later on called the Redfield ratio and its value is 106:16:1 (Redfield, 1934). This ratio also represents generally the nutrient requirement of marine life (Voss et al., 2013).

Nitrogen occurs in water mainly in its non-reactive form, dissolved N_2 gas (about 95%). The remaining dissolved reactive forms consist of nitrite (NO_2), nitrate (NO_3), ammonia (NH_4). It also exists as organic nitrogen either in the dissolved (refractory, DONr, or non-refractory, DONnr, dissolved organic nitrogen) or particulate (PON) phase.

Phosphorus is present as dissolved or suspended matter, in both inorganic and organic forms. Dissolved organic forms include dissolved organic refractory and non-refractory phosphorus (DOPr and DOPnr, respectively), while dissolved inorganic phosphorus may appear as orthophosphate (PO_4). As for suspended forms, it appears as particulate inorganic phosphorus (PON).

According to figure 2 of Voss et al. (2013) and figure 2 of Paytan and McLaughlin (2006), nutrient dynamics in coastal systems can be described as follows.

Nitrogen and phosphorus are supplied into the ocean mainly by continental river discharges and by atmospheric deposition in a very smaller scale (Benitez-Nelson (2000) and Seitzinger et al. (2005)). After they reach the ocean, nitrate, ammonia, and orthophosphate are utilized by autotrophs in the photic zone to perform photosynthesis, which incorporates them into their system. At the same time, nitrogen fixing

bacteria convert molecular nitrogen into ammonia. Through grazing by heterotrophs, nitrogen and phosphorus are incorporated in the following trophic level. Both autotrophs and heterotrophs can expel nutrients by exudation, releasing refractory and non-refractory dissolved organic matter and exude nitrogen in the form of ammonia during respiration. Non-refractory organic matter is remineralized in the water column. When both autotrophs and heterotrophs die, these nutrients become again available in the water column as particulate organic matter, which sink into the ocean until they reach the bottom, undergoing slow remineralization as they slowly descend. Having fully sedimented, bottom bacteria in the aphotic zone remineralize a portion of the nutrients back into their inorganic form and release them into the water, while what was covered by the sediments remains at the bottom (Paytan and McLaughlin, 2006). In the sediment layers or in other oxygen deficient places in the water column, denitrifying bacteria reduce nitrate back into molecular nitrogen.

Adsorbed phosphorus by the sediments can then be released back in the water column due to increases of temperature and salinity (Zhang and Huang, 2011).

Remineralized nutrients remain and accumulate deep into the water near the bottom where they were remineralized, until they are transported back into the surface. According to Voss et al. (2013), there are four major processes that bring nutrient rich waters to the surface to be used again by autotrophs: thermal stratification and mixing, eddies, upwelling, and diffusion.

Thermal Stratification and Mixing

The thermal amplitude along the year is the main driving force behind the vertical mixing of the water. During summer, due to heat transfer and solar irradiation from the atmosphere, the temperature of the water close to the surface is higher than the temperature in higher depths, meaning that the density of the uppermost layer is lower, and there is little to no mixing. But when the atmospheric temperature decreases in autumn and through winter, the uppermost layer will be cooler and denser than the lower layers, causing the layer to sink in and, with the help of the wind, mix vertically with the lower water layer. This mixing phenomenon helps to distribute evenly the nutrients that were stored at the bottom, providing optimal conditions for the proliferation of primary autotrophs and consequently heterotrophs when the incident light and solar radiation increases in the beginning of spring through summer

Eddies

Eddies are circular currents of water caused by baroclinic and barotropic instabilities and their swirling motion bring nutrients from the colder, deeper waters to the surface.

Upwelling

The wind direction is also an important factor of vertical mixing and horizontal transport in the ocean, as it directly affects the currents. One of the most important components of wind-driven ocean currents is the Eckman Transport, and it is especially important for the currents near the coast of Portugal. The Eckman transport is the phenomenon where the wind going on a certain direction exerts friction on the water in the ocean surface. Due to the rotation of the Earth, the Coriolis effect shifts the direction of the surface water to about 45° to the right in the northern hemisphere (NOAA: https://oceanservice.noaa.gov/education/tutorial_currents/04currents4.html) . As the depth increases, the speed and direction of the water changes. due to the combination of the Coriolis effect and the wind The direction of the moving water gradually turns to the right, creating a spiral of moving water up to 100 to 150 m deep. The average direction of the turning water is therefore the Eckman transport. In the summer, Portugal's weather is characterized by high relative temperatures and a regional wind from the North to the South, the "nortada" (Soares et al. 2014), due to the pressure differences caused by the thermal gradients between the warmer Iberian Peninsula and the colder ocean. This Northern wind parallel to the occidental coast of Portugal creates an Eckman transport that drags the superficial layers of water away from the coastline, originating a pressure of water height and pressure on the coast. These waters are then replaced by the colder, nutrient rich waters that ascend to the surface in their place. This increase of nutrients stimulates the growth of phytoplankton and consequently the growth of heterotrophs like sardines, which feed on it (adapted from Lopes, 2012).

Diffusion

Finally, diffusion is the movement of a substance from a location of high concentration to a location with lower concentration. Through the combination of all these processes, nutrients are transported with the water from the depths to the surface layers, providing nutrients that stimulates primary production in the spring of the following year.

3 - Methodology

Modeling ecosystems requires to simulate each component of the environment and their interactions among themselves, so for the purpose of further understanding the dynamics between macroalgae and their surroundings, a mathematical model that can replicate natural processes with some accuracy and the interactions between the several components of water bodies was needed.

MOHID Water is a 3D numerical model that simulates rivers, estuaries, coastal areas and the ocean written in Fortran language. It splits aquatic systems into three compartments that correspond conceptually to the medium where the processes occur: air, water and land, and it possesses two interfaces modules that

compute and manage the fluxes between sediment and water (Module InterfaceSedimentWater) and between water and air (Module InterfaceWaterAir).

The environmental components of those compartments are represented by several modules that are responsible for calculating the relevant physical and biogeochemical processes. These modules are linked to each other just as every environmental medium, through the exchange of mass and energy from one another. As in nature, some modules (processes) are required to be active, while other modules can be added, depending on the aim and the ecosystem composition in study. This is the case of the Module MacroAlgae, which is the focus of this thesis.

3.1 - A Macroalgae Model

The model to test macroalgae was built using Module MacroAlgae. Module MacroAlgae is a zero-dimensional module that calculates the growth of macroalgae and how they interact with the nutrients. Other processes involving nutrients in the water column (described as the biogeochemical cycle of nutrients) are described in the Module WaterQuality. The description of this module and its equations was done on Trancoso et al. (2005) and on the MOHID Technical Manuals (http://wiki.mohid.com/index.php?title=Mohid_Bibliography). The model relies on the formulations of EPA (1985) that should be consulted for more details. Figure 3 shows the conceptual model of all macroalgae mass interactions described in the module:

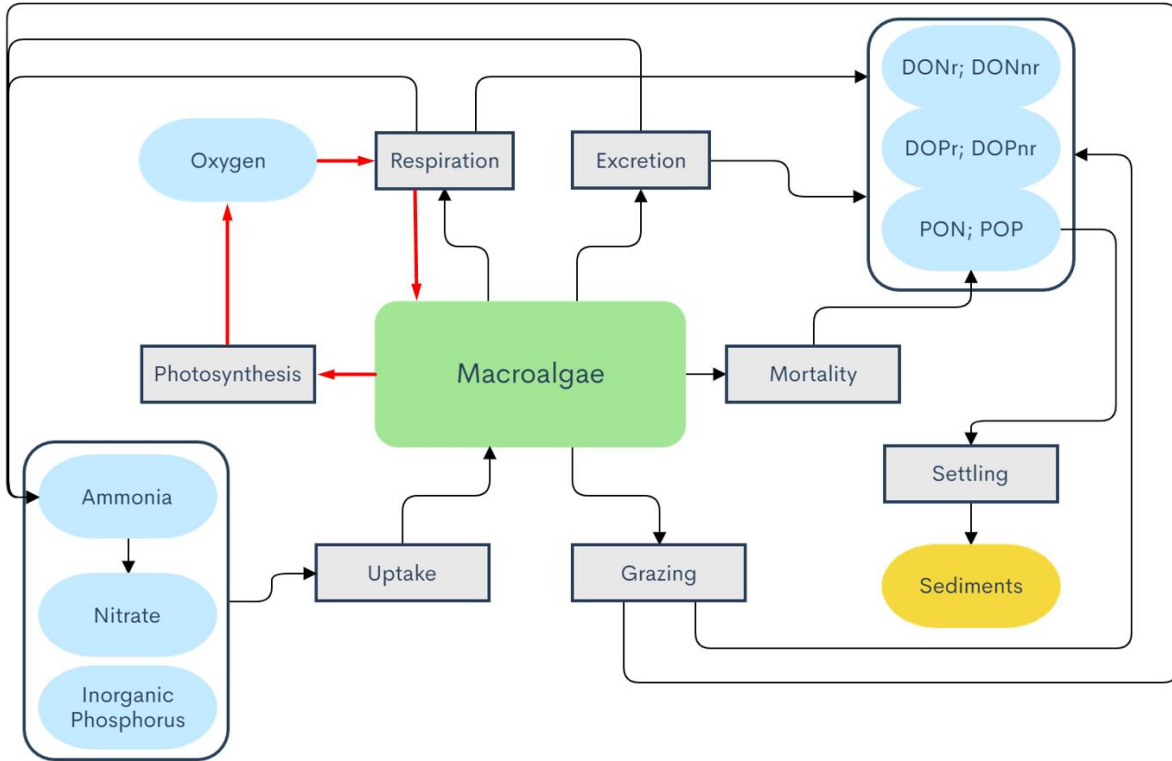


Figure 3 - Conceptual model of macroalgae biomass and nutrient flows. Black lines represent nutrient and carbon fluxes, red lines represent oxygen fluxes.

3.2 – Governing Equations

General macroalgae growth

The main equation to account for macroalgae biomass growth is:

$$\frac{\partial M_x}{\partial t} = (\mu_x - r_x - e_x - m_x - G_x) \cdot M_x \quad (5)$$

Where x is the type of macroalgae (attached in this experiment), M_x ($\text{gC}\cdot\text{m}^{-3}$) is the macroalgae concentration in the water column, μ_x (day^{-1}) is the gross growth rate or gross production rate, r_x (day^{-1}) is the respiration rate, e_x (day^{-1}) is the exudation rate, m_x (day^{-1}) is the natural mortality rate and G_x (day^{-1}) is the grazing rate (or mortality rate by predation). The net production rate is then the balance of the gross production rate minus the respiration, exudations, mortality and grazing rate.

These variables are also defined by their own set of equations, as described below.

Gross production rate

Macroalgae growth depends heavily on the conditions of the surroundings, like the availability of nutrients, light, water temperature and salinity. The gross growth rate is the product of the limitation factors of those conditions with a fixed parameter that is the maximum gross production rate.

$$\mu_x = \mu_x^{max} \cdot \min(\psi(N)_x, \psi(P)_x) \cdot \psi(E)_x \cdot \psi(T)_x \cdot \psi(S)_x \quad (6)$$

Where $\psi(N)_x$, $\psi(P)_x$, $\psi(T)_x$, $\psi(E)_x$ and $\psi(S)_x$ are, respectively, the limiting factors of nitrogen, phosphorus, temperature, solar irradiance, and salinity and μ_x^{max} (day^{-1}) is the maximum growth rate. These factors range from 0 to 1. 1 means that the factor is not limiting the growth and 0 means that it is completely limiting growth, functioning respectively as the neutral and the absorbing elements of multiplication.

Nutrient Limiting Factors

The nutrient limiting factors follow a Michaelis-Menten kinetics for substrate, in which the fraction of the available substrates divided by the sum of those substrates with the half-saturation constant K, dictates the current rate as a fraction of its maximum (μ_x^{max} of Equation 6).

The equation for nitrogen related nutrients is shown below:

$$\psi(N)_x = \frac{[NH_4] + [NO_3]}{K_x^N + [NH_4] + [NO_3]} \quad (7)$$

Where $[NH_4]$ and $[NO_3]$ are the ammonia and nitrate concentrations, respectively, and K_x^N is the nitrogen half-saturation constant, all in mgN.L^{-1} .

In accordance with the equation above, the phosphorus limiting equation is then:

$$\psi(P)_x = \frac{[PO_4]}{K_x^P + [PO_4]} \quad (8)$$

Where $[PO_4]$ is the inorganic phosphorus concentration and K_x^P is the phosphorus half-saturation constant, all in mg.L^{-1} too.

The next figure (Figure 4) presents the evolution of nitrogen and phosphorus limiting factor with the increase of the specific nutrient concentration.

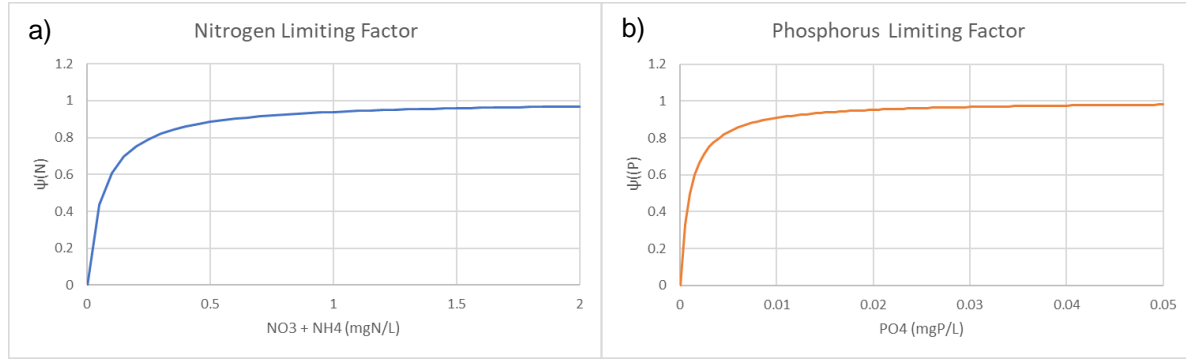


Figure 4 - a) Nitrogen limiting factor (left) and b) Phosphorus limiting factor (right) in function of nitrogen and phosphorus concentrations, respectively, with $K_x^N = 0.065 \text{ mgN/L}$ and $K_x^P = 0.001 \text{ mgP/L}$

Figure 4 shows that the higher the concentration of nitrate or phosphate, the higher the respective limiting factor. It means that high availability of nitrate or phosphorus translates into the respective limiting factor tending asymptotically to 1 (uninhibited growth). They're both needed for algae growth, hence the "minimum" operator of the two nutrient limiting factors in the gross production Equation 6. The nutrient limitation factor decreases until either the nitrogen or phosphorus limiting factor tends to 0, completely inhibiting growth, even if the other nutrient is available.

Temperature Limitation Factor

Temperature limiting factor for macroalgae is calculated by the following equation:

$$\psi(T)_x = K_A(T)_x \cdot K_B(T)_x \quad (9)$$

Where:

$$K_A(T)_x = \frac{K_1 \cdot e^{\gamma_1(T-T_{min})}}{1 + K_1 \cdot (e^{\gamma_1(T-T_{min})} - 1)} \quad (9.1)$$

$$\gamma_1 = \frac{\ln \frac{K_2(1-K_1)}{K_1(1-K_2)}}{T_{opt_{min}} - T_{min}} \quad (9.2)$$

and

$$K_B(T)_x = \frac{K_4 \cdot e^{\gamma_2(T_{max}-T)}}{1 + K_4 \cdot (e^{\gamma_2(T_{max}-T)} - 1)} \quad (9.3)$$

$$\gamma_2 = \frac{\ln \frac{K_3(1-K_4)}{K_4(1-K_3)}}{T_{max} - T_{opt_{max}}} \quad (9.4)$$

$T_{opt_{min}}$ and $T_{opt_{max}}$ (°C) define the range of temperatures where macroalgae grow at optimal rate, T_{max} and T_{min} define respectively the maximum and minimum temperatures macroalgae can grow. Should the water temperature exceed the maximum or be lower than the minimum, growth is completely inhibited. The constants K_1 , K_2 , K_3 and K_4 control the shape of the temperature response curve and are left by their default values, equal for all organisms in this model.

Figure 5 illustrates the temperature limitation factor as a function of temperature.

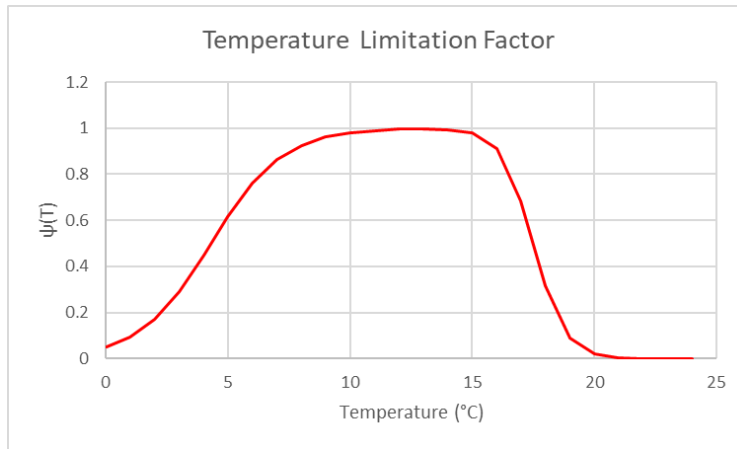


Figure 5 - Temperature limitation factor in function of the temperature (°C) for $T_{opt_{min}} = 10^\circ\text{C}$; $T_{opt_{max}} = 15^\circ\text{C}$; $T_{min} = 0^\circ\text{C}$ and $T_{max} = 20^\circ\text{C}$, with $K_1 = 0.05$, $K_2=K_3=0.98$ and $K_4 = 0.02$.

Salinity Limitation Factor

The salinity limitation factor can be described by:

$$\psi(S)_x = \begin{cases} 1 - \left(\frac{S - S_{opt}}{S_x - S_{opt}} \right)^\alpha, & \text{if } S > S_c \\ \frac{S - S_{min}}{S_{opt} - S_{min}}, & \text{otherwise} \end{cases} \quad (10)$$

and

$$S_x = \begin{cases} S_{min}, & \text{if } S < S_{opt} \\ S_{max}, & \text{otherwise} \end{cases} \quad (10.1)$$

$$\alpha = \begin{cases} 2.5, & \text{if } S < S_{opt} \\ 2.0, & \text{otherwise} \end{cases} \quad (10.2)$$

Where S is salinity (psu), S_{min} , S_{opt} , S_c and S_{max} are, respectively, minimum, optimal, critical and maximum salinity (psu). Below the minimum and above the maximum salinity, the entity can't tolerate those conditions and growth is completely inhibited. From the minimum to the critical salinity, growth is severely limited, but not null ($\Psi(S)_x \approx 0$). Above S_c , growth limitation decreases until it is completely uninhibited at the optimal salinity ($\Psi(S)_x = 1$). Above the optimal salinity, growth limitation rises until the maximum salinity, where growth is inhibited from that value on forward. These statements can be verified by observing Figure 6.

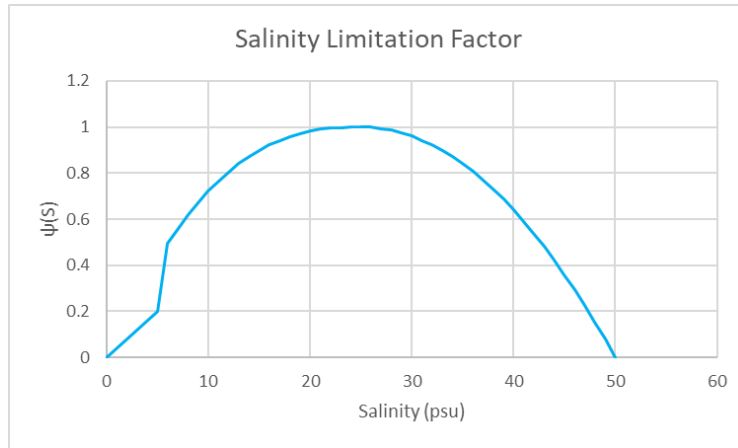


Figure 6 - Salinity limitation factor in function of salinity (psu) with $S_{min} = 0$, $S_{max} = 50$, $S_{opt} = 25$ and $S_c = 5$ psu.

Light Limitation Factor

Solar irradiation is a key factor in the development of photoautotrophs like terrestrial plants, seaweeds, and algae, who perform photosynthesis to grow. The light limitation factor translates the response of producer's photosynthetic rate with the environments available irradiance. Below is shown the equation for photosynthetic rate, as described in the MOHID Technical Manuals (http://wiki.mohid.com/index.php?title=Mohid_Bibliography).

$$\frac{P}{P_{max}} = \frac{Sw_z}{Sw_{opt_x}} \cdot e^{-\frac{Sw_z}{Sw_{opt_x}}} \quad (11)$$

Where P and P_{max} (day^{-1}) are the current photosynthesis rate and the maximum photosynthesis rate that the algae can perform, Sw_z ($W.m^{-2}$) is the shortwave solar radiation available at depth z (m) and Sw_{opt_x} ($W.m^{-2}$) is the optimal shortwave solar irradiance for photosynthesis of the primary producer's species.

By integrating Equation 11 in depth dz, the expression for the light limitation factor, can be derived.

$$\Psi(E)_x = \frac{1}{z} \int_0^z \frac{P}{P_{max}} dz = \dots = \frac{e^1}{k_x \times z} \times \left(e^{-\frac{S_0}{Sw_{opt_x}} e^{-k_x \times z}} - e^{-\frac{S_0}{Sw_{opt_x}}} \right) \quad (12)$$

In Equation 12, k_x (m^{-1}) is the light extinction coefficient, Sw_{opt} ($W.m^{-2}$) is the optimal shortwave irradiation value of the algae, Sw_0 ($W.m^{-2}$) is the shortwave solar radiation at the top of the water column, and z (m) is the depth where macroalgae are fixed.

When the solar radiation at a fixed depth equals the optimum solar irradiation, photosynthesis rate is maximum, and the limitation factor is one. On the other hand, if macroalgae are placed too deep, little to no radiation can penetrate the water column, meaning that the limitation factor will be zero or nearly zero, and totally inhibit any possible growth. When solar radiation is higher than the optimum and solar radiation is too intense, photoinhibition begins to take place. So, placing macroalgae at very shallow depths could be harmful. As solar radiation keeps intensifying beyond the optimum value, the greater is the photoinhibition, the lesser is the growth. This can be visualized in Figure 7 that represents the light limitation factor ($\Psi(E)_x$) as a function of the solar radiation at the top of the water column (Sw_0), for three optimal solar irradiance values (Sw_{opt}).

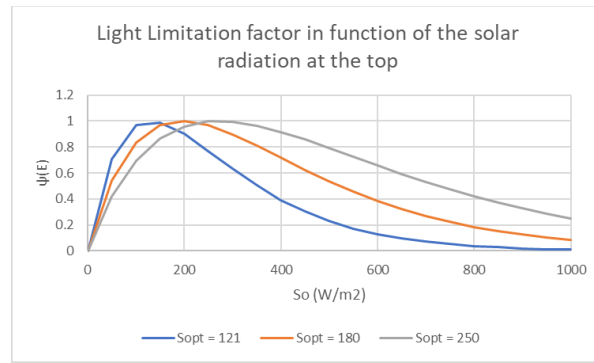


Figure 7 - Light limitation factor in function of the solar irradiance at the top of the water column, for $k = 0.08 m^{-1}$ and $z = 2$ meters.

Since daily solar irradiance at the top of the water varies between 0 $W.m^{-2}$ and a maximum value, if algae are placed at a 2 m depth and their optimal irradiance is 121 $W.m^{-2}$, their potential maximum growth in regard to light will only occur at the time of the day where solar irradiance at the top is 150 $W.m^{-2}$. The same logic can be applied for optimal irradiances of 180 and 250 $W.m^{-2}$, where the light limitation factor will be maximum at the time of the day where solar irradiance is 200 and 250 $W.m^{-2}$, respectively.

There are several estimations for the light extinction coefficient, which is the variable that dictates how much light is attenuated with depth. The formulation used in this study is a multiparametric expression, which considers the natural water coefficient and additive terms that are a function of the concentrations of sediments, particulate organic matter, like phytoplankton, and the self-shading effect of macroalgae that obstruct the passage of light.

$$k = k_w + k_p C_p + k_s C_s + k_m C_m \quad (13)$$

Where k is the light extinction coefficient (m^{-1}), k_w is the natural light extinction coefficient (m^{-1}), k_p , k_c and k_m are the specific phytoplankton, cohesive sediments and macroalgae light extinction coefficients ($m^{-1} \cdot (mg \cdot L^{-1})^{-1}$) and C_p , C_s and C_m are the phytoplankton, cohesive sediments and macroalgae concentrations ($mg \cdot L^{-1}$).

Figure 8 shows the plots of Lambert-Beers law for a surface shortwave irradiation of $400 W \cdot m^{-2}$, with an extinction coefficient of $k = 0.08 m^{-1}$, approximately the natural light extinction for water, $k = 0.1 m^{-1}$ and $k = 0.5 m^{-1}$. The higher the k , the faster light is attenuated. In Figure 8) with $k = 0.08 m^{-1}$ light extinguishes at around 50 m, with $k = 0.1 m^{-1}$ at 30 m and with $k = 0.5 m^{-1}$ in less than 10 m.

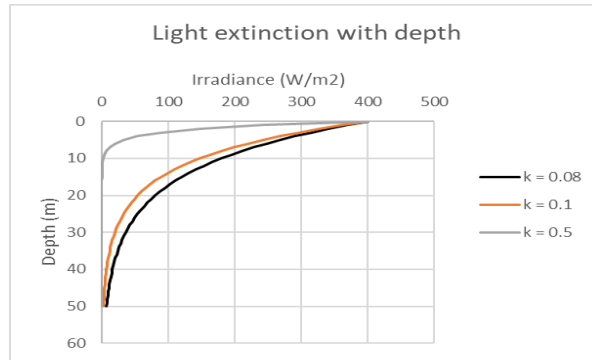


Figure 8 - Light extinction in function of depth, for different light extinction coefficients

Grazing

Fish schools and other primary consumers and their behaviors, apart from zooplankton, are not described by the current model and for that reason the grazing rate G_x (day^{-1}) on macroalgae is a fixed fraction of their biomass. Through grazing, ammonia, dissolved and particulate organic matter are released into the system, as a product of the metabolic processes of the being that grazed on the macroalgae.

Respiration rate

Macroalgae possess two types of respiration, endogenous respiration (cellular maintenance) and photorespiration (a wasteful cycle that lowers the efficiency of photosynthesis), consuming oxygen and releasing carbon in the form of CO_2 to the environment (EPA, 1985).

$$r_x = k_x^{re} \cdot e^{(0.069 \cdot T)} + k_x^{rp} \cdot \mu_x \quad (14)$$

Where r_x is the respiration rate in day^{-1} , k^{re} is the endogenous respiration constant, k^{rp} is the photorespiration constant, T the water temperature in $^{\circ}C$ and μ the growth rate also in day^{-1} .

Through respiration, macroalgae also lose ammonia, dissolved and particulate organic matter.

Exudation rate

Primary producers exudate nutrients that can't be used as substrate anymore in the form of ammonia, dissolved and particulate organic matter.

$$e_x = \varepsilon_x \cdot \mu_x \cdot (1 - \Psi(E)_x) \quad (15)$$

The exudation rate e_x (day^{-1}) is a function of the reference exudation rate ε_x (day^{-1}), growth rate μ (day^{-1}) and the light limiting factor $\Psi(E)_x$. The model admits that in more favorable light availability conditions, exudation is reduced because the macroalga is performing photosynthesis and assimilating nutrients from its surroundings. When faced with unfavorable light conditions or during the night, the light limitation factor is very small or even zero respectively, increasing the exudation rate.

Natural mortality rate

Natural mortality is the rate at which algae, phytoplankton or another primary producer loses some of mass that reaches its end of life. By mortality, particulate organic matter concentrations (PON and POP) in the system are increased.

$$m_x = m_x^{\max} \cdot \frac{\frac{M_x}{\mu_x}}{K_x^m + \frac{M_x}{\mu_x}} \quad (16)$$

Where m_x (day^{-1}) is the instantaneous mortality rate. m_x^{\max} is the maximum mortality rate (day^{-1}), M_x is the current macroalgae biomass ($\text{gC} \cdot \text{m}^{-3}$), μ_x is the gross growth rate (day^{-1}) and K_x^m is the mortality half-saturation constant.

This equation for the mortality of the macroalgae works with a concept similar to the Michaelis-Menten formulations, where a maximum growth rate is achieved or not depending on the value of the fraction, which can vary from 0 to 1, depending on the macroalgae mass and growth rate.

All these fluxes from respiration, mortality, grazing and exudation are displayed in Figure 3.

Finally, it is worth pointing that these equations are analogous for phytoplankton, with the only differences being the parameters defined for both groups and that phytoplankton is suspended in the water columns instead of being fixed at the bottom.

3.3 - Mesocosms, a simpler approach to study ecosystems

The first approach for modelling macroalgae on MOHID was to test the model performance and consistency by building different theoretical and schematic scenarios with different configurations, for instance, assuming that nutrients are being discharged into the tank by a flowrate or simply to see how algae develop in a closed system. By inserting an inflow and outlets, it was possible to mimic what happens in rivers, estuaries, or the open sea. These experiments that attempt to simulate a natural environment in a closed or partially enclosed system in a laboratory, or in this case, a computer simulation are dubbed mesocosms. Three different mesocosms were presented in this report.

- The first one consisted of a small one cell tank of water where no hydrodynamic processes, such as advection and diffusion, occur. The purpose of this tank was to evaluate how macroalgae would grow in response to variations of properties (temperature, light, depth) in a nutrient deficient closed environment.
- The second tank was a 15-cell tank with hydrodynamics, where properties are discharged in the 3 cells south of the tank at a fixed rate and water is removed on the 3 north cells at that same rate, keeping the control volume constant and therefore mimicking a segment of a fictional river. In this case, the purpose was to assess the feedback of the algae to a domain with constant nutrient availability
- The third and final testing tank is an irregular shaped schematic estuary used to describe the growth of algae when subject to physical conditions such as water velocity, shear stress and eddies that may cause algae to dislodge or break at high tension.

Values for macroalgae parameters used in the simulations are summarized in Table 2:

Table 2 - Macroalgae parameters assumed in the tests (from [1] Default program values http://wiki.mohid.com/index.php?title=Mohid_Bibliography/ and [2] This study).

Parameter	Value	Unit	Description	Source
μ_{\max}	0.5	d^{-1}	maximum growth rate	[2]
$T_{opt_{\min}}$	10	$^{\circ}C$	optimum minimum temperature for growth	[2]
$T_{opt_{\max}}$	15		optimum maximum temperature for growth	[2]
T_{\min}	5		minimum temperature for growth	[1]
T_{\max}	40		maximum temperature for growth	[1]
K1	0.05		-	constant to control temperature response curve shape
K2	0.98	-	constant to control temperature response curve shape	[1]
K3	0.98	-	constant to control temperature response curve shape	[1]
K4	0.02	-	constant to control temperature response curve shape	[1]
I_{opt}	121	$W.m^{-2}$	optimum radiation value	[2]
k^{re}	0.009	d^{-1}	endogenous respiration rate	[1]
k^{rp}	0.018		photorespiration rate	[1]
ϵ_x	0.008		exudation rate	[1]
m_x^{\max}	0.001		natural mortality rate	[1]
K_x^m	0.001	$gC.d^{-1}.m^{-3}$	mortality half saturation constant	[1]
G_x	0.00008	d^{-1}	grazing rate over macroalgae	[1]
K_x^N	0.065	$mgN.L^{-1}$	nitrogen half-saturation constant for macroalgae	[1]
K_x^P	0.001	$mgP.L^{-1}$	phosphorus half-saturation constant for macroalgae	[1]
rNC	0.18	-	macroalgae nitrogen/carbon ratio	[1]
rPC	0.024	-	macroalgae phosphorus/carbon ratio	[1]
V_{crit}	1	$m.s^{-1}$	Critical velocity for detachment (m/s)	[2]
S_{opt}	35	psu	macroalgae optimum salinity for growth	[2]
S_{crit}	5		macroalgae critical salinity limit growth	[1]
S_{\max}	0		macroalgae minimum salinity for growth	[1]
S_{\min}	45		macroalgae maximum salinity for growth	[1]

As these three scenarios serve to comparatively display the behavior of macroalgae. Both modified and default parameters emulate a fictional, generalized species of macroalga.

4 – Results and Discussion

This sensibility analysis served to understand and explain how algae grew with different scenarios of nutrient and light availability.

4.1 - First Mesocosm - Sensibility Analysis on a nutrient limited environment

4.1.1 - Setup and components of the simulations

Hydrodynamics

The first set of experiments were performed on a tank with no hydrodynamics. It was represented by an unique cell in the domain, isolated, meaning that it doesn't have any exchange with other cells and that the water and particles inside the cell have no horizontal or vertical movement.

Atmosphere

By defining the geographical latitude and longitude of the location where the model is being implemented, the model computes the solar radiation corresponding to the number of daylight hours at a given time of the year for that position. In this case, solar irradiance was simulated in on 38.42°W; -8.69°N, which corresponds to a location in the coast of Portugal. The solar radiation that reaches the surface of the water is further affected by the cloud cover that the model can either calculate or take on a fixed value. For this experiment, the cloud cover was kept at 50%. Since the temperature of water needed to remain constant, heat fluxes were turned off except for radiative properties. Oxygen fluxes between water and atmosphere were also simulated.

Water Quality and Water Properties

Nutrient cycles are complex processes that take place in nature. They make up the interactions between each component of an ecosystem. MOHID Water modelling system includes a set of conservative differential equations that describe as adequately as possible those inter-component relationships. It simulates the nitrogen, phosphorus, oxygen, and silica cycles, but here, as no diatoms are being considered, the silica cycle was left out. Therefore, it computes each one of those nutrients by sink and source relationships in the water column (mineralization, nitrification, denitrification) with each other and living organisms, like phytoplankton, zooplankton. Model detail on the assumptions and structure of the

biogeochemical model can be found in the MOHID Technical Manuals (http://wiki.mohid.com/index.php?title=Mohid_Bibliography).

Macroalgae processes are described before on the Module Macroalgae.

Light Extinction

This module is coupled with the water properties and simulates the decay of solar irradiance inside the water body. The light extinction is assumed as a multiparameter function and the natural water extinction coefficient k_w was kept always as 0.08 m^{-1} (default value in the model). For phytoplankton and macroalgae in this study, their specific light extinction coefficients, (k_p and k_m in Equation 13) were arbitrarily assumed as 0.02 and $0.01 \text{ m}^{-1} \cdot (\text{mgC} \cdot \text{L}^{-1})^{-1}$, respectively. Sediments contribute to light extinction as a function of their concentration, the same manner as phytoplankton. Sediments and phytoplankton behave as suspended particles that block the passage of light.

4.1.2 – Simulations

Control – Simple nutrient tank

To be able to compare results, a control simulation was computed, where no living organisms are present, representing how nutrients would behave without the presence of primary producers and first order consumers in the system. After the control, the second simulation includes phytoplankton and zooplankton but no macroalgae. Since the control volume of the tank was small, and the timestep used to compute these processes was also small ($dt = 60 \text{ s}$), computational time was very short, which made it possible to perform several scenarios assuming one fictional year, from the 1st of January to the 31st of December. Outputs were recorded every 12 hours during simulation time.

Surface heat fluxes were null, therefore keeping the tank at its default temperature, except in the temperature experiments.

The control presented here was simulated for depths of 2 meters, because no relevant difference could be observed for simulations with different depths, since they possessed no macroalgae. Depth will affect the system when macroalgae are turned on, as explained later on. Table 3 displays the water properties and their default values on the tank.

Table 3 - Water properties and their default values on the tank.

Property	Value	Units
Temperature	15	°C
Salinity	35	psu
Dissolved Oxygen	8	mg.L ⁻¹
Nitrate	0.1	mgN.L ⁻¹
Nitrite	0.01	
Ammonia	0.001	
DONnr	0.01	
DONr	0.001	
PON	0.1	
Inorganic Phosphorus	0.05	mgP.L ⁻¹
DOPnr	0.001	
DOPr	0.001	
POP	0.1	
Phytoplankton	0	mgC.L ⁻¹
Zooplankton	0	mgC.L ⁻¹
Macroalgae	0	gC.m ⁻³
Cohesive Sediments	0	mg.L ⁻¹

On this control (Figure 9), several processes of the nitrogen, phosphorus and oxygen cycle could be observed. During the first half of January, oxygen was consumed to mineralize particulate organic matter (PON and POP) into dissolved refractory organic matter (DONr and DONnr; not shown) and ammonia. Oxygen was also spent on the nitrification of ammonia into nitrite and nitrite into nitrate.

Nitrate then decreased until it was eventually depleted, by denitrification. In reality this should not have happened. Denitrification should've only started when there was no oxygen available, in anaerobic conditions, and there is organic matter to serve as an energy source. This inconsistency was due to the simplistic way that denitrification was coded.

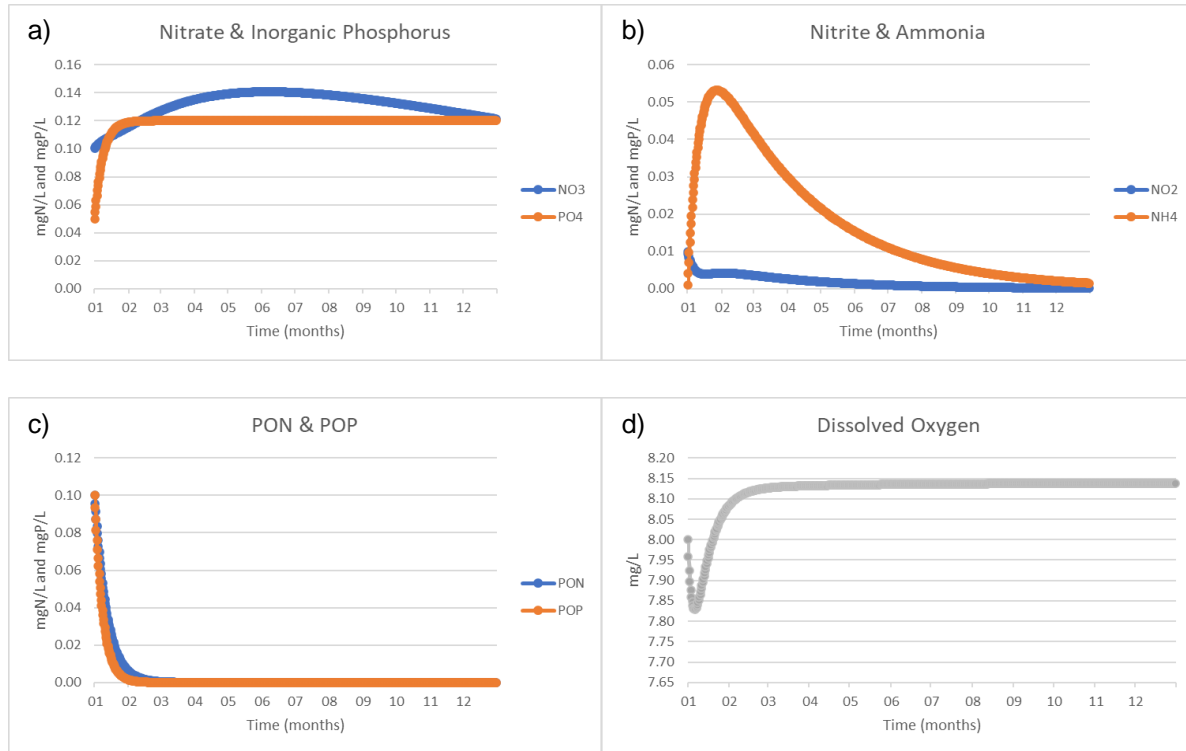


Figure 9 - a) Nitrate and inorganic phosphorus; b) Nitrite and ammonia; c) PON and POP and d) Dissolved oxygen concentrations in the system along the simulation period for the control scenario.

Finally, dissolved oxygen concentration increased due to transfers from the atmosphere, until it reached a new equilibrium.

Nutrients and phytoplankton

This next test included phytoplankton and zooplankton (Table 4) and their effect on nutrients. All other properties start with the values specified on Table 3 and temperature is constant.

Table 4 - Initial concentrations of phytoplankton and zooplankton.

Property	Value	Units
Phytoplankton	0.01	mgC.L ⁻¹
Zooplankton	0.001	mgC.L ⁻¹

With phytoplankton (Figure 10 e)), the dynamic of nutrients changed completely compared with the previous scenario (Figure 9).

Nitrate and phosphorus (Figure 10 a)) increased slowly due to regeneration like in Figure 9 a) until there was a boom in the growth of phytoplankton, and they were consumed and depleted after one month. Phytoplankton then slowly died as a consequence of lack of nutrients.

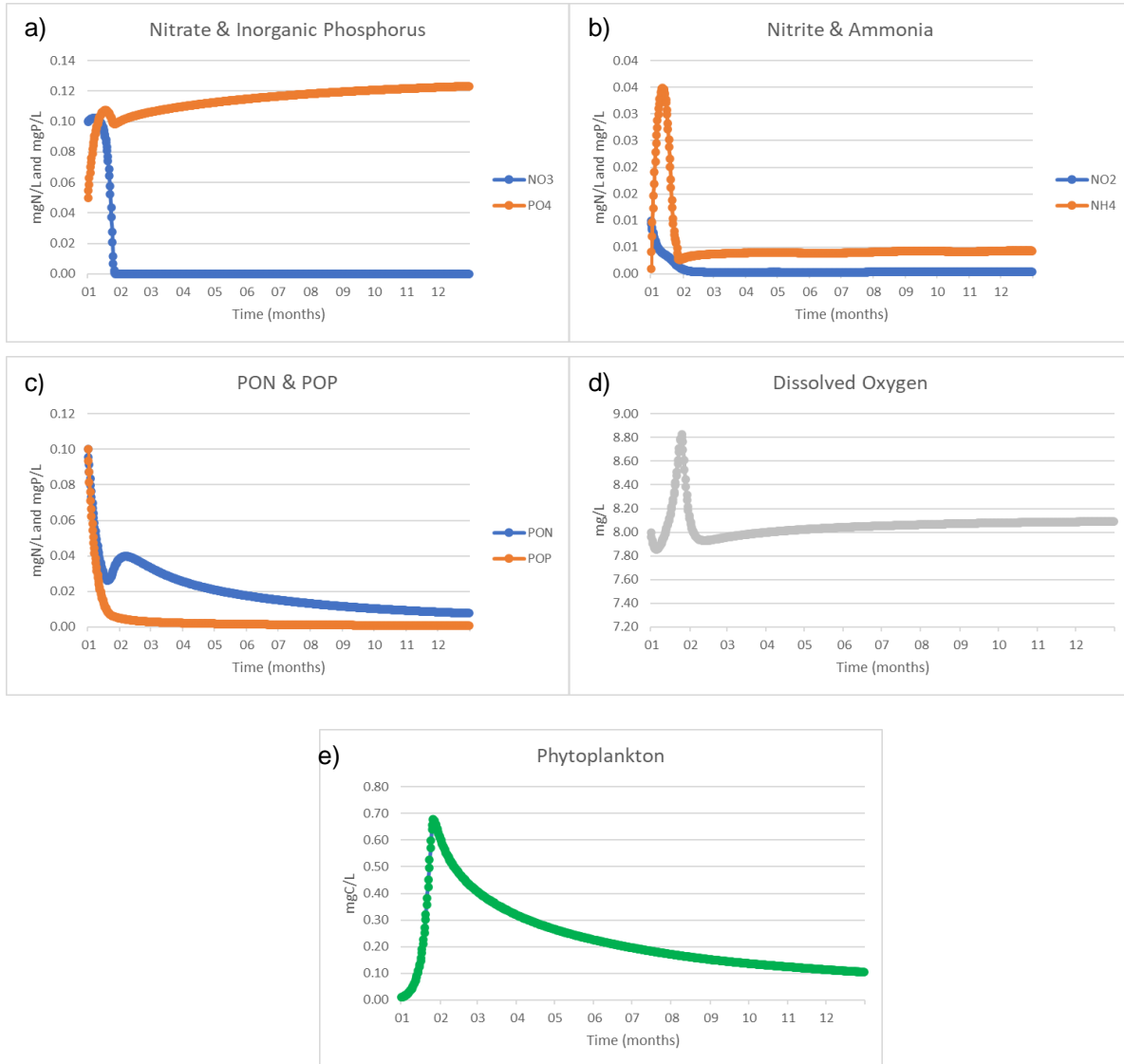


Figure 10 - a) Nitrate and inorganic phosphorus; b) Nitrite and ammonia; c) PON and POP; d) Dissolved oxygen and e) Phytoplankton concentrations in the system along the simulation period for the nutrients and phytoplankton scenario.

Dissolved oxygen (Figure 10 d)) was slightly spent on mineralization at the beginning before increasing again due to photosynthesis from phytoplankton during the growth boom, then decreased as phytoplankton dies. Concerning PON and POP (Figure 10 c)), their concentration initially declined because of mineralization and then started to increase when phytoplankton started to die and its mass became particulate organic matter (more important on PON than POP). Ammonia's sudden increase at the start was a result of the decrease in PON, then it decreased thanks to nitrification. During the phase where oxygen

and phytoplankton increased, oxygen produced by photosynthesis was higher than oxygen consumption for mineralization and oxygen consumed by respiration, resulting in an overall positive net production. When phytoplankton died, no more oxygen is produced and since water was oversaturated with oxygen, it escaped to the atmosphere.

Nutrients and macroalgae

Nutrients are necessary components for the development of living organisms. On this experiment, it was verified how macroalgae grow in response to a fixed concentration of nutrients. The conditions were exactly the same as in Control but with the presence of macroalgae in the bottom at a 2 m depth. All initial properties except for the initial macroalgae density were specified on Table 3. Despite being usually fixed at the bottom, macroalgae were computed as a concentration in the entire volume by the model. Table 5 shows the initial macroalgae concentration value.

Table 5 - Initial macroalgae concentration value.

Property	Value	Units
Macroalgae	0.01	gC.m ⁻³

Macroalgae grew over 3 months before spending all of the nitrate (Figure 11 a) and e)). Nitrate and inorganic phosphorus, analogously with the previous case of phytoplankton (Figure 10), increased by mineralization until macroalgae grew enough to consume moderate quantities of nitrate, depleting it. Nitrite, ammonia, PON and POP (Figure 11 b) and c)) exhibited the same behaviour as in the phytoplankton case. As for dissolved oxygen (Figure 11 d)), it had an initial decrease period until a third of the first month, then it increased until the beginning of the third month, decreased again in the following month and finally started to stabilize, tending to 8.1 mg/L in the following months.

Nutrients can limit the autotrophic organisms growth, as evidenced by the nitrate and phosphorus limiting factor Equations 7 and 8. When these nutrients are abundant, the ratios of the limiting factors gravitate to 1 (no inhibition of growth), meaning that the more nutrients are available, the faster is the growth. As nitrate (ammonia in reduced quantities) and phosphorus are being spent, the limiting factors decrease, slowing down the growth and eventually the limiting factor of the nutrient in lower proportion leans toward 0, stopping growth even if the other nutrient is still available (see Figure 3).

The first decrease in oxygen was due to the consumption by mineralization, by comparing the oxygen with the PON, POP, Nitrite and Ammonia figures (Figure 11 b), c) and d)). Afterwards, the fast increase in oxygen concentration was a consequence of the growth of macroalgae. As algae started to die, the oxygen production decreased and the concentration value decreases as well. Lastly, due to the atmosphere-water gas exchanges, oxygen was slowly getting replenished in the water.

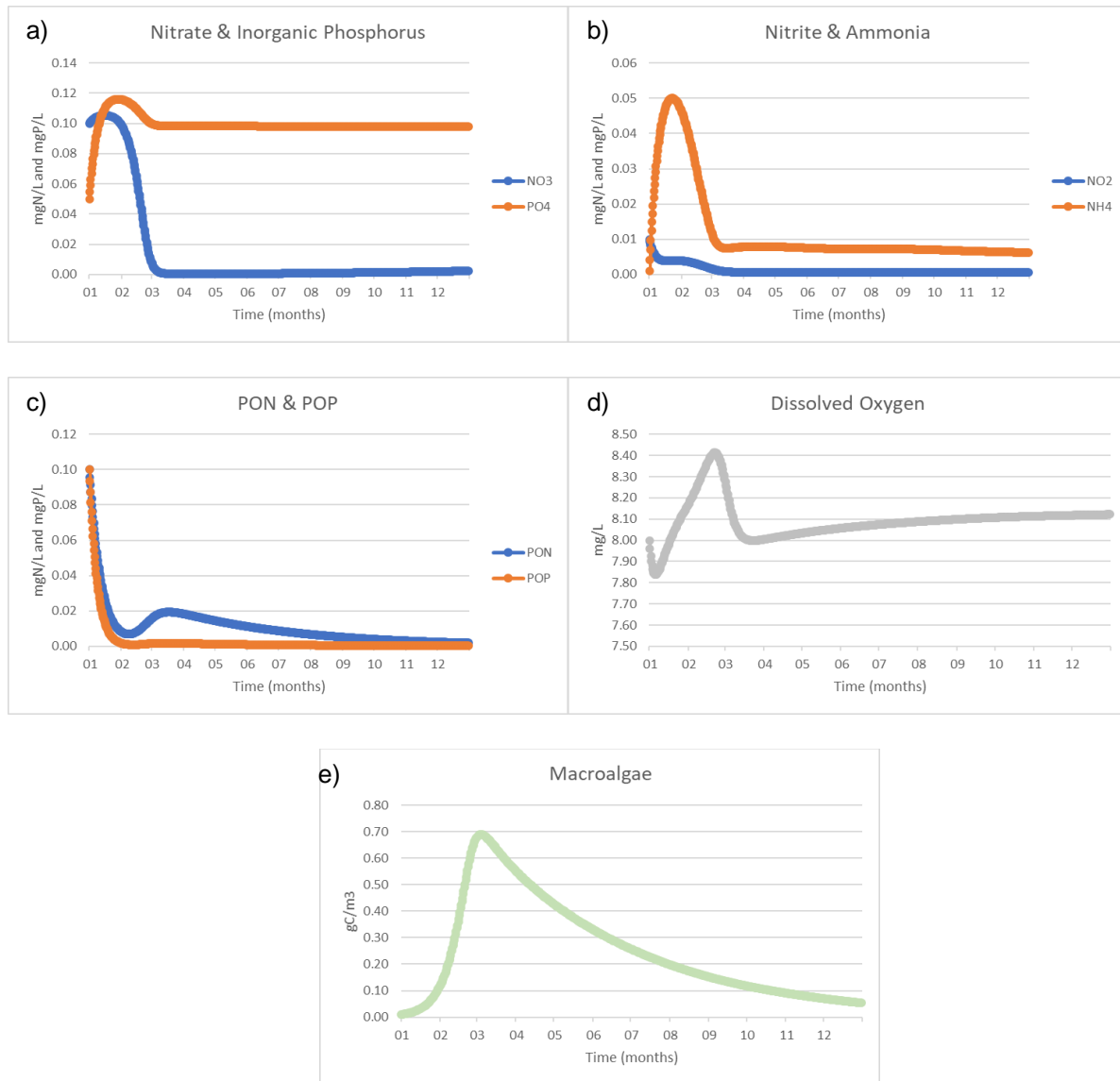


Figure 11 - a) Nitrate and inorganic phosphorus; b) Nitrite and ammonia; c) PON and POP; d) Dissolved oxygen concentrations and e) macroalgae density in the system along the simulation period for the nutrients and macroalgae scenario.

Nitrate was the limiting nutrient, the nutrient which was exhausted first. Generally, to change the limiting nutrient, either the concentration of the current limiting nutrient needs to be increased, or the amount of the other essential nutrient needs to be decreased.

Higher Nitrate

The next test shows what happens when the concentration of nitrate is increased (by a factor of five, Table 6). All other properties are the same as Table 3.

Table 6 - Initial nitrate concentration for the increased nitrate test.

Property	Value	Units
Nitrate	0.5	mgN.L ⁻¹

Like in the previous situation, macroalgae now grew and nitrate was used up in about 3 months (Figure 12), but macroalgae mass grew almost four times than before (Figure 11 e)). Although nitrate concentration was five times the default in these tests, it was still the limiting nutrient.

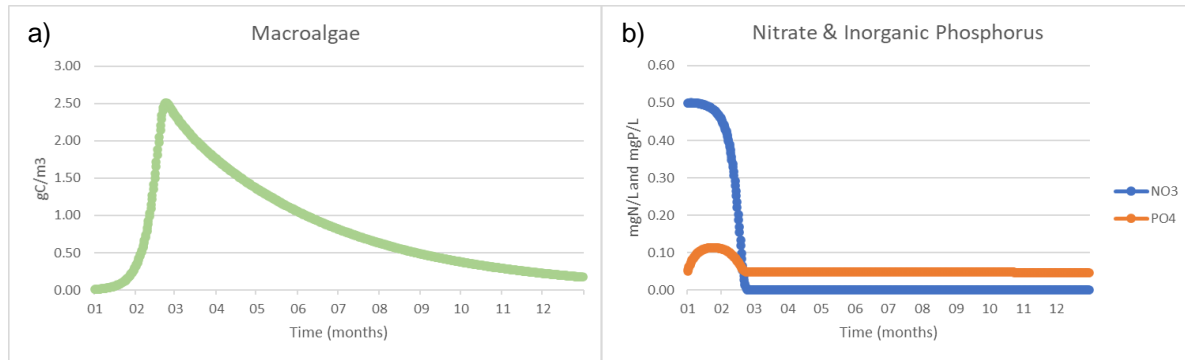


Figure 12 - a) Macroalgae density and b) nitrate and inorganic phosphorus concentrations for the increased nitrate test.

Lower Phosphorus

The concentration of phosphorus always increased in these tests at the beginning due to remineralization. In order to check phosphorus as the limiting nutrient, PON and POP concentrations were set to 0, because their concentrations were high and were responsible for the majority of the nutrient replenishment. The concentration of inorganic phosphorus was lowered to a tenth of it's default value. All properties according to Table 3 except for the ones in Table 7.

Table 7 - Initial nutrient concentrations for the lower inorganic phosphorus test.

Property	Value	Units
Nitrate	0.1	mgN.L ⁻¹
Inorganic Phosphorus	0.005	mgP.L ⁻¹
PON	0	mgN.L ⁻¹
POP	0	mgP.L ⁻¹

Phosphorus was depleted in two and a half months (Figure 13 b)). Overall growth (Figure 13 a)) was very reduced when compared to the first macroalgae case in Figure 11 e). Nitrate still increased in the beginning thanks to nitrification of ammonia.

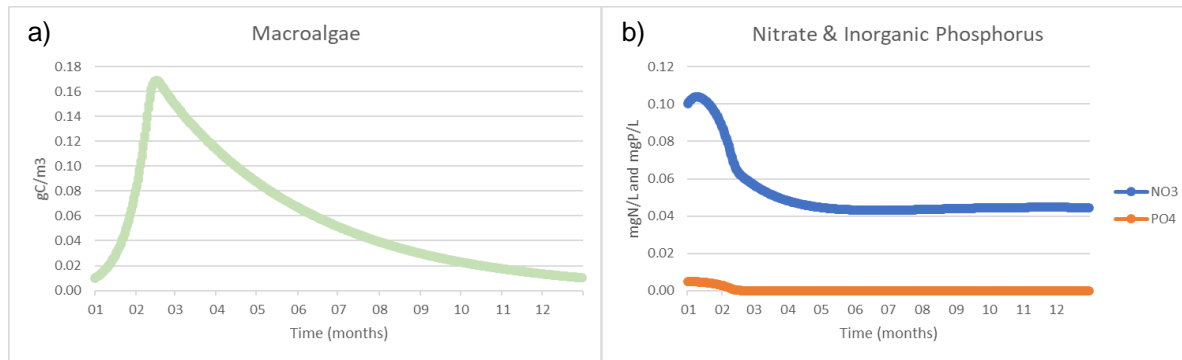


Figure 13 - a) Macroalgae density and b) nitrate and inorganic phosphorus concentrations for the lower phosphate test.

Higher Phosphorus

When phosphorus concentration was higher than nitrate, nitrate was still the limiting nutrient (Figure 14 b) below) because phosphorus generally exists in smaller quantities (Redfield ratio) than nitrate and is consequently needed less. For initial properties see Table 3 and Table 8.

Table 8 - Initial phosphorus concentration for the higher phosphorus test.

Property	Value	Units
Inorganic Phosphorus	0.1	mgN.L ⁻¹

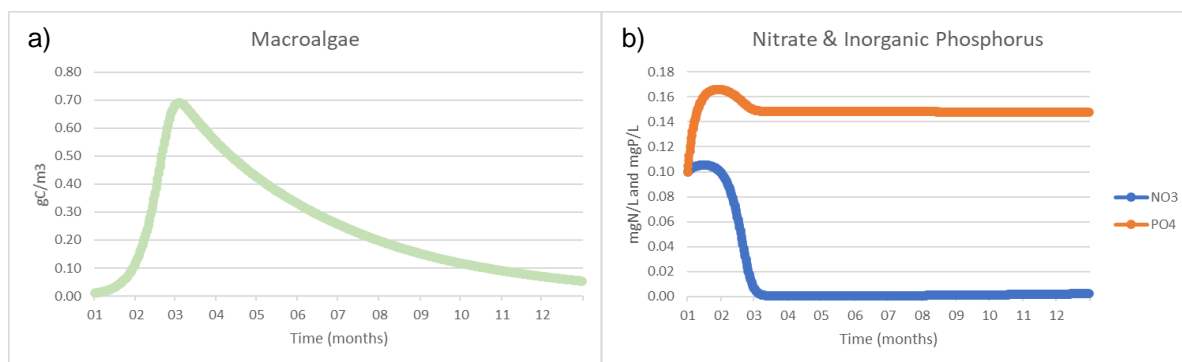


Figure 14 - a) Macroalgae density and b) nitrate and inorganic phosphorus concentrations for the higher phosphate test

In this situation, even though the initial concentration of phosphorus was high, both nitrate and phosphorus dynamics were similar to the first situation (Figure 11 e)). They got consumed until nitrate depleted in 3 months while macroalgae grew and then died off.

Influence of light and depth

Macroalgae need shortwave solar irradiance for their photosynthetic processes. This test's purpose was to differentiate how macroalgae grow when they are fixed at certain depths.

Four tanks with different depths were simulated: 2, 5, 10 and 20 meters. Initial concentrations of nutrients were the same as in Control (Table 3) an initial macroalgae concentration was specified in Table 9.

For the first set of simulations, only macroalgae and nutrients were computed, without the presence of phytoplankton and zooplankton to interfere. It is hypothesized that, under these conditions in clear water, macroalgae will grow more in less amount of time at shallower depths.

Table 9 - Macroalgae initial concentration for all depths.

Property	Value	Units
Macroalgae	0.01	gC.m ⁻³

By examining Figure 15, it's shown that macroalgae placed at 2, 5 and 10 m (overlapped) grew about the same in the same amount of time, while algae at 20 m took more time to develop and ultimately reached a lower concentration.

One thing in common for all the nutrient figures was that in the beginning, both nitrate and inorganic phosphorus concentrations increase progressively until nitrate started to quickly deplete.

By comparing the macroalgae figures with their corresponding nutrient figures (Figure 15 a) and b) with c)), the peaks of growth correspond to the instant when nitrate concentration started to decrease and since macroalgae are the only possible major sink for nutrients (as phytoplankton is non-existent in this system), macroalgae grew until they depleted one of the nutrients. In this case, nitrate was depleted first, making it the limiting nutrient. As for the initial rise in concentration of nitrate and inorganic phosphorus, it increased due to the mineralization that was also observed and described for the control (Figure 9).

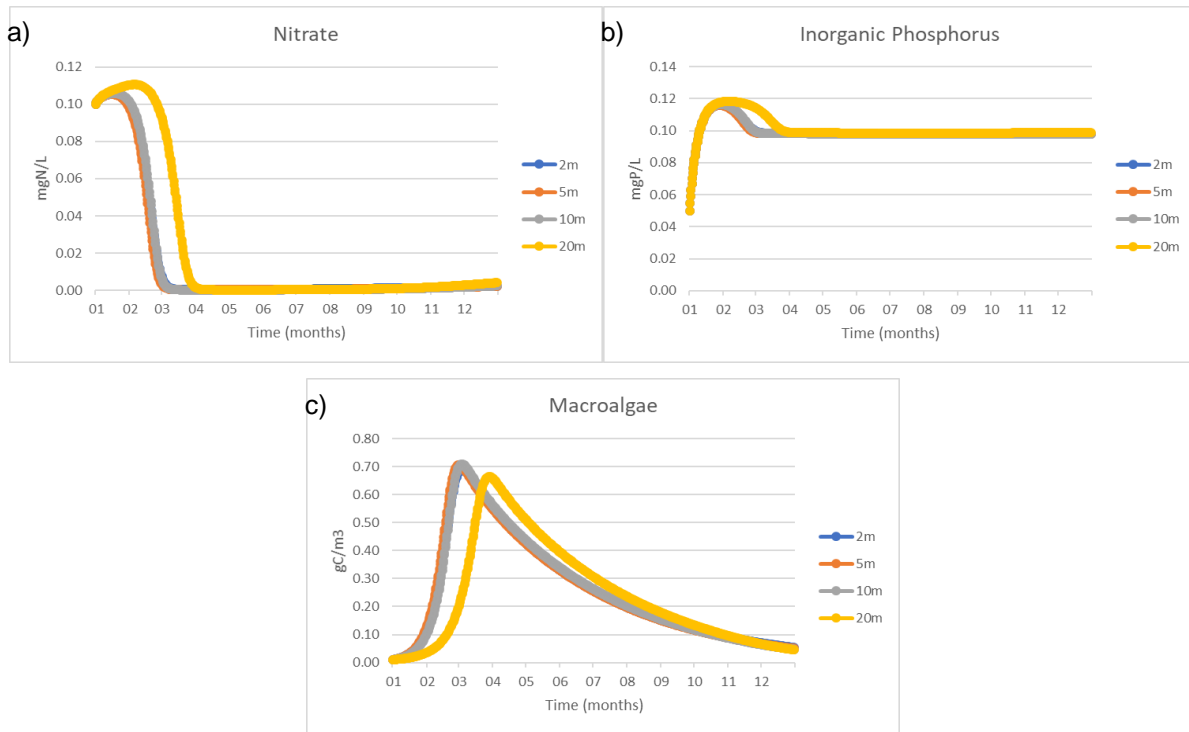


Figure 15 - a) Nitrate, b) inorganic phosphorus and c) macroalgae concentrations at 2, 5, 10 and 20 meters.

Considering the timing of the macroalgae concentration peak and the respective depths, it could be conjectured that light availability was very similar in the first three depths and that at 10 m irradiance was still higher than the optimal light. For 20m, light was already attenuated past the optimal irradiance (Figure 8 a)). Light was slowly extinguished as it traveled deeper and deeper into the tank (Equation 4, upper), constantly diminishing the irradiation available to perform photosynthesis, decreasing the light limiting factor (Equation 12) and consequently decreasing the instantaneous growth rate (Equation 6). There were no suspended sediments or phytoplankton, so the only attenuation of light was from the natural extinction of light in water is a consequence of absorption and scattering. As for macroalgae self-shading, it wasn't very evident due to their low concentrations which weighted very little on light extinction.

In conclusion, given the same initial nutrient conditions for all the scenarios, macroalgae grow until they deplete the limiting nutrient, but the effect of depth still couldn't be observed clearly because of the proximity of the results for the first three depths. The next test will introduce phytoplankton in these same scenarios to aid produce a discernible difference in the results.

Light and depth with phytoplankton

This second test to depth was set in the same conditions as the previous test, but this time with phytoplankton and zooplankton. With the existence of phytoplankton, differences of macroalgae with depth

should become more evident, as phytoplankton concentrations act as a light blocking factor. Table 10 states the initial concentrations for the organisms in this experiment. For the rest of the properties, see Table 3.

Table 10 - Macroalgae, phytoplankton and zooplankton concentrations for this experiment.

Property	Value	Units
Macroalgae	0.01	gC.m ⁻³
Phytoplankton	0.01	mgC.L ⁻¹
Zooplankton	0.001	mgC.L ⁻¹

As demonstrated by Figure 16, macroalgae grew the most when placed at 2 m, then at 5 m, 10 m and lower at 20 m (Figure 16 c)). As for phytoplankton and nutrients, phytoplankton grew about the same for all cases, except for 10 and 20 m where it grew less and took longer to grow respectively, and the nutrients got consumed almost identically in the four cases.

When comparing with the previous simulation (without phytoplankton in the system, Figure 15 c)), the magnitude of macroalgae growth was now significantly reduced. There are two possible explanations for this great disparity in macroalgae growth.

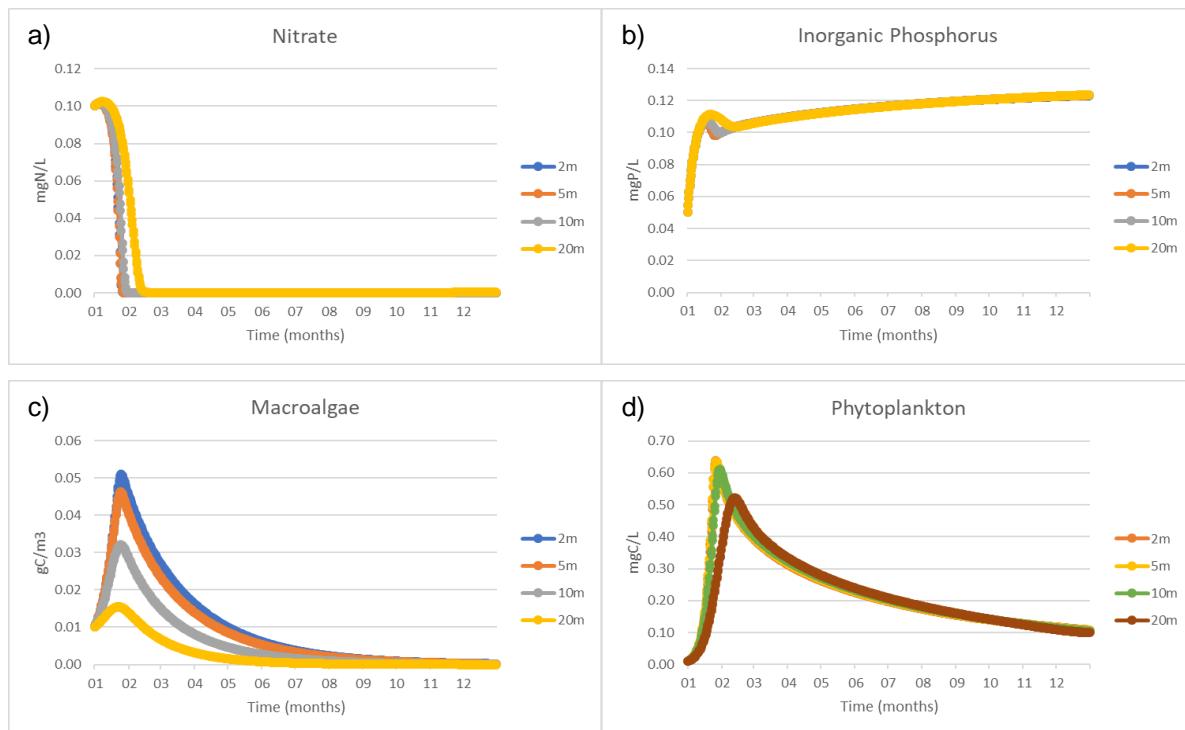


Figure 16 - a) Nitrate, b) inorganic phosphorus, c) macroalgae and d) phytoplankton concentrations at 2, 5, 10 and 20 meters in the first mesocosm experiment.

The first possible reason was because there was a new term for light extinction coefficient equation (Equation 13), the effect of phytoplankton, which inhibited the development of other organisms at the bottom of the tank by competing for light. As phytoplankton grew, it blocked the passage of light to the bottom where macroalgae were fixed. Because the growth limiting factor for light (Equation 12) depends directly on the radiation that reaches the macroalgae, the overall growth was reduced.

The second reason that when competing with macroalgae, phytoplankton absorbed nutrients much faster than macroalgae could (Figure 16 a) and b)), growing much faster until all nutrients were depleted (about only a month) than in the case where macroalgae were alone (3 months), Figure 15 a) and b).

Macroalgae growth was so limited that the amount of nutrients consumed was only a small fraction of what phytoplankton consumed. Even though phytoplankton consumed about the same amount of nutrients, it raised the question of why it didn't grow the same for all depths. The answer was that since the 10 and 20 m tanks were deeper, light was more attenuated in the water column, decreasing the light limitation factor for phytoplankton and additionally increasing the exudation rate (Equation 15). So phytoplankton grew at a slower pace due to light limitation and lost more mass through exudation in deeper tanks, explaining the differences in peaks.

This test was conducted in a poor nutrient environment and nutrients deplete fast, so it didn't really explain how much of this reduced growth is due to the nutrient competition or if it is by the extinction of light caused by phytoplankton. In the next chapter, the effects of light extinction without the effect of nutrient availability will be properly concluded.

Testing the effect of temperature

For this study, the adopted optimal interval for macroalgae growth was between 10 and 15 °C. In this section are displayed the growth graphics for different temperatures lower, within and higher than the optimal range. To evaluate growth being limited by temperature, conditions were the same as Table 3 except for temperature and phytoplankton and zooplankton were turned off. It was expected that macroalgae grow in less time within the optimal temperature range than outside.

The temperatures of the test tanks ranged from 0 to 40°C. These temperatures were divided by two figures because of the differences in scale, with one figure containing the results for 0, 5 and 40°C and the other with 8 through 25°C. Phytoplankton and zooplankton were turned off. All simulations were run with macroalgae at a 2-meter depth.

Below on Table 11 is the initial macroalgae concentration for this experiment.

Table 11 - Macroalgae initial concentration.

Property	Value	Units
Macroalgae	0.01	gC.m ⁻³

By observing Figure 17 a), it's shown that for 0, 5 and 40°C growth was null and macroalgae were dying. The decrease in concentration was more acentuated and practically instantaneous at 40°C, while for 0 and 5°C it was respectively more attenuated.

In the scenarios presented in Figure 17 b), the overall growth was higher at 10°C, then 8°C, followed by 13°C, 15°C, 20°C and finally 25°C. In terms of growth rate, macroalgae grew faster at 10, 13 and 15°C, then at 8°C, 20 and finally 25°C, where they took longer to grow. At these temperatures, growth took place in about two or three months while it took about six months for algae in the 25°C environment.

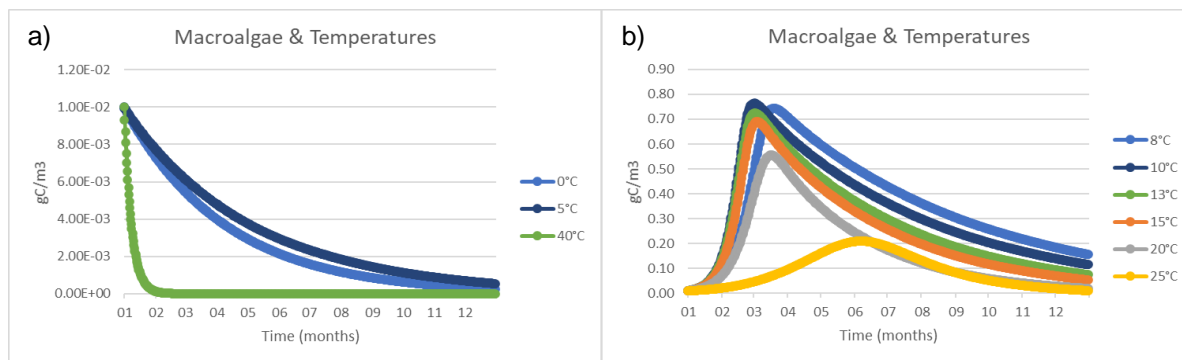


Figure 17 - Macroalgae concentration at a) 0, 5 and 40°C and b) 8, 10, 13, 15, 20 and 25°C.

Results showed that the growth was optimized (as in a great increase in concentration in the shortest amount of time possible), mainly at temperatures inside the specified optimal range, namely between 10 and 13°C.

It was also noteworthy to point that, while in a slightly broader period, macroalgae grew significantly at 8°C, as much as inside the optimal range, so it could be witnessed that growth consistently decreases when macroalgae are subject to consistently higher temperatures. But didn't necessarily decrease when temperatures get lower than the values in the optimal interval, as they should according to the temperature limiting factor equations (Equation 9). The reason for this comes from respiration (Equation 14). If temperature rises, the endogenous respiration term in the equation increases and the macroalgae lose mass that way. So in fact, in the figures on the right (Figure 17 b)), the fact that macroalgae at 13, 15, 20 and 25 didn't grow as much as at 10°C was due to loss through respiration, or the overall growth would've been the same for all cases.

At 8°C, the respiration rate was low so they grew about as much as in the optimal temperatures, but since 8°C was not an ideal temperature, it took more time to grow because the temperature limiting factor is lower

than 1, while in the optimal temperature range it tends to 1 (see Figure 5). At 5°C growth was so shortscaled that the respiration, grazing and mortality terms (Equation 5) end up prevailing. At 0°C macroalgae do not grow and only the terms mentioned before are active. At 40°C the concentration decrease was so accentuated because at that temperature, macroalgae growth was completely inhibited ($\Psi(T)_x = 0$) and the respiration term was substantially large, making what's left of algae lose mass quickly.

Summing up, temperature influences directly the rate at which macroalgae grow, as per the growth equation (Equation 6) and therefore, the amount of time they take to grow, given a fixed initial concentration of nutrients; and influences the respiration rate which in turn controls the maximum amount they can grow at that certain temperature.

But once again, in this case, macroalgae grow only until nutrients deplete so we only see the effect on temperature while nutrients are not the limiting factor. To be able to conjecture the actual effect of temperature as a limiting factor, constant inflow of nutrients are required.

Salinity

Testing the effect of salinity involved a set of simulations similar to temperature's. Macroalgae growth was computed with constant temperature and with default values of the other variables (Table 3), changing only the salinity from case to case. The salinity values tested were 0 (freshwater), 3, 5, 15, 25, 35, 40 and 45 psu. As it's been observed by other properties, macroalgae and other marine organisms grow best when a property takes a specific optimal value or range of values. Salinity is no exception. It's expected that macroalgae respond better to a certain range of salinity and that they grow less the further they stray from it.

Results were separated into two figures (Figure 18 a) and b)) because of differences in magnitude and initial macroalgae concentration was specified in Table 12.

Table 12 - Macroalgae initial concentration.

Property	Value	Units
Macroalgae	0.01	gC.m ⁻³

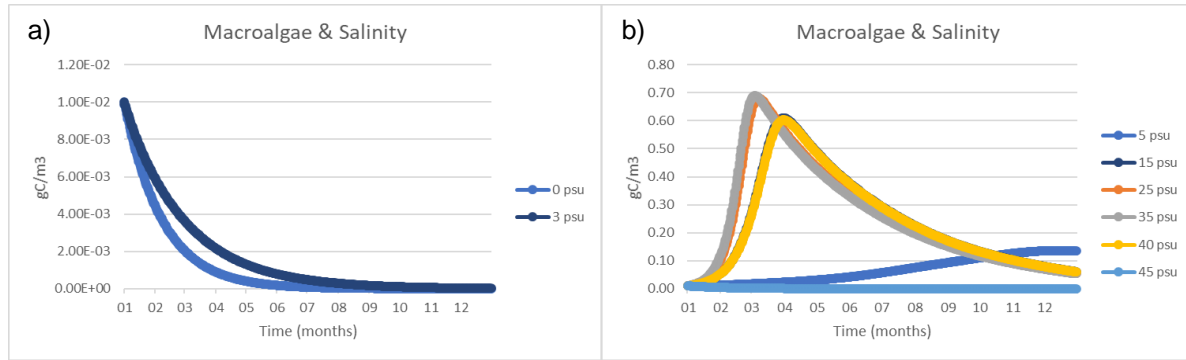


Figure 18 - Macroalgae concentration at a) 0 and 3 psu and b) 5, 15, 25, 35, 40 and 45 psu.

Figure 18 a) displays the evolution of macroalgae at 0 and 3 psu, where the algae concentration decreased in time. At 0 psu, mass decreased faster than at 3 psu. In Figure 18 b), it could be observed that macroalgae grew faster at 35 and 25 psu (overlapped), then at 15 and 40 psu (also overlapped), followed by 5 psu and finally at 45 psu, algae simply died without ever increasing.

From 0 until 5 psu, in the freshwater domain, the salinity limiting factor was very attenuated (Equation 10), meaning that macroalgae grow but not enough to overcome the loss through respiration, mortality and grazing. After 5 psu, which is the critical salinity value for this algae, the salinity limiting factor start to substantially increase with salinity until it reached the optimal salinity value and then started to decrease (see Figure 6). By these results, it could be verified that the optimal salinity value in this case, where the salinity limiting factor was maximized ($\Psi(S)_x = 1$) and growth was completely uninhibited, was at 35 psu. Below and above that salinity, the limiting factor started decreasing until algae could not tolerate the lack or the excess of salinity ($\Psi(S)_x \sim 0$), which in this test corresponds to 0 and 45 psu respectively.

4.1.3 - Final remarks

- This mesocosm model proved to behave in conformity with its defined equations presented in section 2 of chapter 2, since results for all property scenarios were as expected.
- While macroalgae are fixed to a substrate, phytoplankton is suspended in the water column and is easily transported by the current, as were nutrients. So this tank didn't represent how macroalgae would actually fare in nature, unless they were placed in a pond or closed lagoon where water movement is reduced. In reality, nutrients and phytoplankton are passengers in the ocean and estuarine ecosystems where algae grow. The next chapter will focus on simulating that type of environment.
- The scarcity of nutrients in a closed system interferes with the testing of other non-nutrient related properties because nutrients were constantly in deficit and always a limiting factor. These experiments served their purpose in highlighting the importance of nutrients but they didn't allow to conclude the effects of only one limiting property at a time.

4.2 - Second Mesocosm – The influence of nutrient availability

In practice, rivers, estuaries and the open ocean aren't still bodies of water. There are constant horizontal and vertical movements of water that transport nutrients, sediments and organisms from one place to another. As pointed on the previous chapter, macroalgae barely grew in a static environment where phytoplankton absorbs nutrients more efficiently, growing and blocking light.

In this chapter, the goal was to test the macroalgae growth under dynamic systems, where hydrodynamics play a role by changing nutrient availability and to verify which conditions of temperature, salinity and light maximize the proliferation of macroalgae. For that purpose, this mesocosm aimed to simulate the behaviour of a hypothetical saltwater river with horizontal transport of properties.

All simulations corresponded to a day to facilitate comparison between scenarios and to reduce computational time, considering that nutrients are abundant and it would be difficult to see them deplete like in the former cases.

4.2.1 – Setup and conditions of the simulations

Hydrodynamics and Discharges

Cells could now exchange properties with each other through advection-diffusion processes. Simulating the flow akin to a river required two sets of discharges. The discharge of water and nutrients was assumed at the 3 bottom cells, which is thus mixed into the system. The outflow was imposed as “negative discharges” or in reality, as abstraction points that remove the mixed water on the 3 top cells. Water was introduced and removed at the same rate, so the water level was always constant. The flowrate depends on the depth of the tank, in order to keep the hydraulic retention time of the water at about 0.17h for all simulations, which corresponded to a water velocity of $0.5 \text{ m}\cdot\text{s}^{-1}$ (see Table 13).

The tank was assumed as 15 cells, each one 100 by 100 meters (see Figure 19). Their depth and consequently, their volume depends on the depth set for macroalgae, this change in volume does not affect the macroalgae, phytoplankton nor the other properties because the macroalgae concentration proportion to nutrient and phytoplankton concentration remains the same.

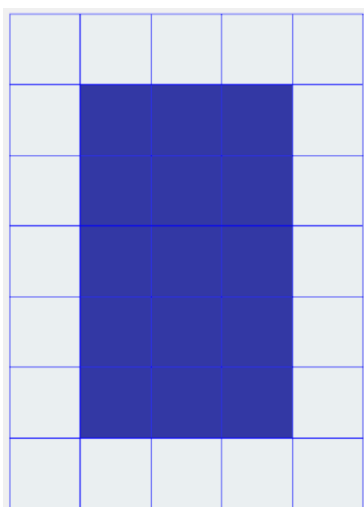


Figure 19 - Second mesocosm tank.

Table 13 - Measurements and flowrates for the tanks of the second mesocosm.

Depth (m)	Section (m ²)	Volume (m ³)	Flowrate (m ³ .s ⁻¹)
2	600	3 x 10 ⁵	300
5	1500	7.5 x 10 ⁵	750
10	3000	1.5 x 10 ⁶	1500
20	6000	3 x 10 ⁶	3000

Atmosphere and light extinction

Solar irradiance was calculated by the model for the specified latitude and longitude of the place we want to simulate. The solar irradiance of the simulations coincides with the 1st of January of a fictional year, so it matches with the initial period of the results of the past chapter. Coordinates were the same for this case, 38,42°N; -8,69°W. Cloud cover was 50% and relative humidity 70%. Light extinction parameters were exactly the same as in the first mesocosm.

4.2.2 – Simulations

Control

In similarity with the control from the closed mesocosm, this first simulation represented the performance of the model on the nutrients processes without macroalgae or plankton influence.

Below in Table 14 are listed the concentrations of properties discharged in the tank:

Table 14 – Inflow water characteristics. property concentration values inside the saltwater river mesocosm and of the discharges entering it.

Property	Value	Units
Temperature	15	°C
Salinity	35	psu
Dissolved Oxygen	8	mg.L ⁻¹
Nitrate	1.5	mgN.L ⁻¹
Nitrite	0.01	
Ammonia	0.001	
DONnr	0.01	
DONr	0.001	
PON	0.1	
Inorganic Phosphorus	0.1	mgP.L ⁻¹
DOPnr	0.001	
DOPr	0.001	
POP	0.1	
Phytoplankton	0	mgC.L ⁻¹
Zooplankton	0	mgC.L ⁻¹
Macroalgae	0	gC.m ⁻³

Examining Figure 20, all properties had a constant concentration. The river segment shaped mesocosm, a control volume, was subject to a continuous stream of water with constant temperature, salinity and concentration of nutrients flowing in by one end, mixing inside the control volume and then leaving it by the other end.

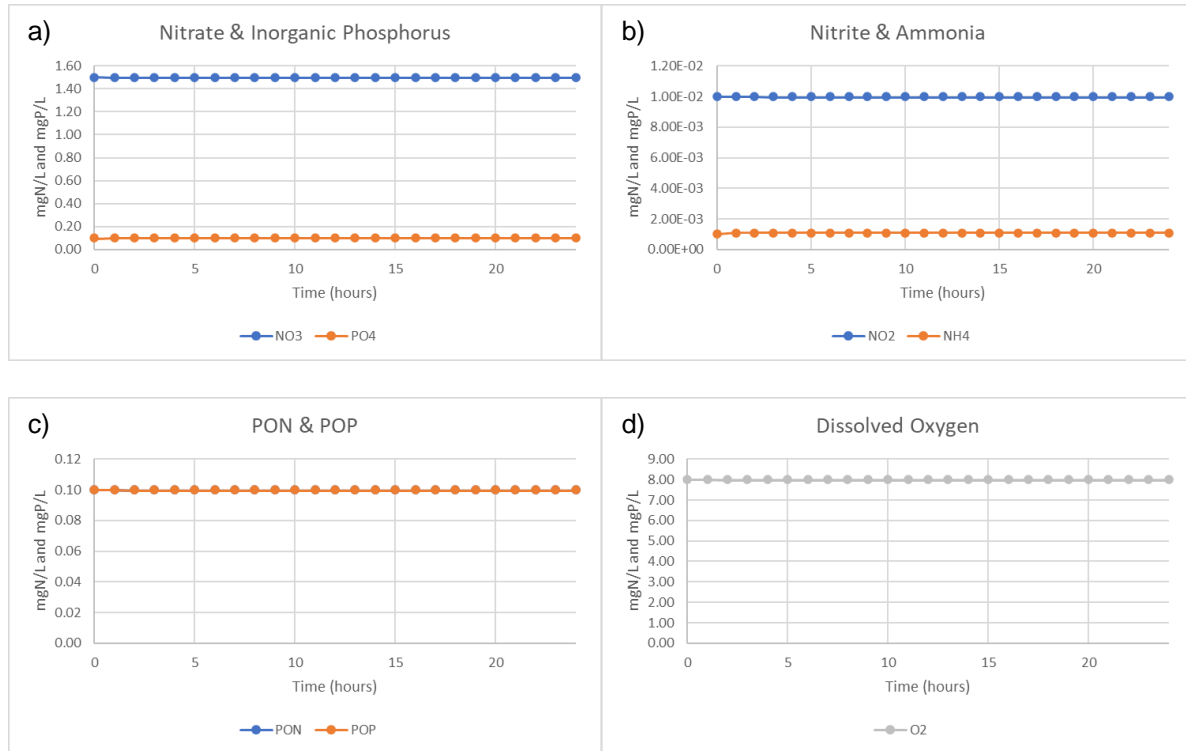


Figure 20 - Control property evolution for the river mesocosm without the presence of phytoplankton or macroalgae. a) Nitrate and inorganic phosphorus; b) Nitrite and ammonia; c) PON and POP and d) Dissolved oxygen concentrations.

Nutrients and phytoplankton

By adding phytoplankton and zooplankton in both initial conditions in the tank and in the discharge, it was anticipated that the concentration of properties in the system will not change due to the constantly discharged properties and a short residence time in the control volume. The conditions of the tank and discharges were the same as Table 14, except for phytoplankton and zooplankton initial concentrations that were specified on Table 15.

Table 15 - Phyto and zooplankton concentrations added to the control scenario.

Property	Value	Units
Phytoplankton	0.5	mgC.L ⁻¹
Zooplankton	0.01	mgC.L ⁻¹

Phytoplankton and oxygen remained practically constant, having suffered a minor increase between 9:00 to 16:00 (Figure 21 d) and e)). Nutrients were seemingly not affected, and thus, remained constant (Figure 21 a), b) and c)).

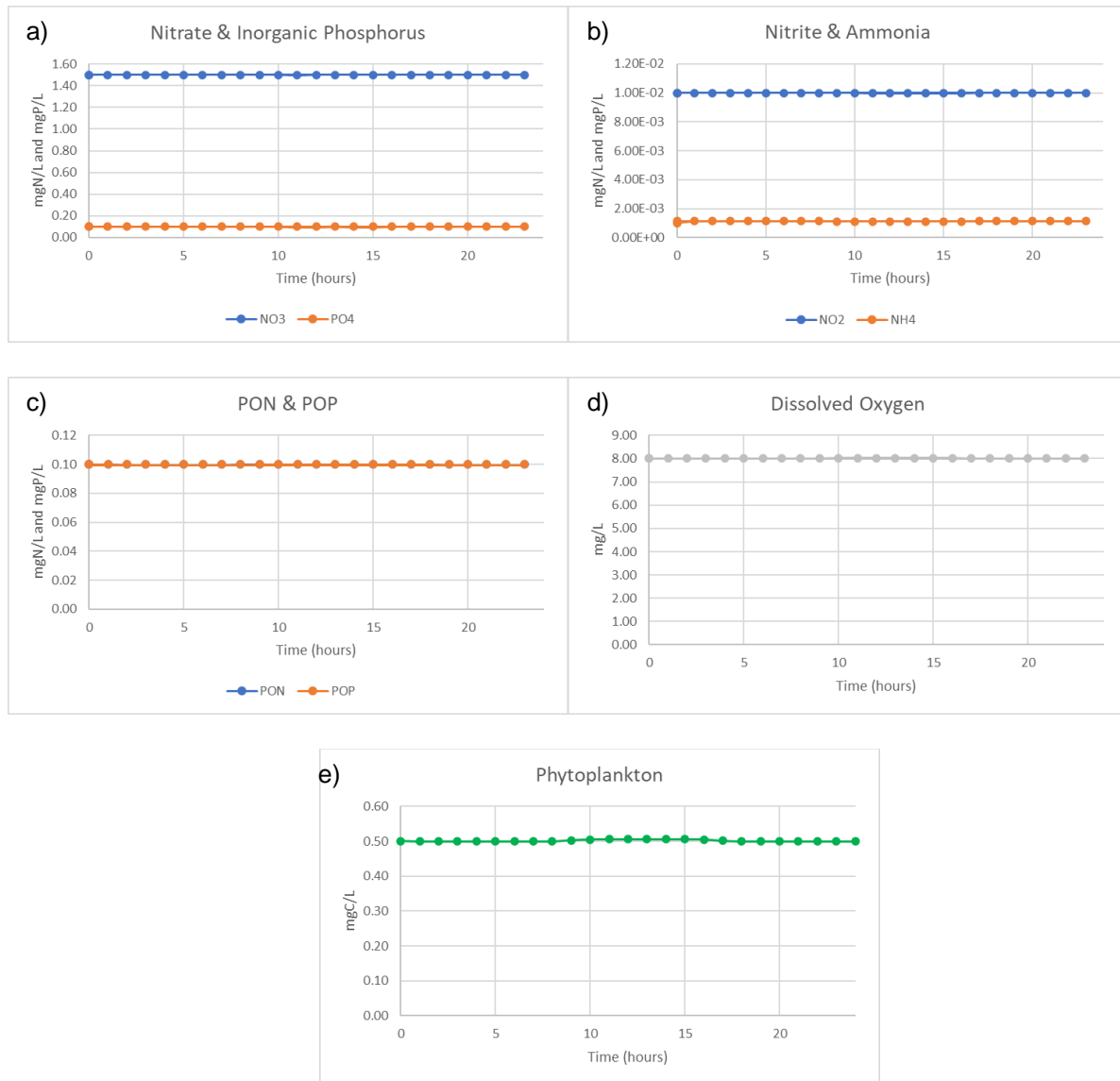


Figure 21 - a) Nitrate and inorganic phosphorus; b) Nitrite and ammonia; c) PON and POP; d) Dissolved oxygen and e) Phytoplankton concentrations in the system along the simulation period for the nutrients and phytoplankton scenario in the second mesocosm.

The slight increase on phytoplankton during that time was due to its growth during daylight hours that can also be noticed in the small increase in dissolved oxygen originated from the photosynthesis of phytoplankton). After the daylight period, phytoplankton and dissolved oxygen reset to their discharged values.

Nutrients and macroalgae

In the scenario with macroalgae, the results for the nutrient dynamics are expected to be the same as in the scenario with only phytoplankton. Because macroalgae are fixed at the bottom and not transported by the water current, macroalgae will be able to grow inside the system, and although they consume more nutrients, the nutrients concentration will be restored by the constant discharge input. Conditions were as stated by Table 14 and in Table 16 it's indicated the initial macroalgae concentration in the tank for this experiment.

Table 16 - Macroalgae initial concentration added to the control scenario.

Property	Value	Units
Macroalgae	0.01	gC.m ⁻³

As it can be seen in Figure 22 e), macroalgae concentration slowly declined from the beginning to 8h, then increased from 8 to 17h and afterwards it decreased again. This was due to the day and night variation combined with the sink terms of the algae. At night, solar irradiance was null, consequently, the light limitation factor (Equation 12) was also null ($\Psi(E)_x = 0$) and therefore, there was no growth. The slow decrease was the combination of respiration, natural mortality, and grazing, as stated by the macroalgae main equation (Equation 5) since the only positive term, growth (μ), was zero.

During the day, with solar irradiance available, macroalgae uptake nutrients and grow with almost no inhibition by the nutrients. By extracting the concentrations of nitrate, ammonia, and phosphorus from Figure 22, one can easily calculate both nutrient factors. In this set of experiments $\Psi(N)_x = 0.996$ and $\Psi(P)_x = 0.999$, which are very close to one.

On the nutrient perspective Figure 22 a), b) and c), since the scale of macroalgae growth in one day was so reduced and there was a constant replenishment of every nutrient, the concentrations of nitrogen and phosphorus stayed the same. The residence time inside the volume was so reduced that there was no time for mineralization reactions to occur.

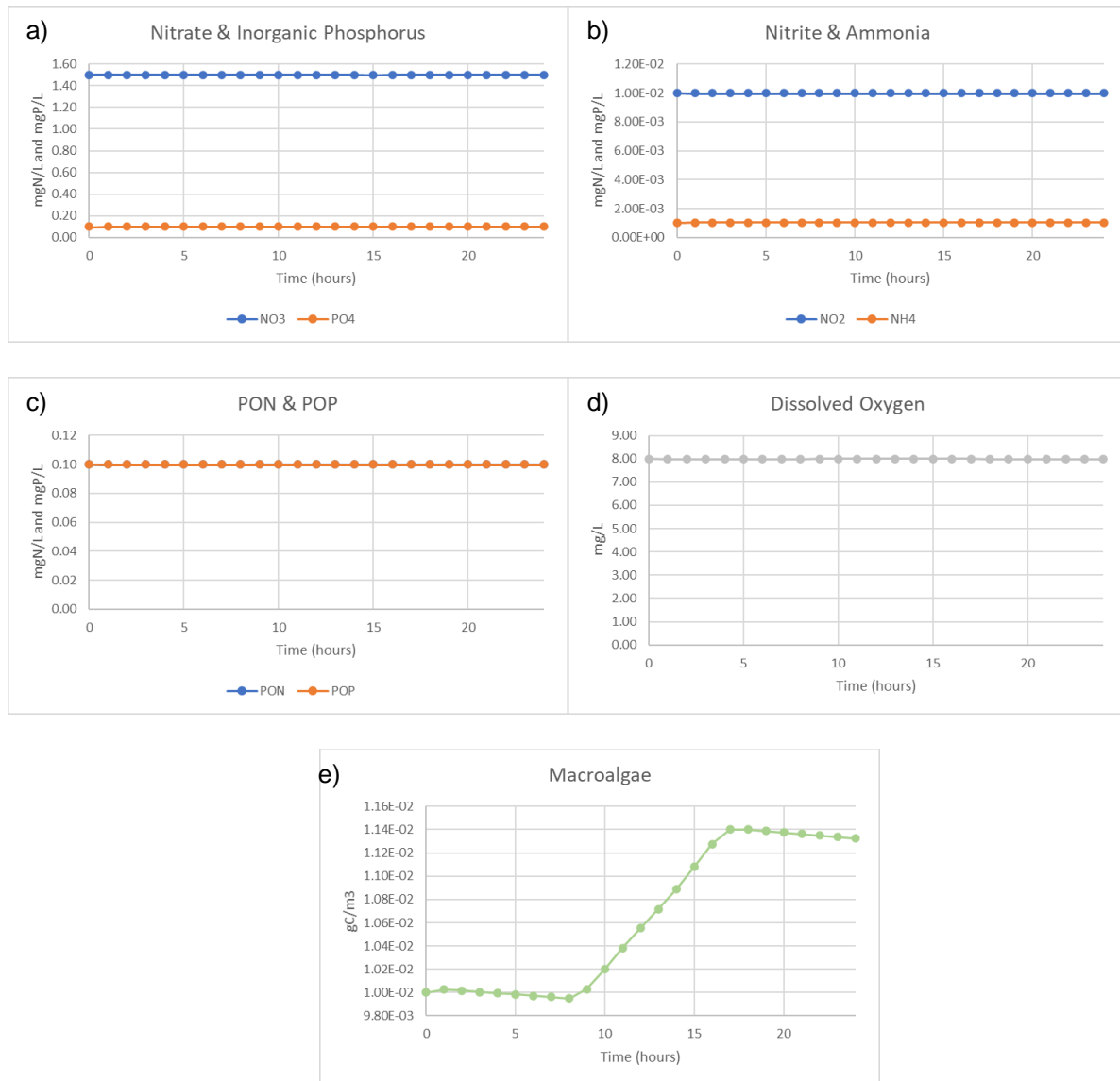


Figure 22 - a) Nitrate and inorganic phosphorus; b) Nitrite and ammonia; c) PON and POP; d) Dissolved oxygen and e) macroalgae concentrations in the system along the simulation period for the nutrients and macroalgae scenario in the second mesocosm.

Influence of light and depth

In similar fashion with the tests of the former mesocosm, this light test placed macroalgae at several depths where light reaches differently, without the presence of other organisms (*plankton*). This time, with no shortage of nutrients, the difference in growth should be more evident. Conditions were as stated by Table 14 and in Table 17 it's indicated the initial macroalgae concentration in the tank for this experiment.

Table 17 - Macroalgae initial concentration in the light and depth test of the second mesocosm experiment.

Property	Value	Units
Macroalgae	0.01	gC.m ⁻³

As expected, the greatest growth rate was found at a 2 m depth followed immediately by 5 m, then 10 m and finally 20 m (Figure 23). Once again, taking only into account the specific light extinction of water ($k_w = 0.08 \text{ m}^{-1}$) and the shortwave irradiance extinction equation (Equation 4, upper), the greater the depth, the greater the distance light must travel through the water, the greater the light extinction and the less irradiance reaches the level where macroalgae are and lower is their growth.

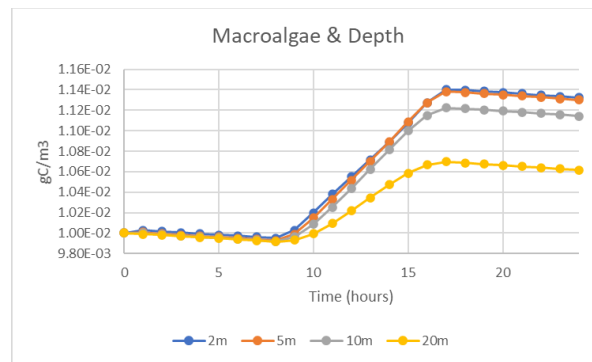


Figure 23 - Macroalgae concentration evolution at depth 2, 5 10 and 20m in the second mesocosm experiment.

Influence of light, depth and phytoplankton

As the residence time of the water inside the system is very small, phytoplankton growth is not significant and it's expected that the main effect on macroalgae is on blocking light. Table 18 states the initial concentration of all three organisms in the system and simultaneously the concentration of phytoplankton and zooplankton in the discharges. All other properties are according to Table 14.

Table 18 - Macroalgae, phytoplankton and zooplankton initial concentrations in the light and depth test of the second mesocosm experiment.

Property	Value	Units
Macroalgae	0.01	gC.m ⁻³
Phytoplankton	0.5	mg.L ⁻¹
Zooplankton	0.01	mg.L ⁻¹

Results showed that macroalgae growth rate was still highest at 2 m, then 5 m, 10 m and finally 20 m, but the difference between them from the previous test (Figure 23) has increased.

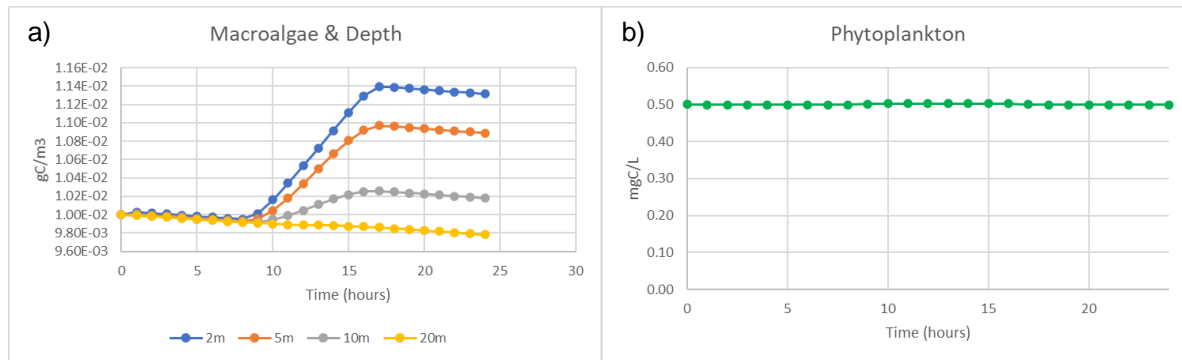


Figure 24 – Macroalgae and phytoplankton concentration evolution at depths 2, 5 10 and 20m in the second mesocosm experiment.

Since phytoplankton doesn't remain enough time in the system to assimilate any significant amount of nutrients, they don't compete with macroalgae for nutrients. The only resource they both competed for was light. Phytoplankton adds to the light extinction inside the water column (Equation 13), decreasing the light that reaches the macroalgae at greater depths and therefore creating this difference in growth rates between Figure 23 and Figure 24.

Testing the effect of temperature

With nutrients not being a limiting factor, it was possible to verify the effects of temperature as a limiting factor. Phytoplankton was kept turned off. Conditions are as in Table 14 and macroalgae initial concentration is specified in Table 19.

Table 19 - Macroalgae initial concentration in the temperature experiment of the second mesocosm.

Property	Value	Units
Macroalgae	0.01	gC.m ⁻³

For Figure 25 a), faster growth was verified at 10 and 13°C, then at 8°C, almost no growth at 5 and no growth at 0°C. As for Figure 25 b), the most significant growth was 15°C, then followed closely by 20°C and finally 25°C. No growth was verified at 40°C. Contrarily with the analogous test in the closed mesocosm, here the effect of respiration was attenuated. The overflow of nutrients kept the nutrient limitation factors high, near the maximum consequently keeping the growth rate also high compared to the respiration rate.

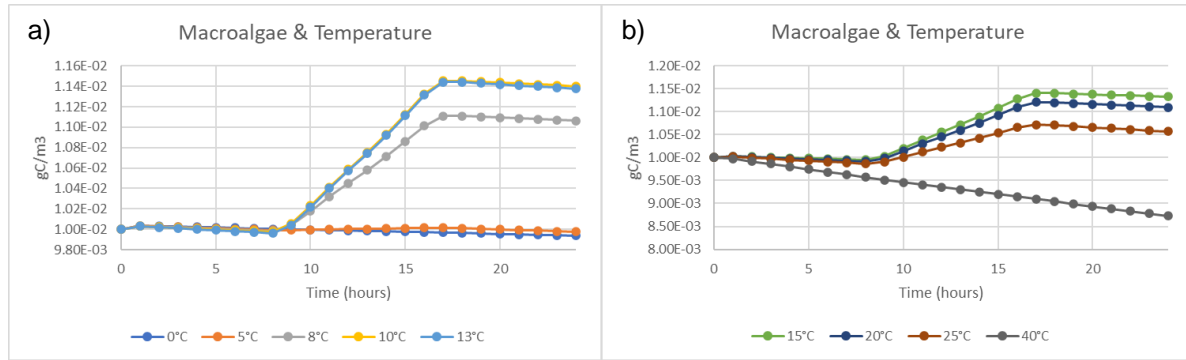


Figure 25 - Macroalgae evolution at temperatures a) 0, 5, 8, 10 and 13°C and temperatures b) 15, 20, 25 and 40°C in the second mesocosm experiments.

At last, as dictated by the temperature limiting factor, growth was in fact optimized for the temperatures inside the optimal range, in this case, 10, 13 and 15°C, growing lesser and lesser as temperature strays higher or lower than that ideal scope, until reaching temperatures where they don't grow anymore (0 and 40°C).

Salinity

Lastly, for this salinity test without nutrient limitation, it's expected that results will be like the analogous test in the first mesocosm. Conditions were as in Table 14 and macroalgae initial concentration was specified in Table 20.

Table 20 - Macroalgae initial concentration in the salinity experiment of the second mesocosm.

Property	Value	Units
Macroalgae	0.01	gC.m ⁻³

This time, with salinity being the only limiting factor, growth was once again higher at 35 psu, then followed by 25 psu, 15 and 40 (overlapped), 5, 3, 0 psu and finally null 45 psu (Figure 26).

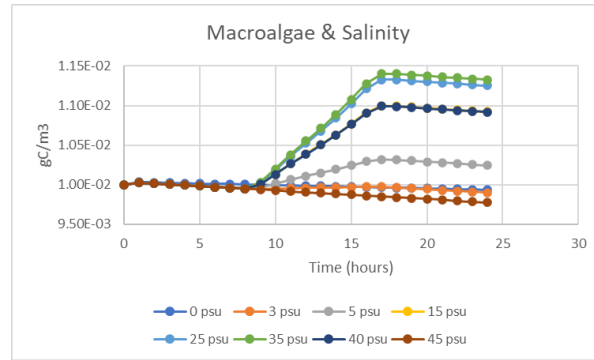


Figure 26 - Macroalgae evolution in salinities 0, 3, 5, 15, 25, 35, 40 and 45 psu in the salinity experiment of the second mesocosm.

Therefore, it was evidenced that these hypothetical macroalgae grow ideally at 35 psu where the salinity limiting factor was maximized. For the surrounding values of salinity, macroalgae still grew well at 25 psu, relative to the maximized growth at 35 psu. For salinities lower and higher than 35, growth got consistently inhibited until it reached values where algae could not grow anymore or where their own maintenance overwhelms the growth, like in salinities below 5 psu or 40 psu and higher.

4.2.3 - Final remarks

Eliminating nutrients as the limiting factor, the effect of the other properties on growth could be clearly evidenced. Macroalgae proved to grow better inside the ideal range of temperatures, at ideal salinity and shallow depths where light is available without much interference from their main competitor, phytoplankton, thus proving the model is working accordingly in response to the input parameters.

4.3 - Third Mesocosm – Schematic Estuary

These last sets of tests emulate a mesocosm of an estuary, where two rivers discharge and eventually join, with the objective of testing macroalgae resilience against physical stresses, as well as the gradients of nutrients, salinity, and light. The simulation period was one year and the timestep used to perform all computations was 60 seconds. For this objective, flowrate was initially low and constant to allow for macroalgae to develop and then, from the seventh month onwards, flowrate was increased by a factor of four to increase the water velocity and verify the possible occurrence of macroalgae detachment or dislodgement.

Regarding nutrients, only nitrate will be presented as a representation of both nitrogen and inorganic phosphorus and their derived nutrients (although they were also computed), since they possess the same behavior in advection-diffusion phenomena, to keep the figure displays simple.

4.3.1 - Estuary characteristics

Figure 27 displays schematic estuary and its variable bathymetry.

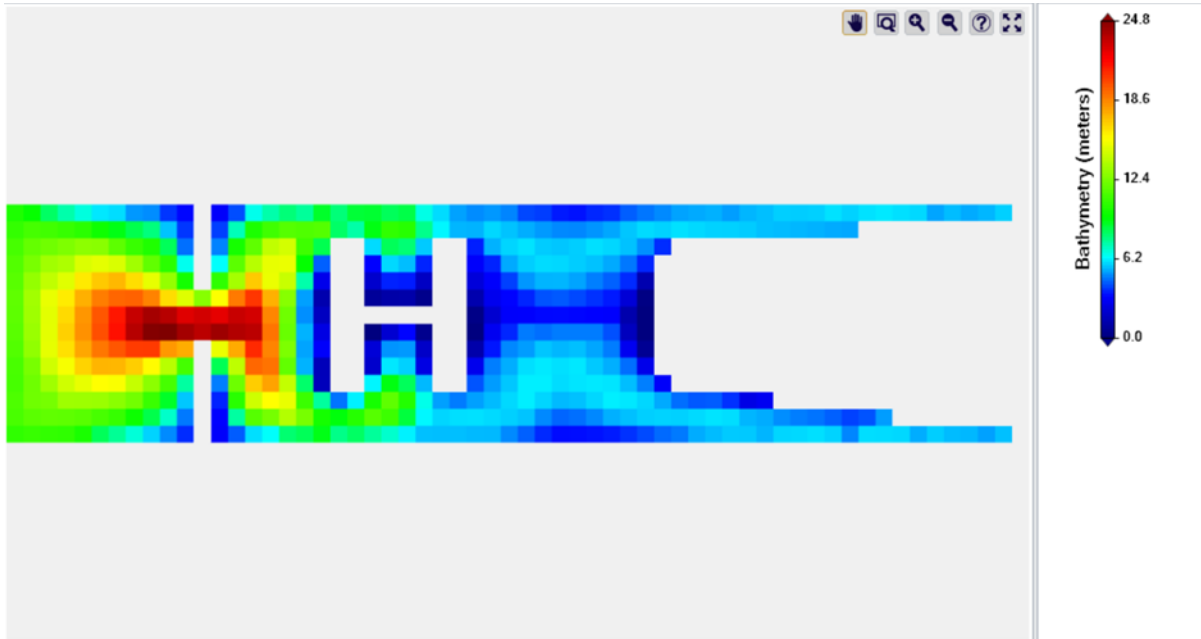


Figure 27 - Bathymetry of the schematic estuary.

The estuary was composed by two rivers located at right-side of Figure 27. Then, water encounters and encompasses an “H” shaped bank, followed by passing through a gap with a small width but great in depth and finally discharging into the open ocean. The left side frontier with the ocean has imposed concentrations of nutrients, temperature and salinity, mimicking an actual frontier with the ocean. Estuarine hydrodynamics has two major driving forces in this simulated environment, flow and water velocity from the two rivers flow and a simulated simple M2 tide. Table 21 and

Table 22 display, respectively, the variation of flowrated in time and the initial properties of the river and discharges.

Table 21 - River discharge flows along the simulation.

Month	Northern flow ($\text{m}^3 \cdot \text{s}^{-1}$)	Southern flow ($\text{m}^3 \cdot \text{s}^{-1}$)	Total flow ($\text{m}^3 \cdot \text{s}^{-1}$)
1 to 6	100	100	200
7 to 12	4000	4000	8000

Table 22 - Estuary initial property values and river discharge characteristics.

Property	Estuary initial value	River discharges value	Units
Temperature	15		°C
Salinity	35	3	psu
Dissolved Oxygen	8		mg.L ⁻¹
Nitrate	0.5		mgN.L ⁻¹
Nitrite	0.001		
Ammonia	0.001		
DONnr	0.001		
DONr	0.001		
PON	0.001		
Inorganic Phosphorus	0.1		mgP.L ⁻¹
DOPnr	0.001		
DOPr	0.001		
POP	0.001		
Phytoplankton	0.001		mgC.L ⁻¹
Zooplankton	0.0001		mgC.L ⁻¹
Macroalgae	0.01	-	gC.m ⁻²

4.3.2 – Simulation

Beginning of the Simulation

At the first instant of the simulation, macroalgae were evenly distributed in the bottom with a total concentration of 0.01 gC.m⁻³ in the system, water velocities were very small and nitrate concentration, phytoplankton concentration and salinity were uniform throughout the estuary (Figure 28).

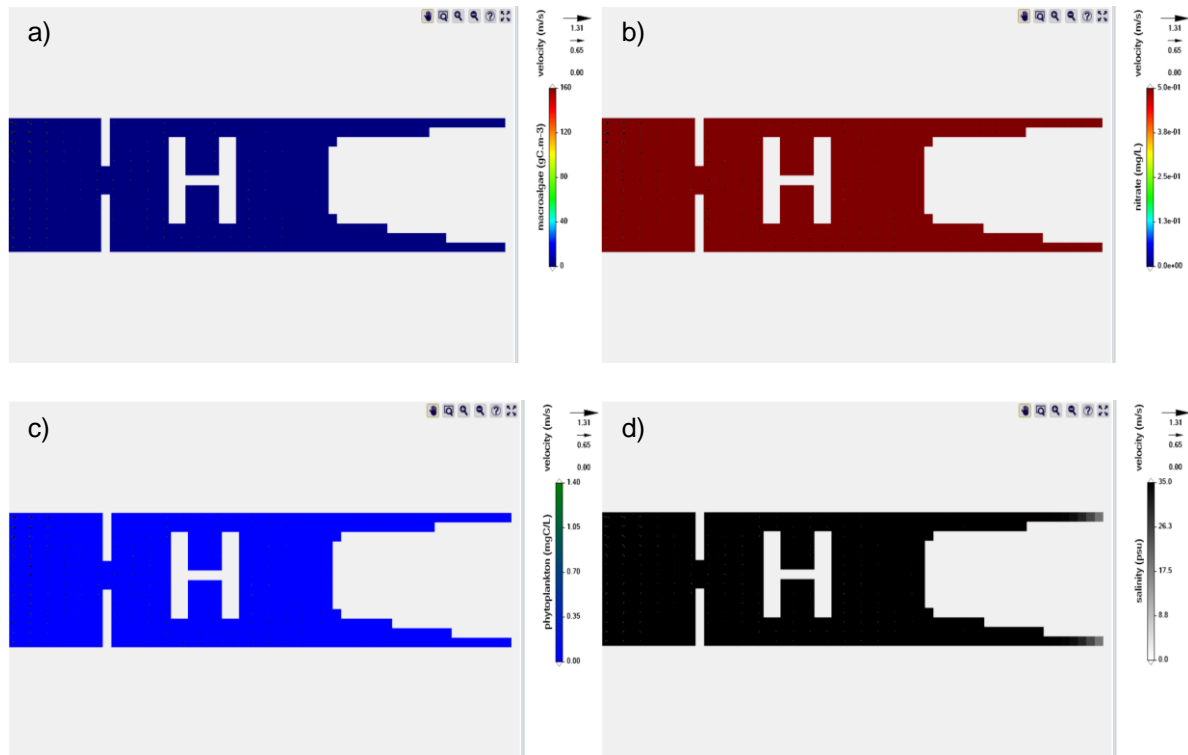


Figure 28 - a) Macroalgae, b) Nitrate, c) Phytoplankton and d) salinity concentration distribution maps at the beginning of the schematic estuary simulation (01/01 – 06h00).

Instant before flowrate increase

Over the following 7 months, with a constant inflow of water, macroalgae ended up developing more on the frontier with the open ocean, a little at the end of the two confluent rivers and faintly to the left of the “H” shaped bank (Figure 29 a)). There were three reasons for this localized growth.

The left imposed boundary condition and the backward-forward motion caused by the tides kept nutrients on the left side relatively high and available for algae use (Figure 29 b)). The same happened with the salinity conditions, as salinity decreased from the left to the right of the picture (Figure 29 d)).

The two rivers brought fresh water (very low salinity, 3 psu) into the estuary, so algae only started to develop on brackish waters, places where saltwater mixes with the two rivers’ freshwater, which coincided with the end of the rivers or the start of the open middle estuary area.

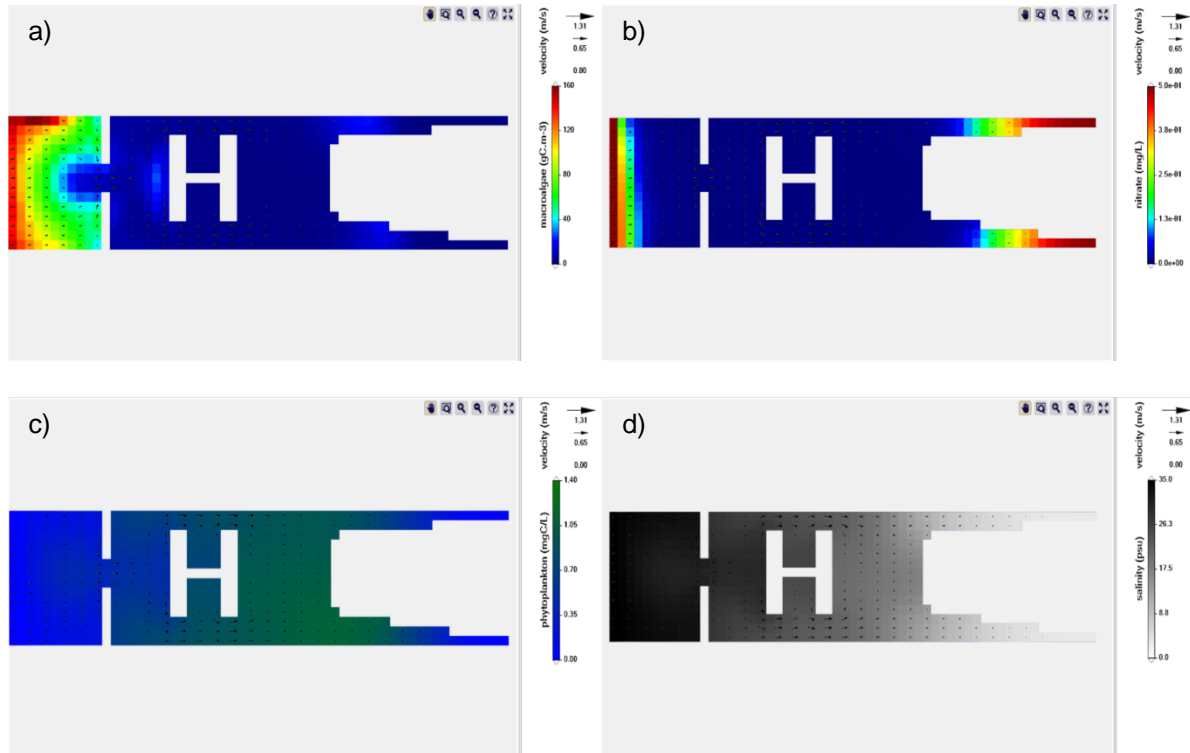


Figure 29 - a) Macroalgae, b) Nitrate, c) phytoplankton and d) salinity concentration distribution maps at the instant before flowrate increases in the schematic estuary simulation (30/06 – 18h00).

Here macroalgae grew less than in the other locations due to nutrient consumption by phytoplankton (Figure 29 d)). As observed by the nutrient and phytoplankton figures ((Figure 29 b) and d)), phytoplankton depleted nutrients in that middle area. Right to the left of the “H” shaped bank, nutrient concentrations were low, but water was shallow compared to the surroundings (Figure 27), which enables algae to perform photosynthesis, uptake the small concentration of nutrients and grow slightly.

Instants right after the flowrates increase

Right after the overwhelming increase in river flow, it could be seen the immediate reduction of macroalgae mass at the end of the north river as a consequence of the high velocity imposed by a high water volume flowing through a narrow section (Figure 30).

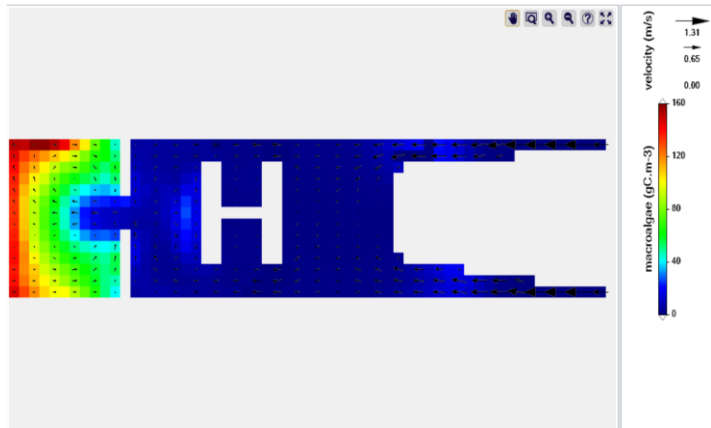


Figure 30 - Macroalgae concentration distribution map 6 hours after the flow increased.

With this new high flow rate, phytoplankton grown before was quickly transported out of the estuary by advection (Figure 31).

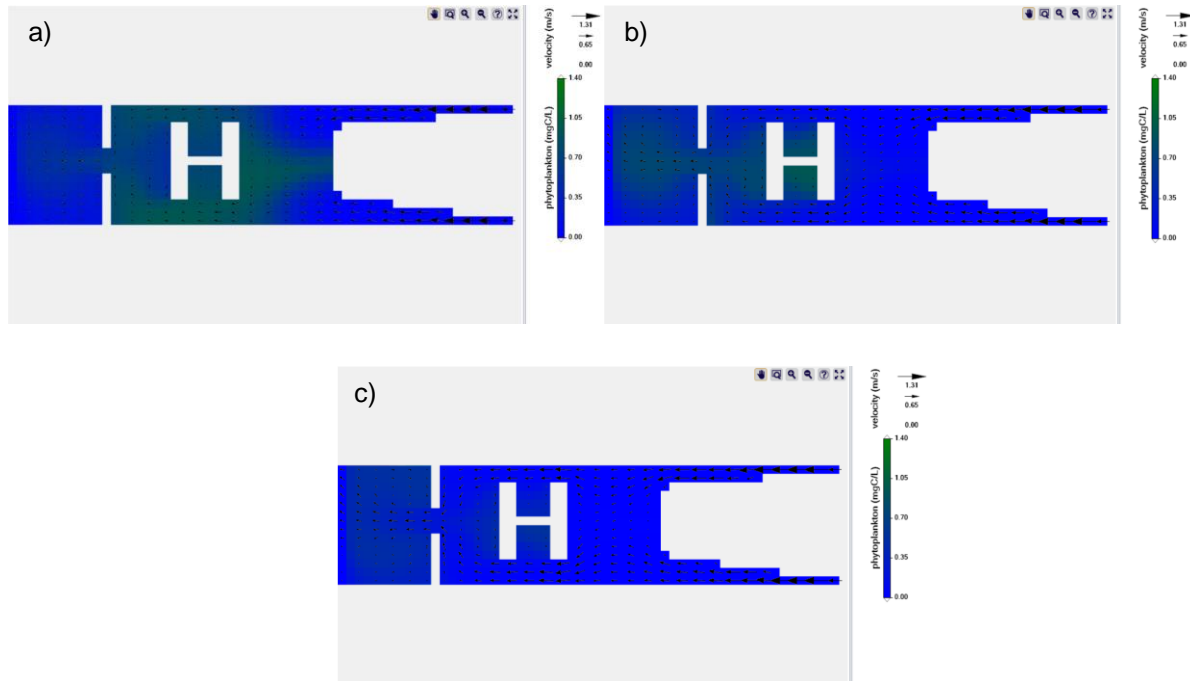


Figure 31 - Instantaneous phytoplankton evolution a) 6 hours, b) 18 hours and c) 30 hours after the flow increase (ebb tides only).

Nutrients from freshwater quickly flooded the estuary, which in overall, increased the nutrients (Figure 32) and decreased salinity (Figure 33) in the whole control volume, as displayed in the figure sequence below.

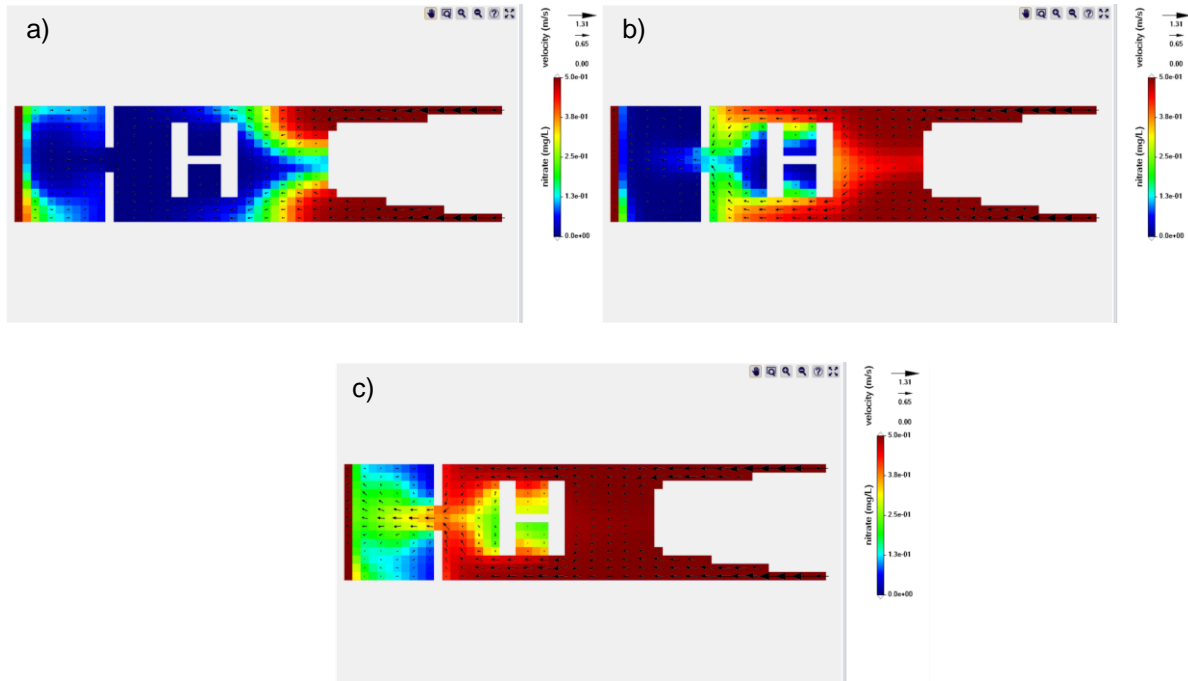


Figure 32 – Instantaneous nitrate evolution a) 6 hours, b) 18 hours and c) 30 hours after the flow increase (ebb tides only).

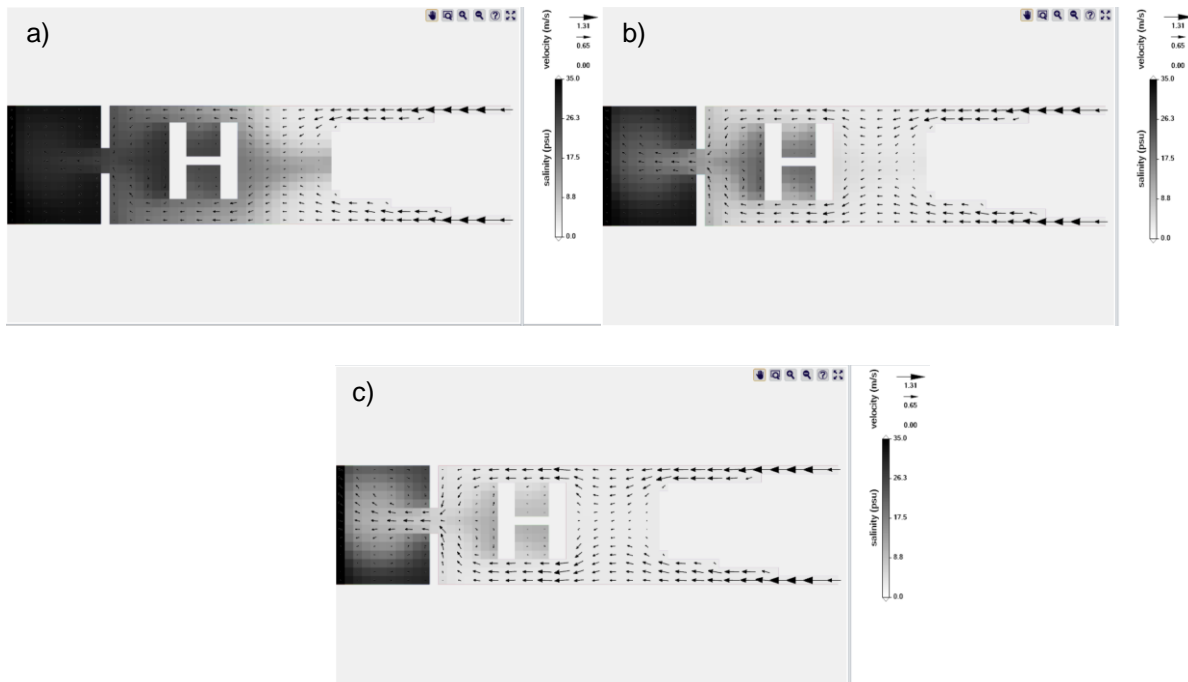


Figure 33 - Instantaneous salinity evolution a) 6 hours, b) 18 hours and c) 30 hours after the flow increase (ebb tides only).

Subsequent macroalgae die-off

Afterwards, it could be observed that the concentration of macroalgae that grew on the confluent ends of the rivers started to slowly die-off (Figure 34 a)). Even though nutrient concentrations were plenty (Figure 34– b)), these locations now consisted solely of fresh water (Figure 34 c)), where salinity levels were below the critical salinity threshold, limiting growth.

Nutrient concentration was uniform in most of the estuary, except in the ocean segment on the left side (Figure 34 b)). Since the flowrate brought along a constant concentration of nutrients, it was expected that the concentration remained uniform, but it wasn't, because there's nutrient consumption by macroalgae in that area.

Phytoplankton that grew before, got carried away when the flowrate increased. Since the flowrate was very high, water and phytoplankton's residence time was low, so it didn't have time to grow, despite having nutrients and light.

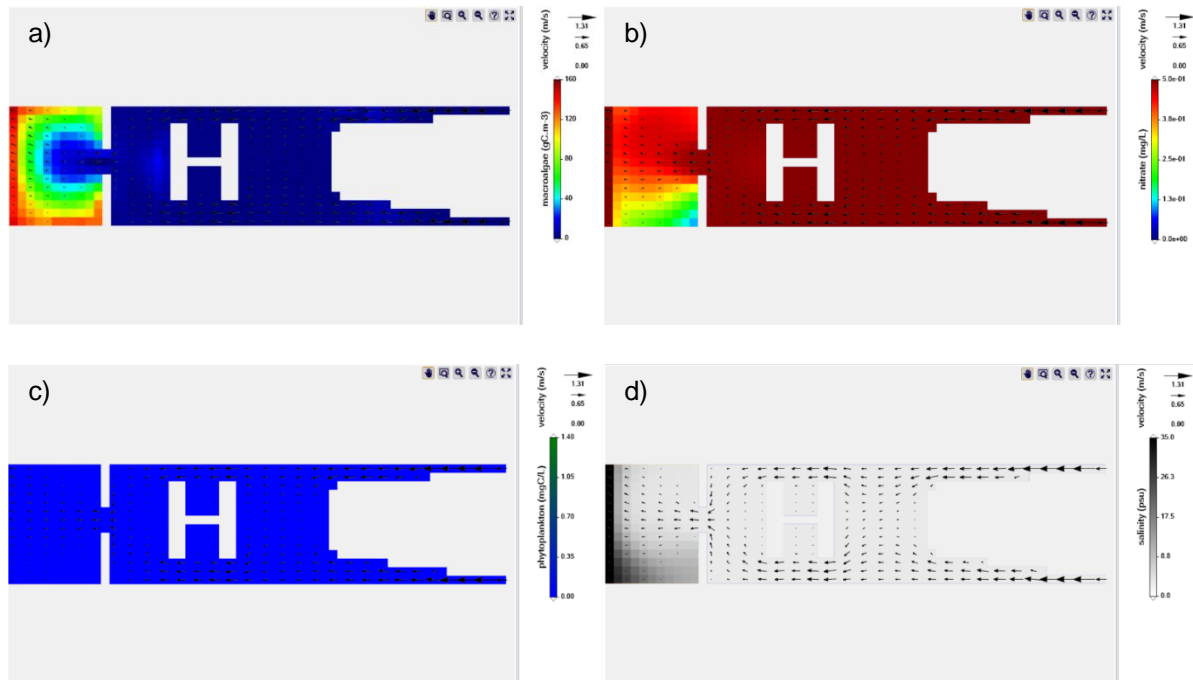


Figure 34 - a) Macroalgae, b) Nitrate, c) phytoplankton and d) salinity concentration distribution maps at (12/09 – 12h00). in the schematic estuary simulation

The blue and green corner on the nutrient figure (Figure 34 b)) corresponded to the place where consumption was most significant at this time, due to macroalgae growth.

A product of the motion of water produced by the tide and the irregular bathymetry of the estuary, which brings salinity from the ocean to that corner, enabling the existence of a small pocket of brackish water in the middle of freshwater, where macroalgae could develop.

In the narrow transition section of the ocean with the rest of the estuary, it could be verified a high water velocity, meaning that macroalgae could not grow there. Even if the velocity was lower than the critical velocity, that section possessed the biggest depth in this estuary, of about 20 to 24 m, so growth would also be limited from having the highest light limitation factor of the system.

End of the simulation

Close to the end of the simulation, the new right-side flow stabilized with the tidal flows, keeping nutrients and other properties continuously going back and forth in the same place (Figure 35).

Macroalgae completely disappeared from the two river areas and decreased significantly (when compared to the previous case in (Figure 34 a)) in the ocean side of the estuary, with the exception of the corner cell represented by orange (Figure 36). Nutrients became abundant in the great majority of the estuary, except for the exterior ocean segment on the Figure 35 a) and b), where macroalgae were consuming them.

Macroalgae were consuming nutrients but generally slowly dying except in that corner, where they were thriving. As for salinity, the great river discharges overwhelmed the estuary with freshwater, leaving only the ocean side with some concentration of salinity (Figure 35 c) and d)), especially in the southern segment due to recirculation, as explained before.

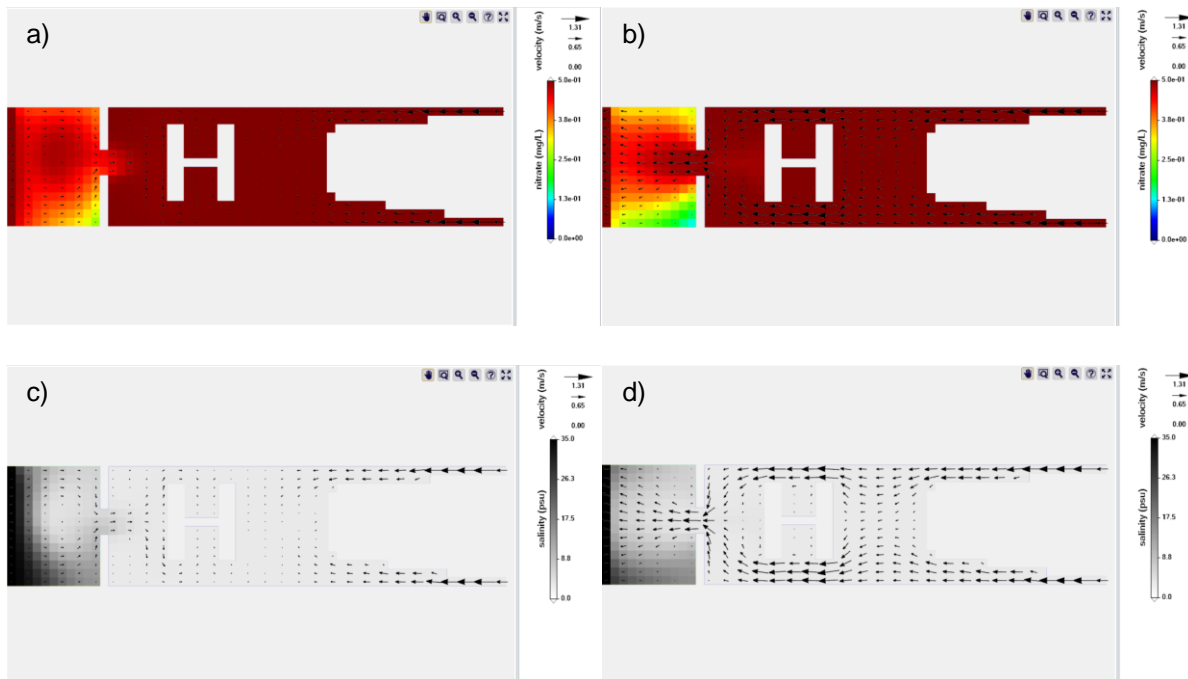


Figure 35 - a) nitrate concentration at 30/12 – 12h00 in flow tide and b) at 18h00 in ebb tide. c) salinity at 30/12 – 12h00 in flow tide and d) at 18h00 in ebb tide.

Ebb tides brought nutrients from the interior to the exterior segment (Figure 35 a) and b)). Those nutrients should have enabled macroalgae to grow in the ocean side, but freshwater inflow and recirculation was so strong, that only the algae in brackish and shallow waters where salinity and light are available (see Figure 35 c), b) and, Figure 27 respectively), like in the aforementioned corner, managed to survive.

In the section that divides the two parts, the bottom was very deep and the flow consisted mainly of freshwater (which mixes more on the left-side), depriving algae of light and salinity conditions.

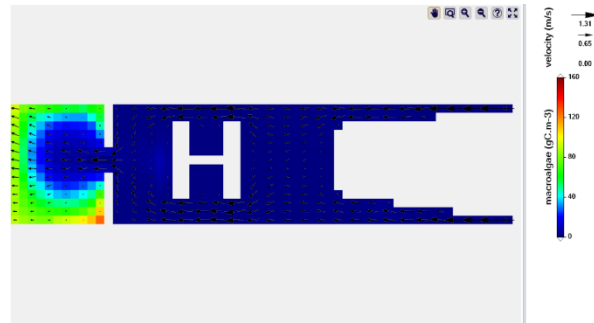


Figure 36 – Macroalgae distribution at the end of the simulation - 30/12 - 18h00 (ebb tide).

Looking directly at the nitrate and salinity in ebb and flow tides six hours apart (Figure 35), the flow of nutrients and freshwater to the direction of the ocean could be observed in the ebb period and the opposite, of brackish nutrient mixed water flow could be observed in the river direction in flow period.

4.3.3 – Final remarks

Macroalgae can grow in several different conditions of salinity, light, nutrients, and velocity but have preferential conditions.

Even if there's abundance of nutrients, if another growth limiting factor is completely amiss, macroalgae won't be able to develop. The same could be said for light. There can be enough nutrients available for growth, but if algae are so deep that light cannot reach them, they won't be able to use it and assimilate nutrients for proliferation. Algae grew under those three factors present, but as soon as the flowrate increased and lowered salinity values from most of the system, they slowly started to die.

With respect to water velocity, immediate detachment of algae occurred the moment the flowrate increased to match that critical velocity (Figure 30), as it was expected.

4.4 – *Saccharina latissima* in the Tagus Estuary

4.4.1 – Contextualization

After testing how different factors affect macroalgae growth in small, controlled environments, in this last chapter the aim was to simulate how a specific macroalga, *Saccharina latissima*, a species of brown kelp copes with the seasonal variability of temperature, nutrients and other factors of a real estuary, the Tagus Estuary (*Estuário do Rio Tejo*).

The Tagus Estuary, situated in the middle of the Lisbon metropolitan area, is the largest estuary of the largest river in Portugal and is one of the largest estuaries in western Europe. It encompasses a natural reserve of the same name, whose wetlands are of great biodiversity importance, especially because it's an important feeding location for the migratory wading birds, like flamingos and pied avocets and it's a nursery for several fish species (Infopedia: [https://www.infopedia.pt/\\$rio-tejo](https://www.infopedia.pt/$rio-tejo)).

The Tagus River is about 1009 km long, rises in *Sierra de Albarrazín* in Spain, crossing Spain into Portugal until it discharges into the Atlantic Ocean in Lisbon. Tagus Rivers' basin is 79 800 km², where Spain is the major contributor by drainage area. Its annual discharge is, on average 17 080 hm³, with an average flow of about 500 m³.s⁻¹.

4.4.2 – Setup and simulation conditions

The process of modelling *S. latissima* in the Tagus Estuary uses the results from a 3D hydrodynamic and biogeochemical operational model created, operated, and maintained by IST Maretec (<http://forecast.maretec.org/>), using MOHID Water modelling system for the Tagus region. The results of this model setup have been used in multiple studies and services with good results. References and more information can be found at the website and the most recent validations can be found in de Pablo et al. (2019) and de Pablo et al. (submitted). The results of the operational model on the dynamics of temperature, salinity, nutrients, phytoplankton, sediments and water velocity were used as inputs for this final experiment, simulating kelp growth in the estuary using the same single celled model setup (see chapter 3). By placing *Saccharina* at the desired depth and by making some conversions, it was possible to simulate the growth of this algae along a longline, just like how it's practiced in today's kelp aquaculture. The model calculated the output in grams of carbon, without taking into account the water content of the organism, needing further conversion to real weight. With this design in mind, twenty-one sites were chosen for the simulations. Ten inside the estuary, and eleven along the coast near the mouth. For each of these sites, time series with property results for the year 2019 for three distinct depths (approximately one, five and ten meters) were extracted from the operational model to use as inputs. The locations of these stations in function of the bathymetry are represented below in Figure 37.

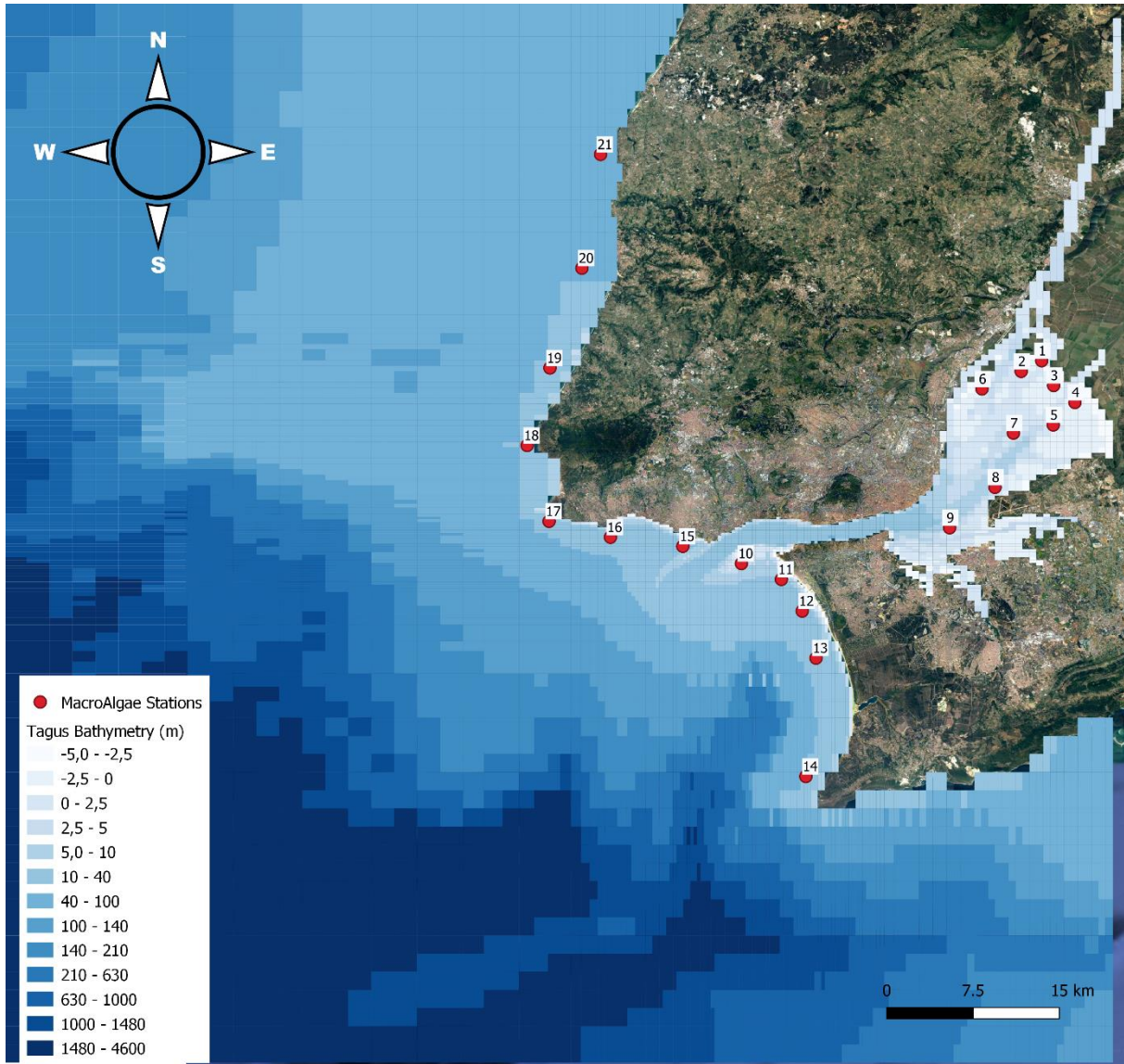


Figure 37 - Map of the Tagus Estuary in Lisbon, Portugal overlaid with the bathymetry and location of the points where macroalgae were simulated.

The river flows into the estuary from the North-east, bringing freshwater, nutrients and sediments washed from the soils in the Tagus watershed. The estuary itself is characterized by relatively low water depths, distributed along a 10 km wide region that divides the Lisbon Metropolitan Area and houses some wetlands, converging and getting deeper at the mouth of the estuary and discharging into the Atlantic Ocean.

Water has a different composition across the estuary, a particularity of being a transition zone between a river and the ocean.

On Table 23 are displayed the parameters to model *S. latissima* in the Tagus Estuary.

Table 23 - Parameters for *Saccharina latissima*, adapted from Broch and Slagstad (2012).

Parameter	Value	Unit	Description	Source
μ_{\max}	0.18	d ⁻¹	maximum growth rate	Chapman et al. (1978)
$T_{\text{opt}_{\min}}$	10	°C	optimum minimum temperature for growth	Fortes and Lüning (1980)
$T_{\text{opt}_{\max}}$	15		optimum maximum temperature for growth	
T_{\min}	0		minimum temperature for growth	Bolton and Lüning (1982)
T_{\max}	23		maximum temperature for growth	
K1	0.05	-	constant to control temperature response curve shape	This study
K2	0.98	-	constant to control temperature response curve shape	This study
K3	0.98	-	constant to control temperature response curve shape	This study
K4	0.02	-	constant to control temperature response curve shape	This study
I_{opt}	180	W.m ⁻²	optimum radiation value	Ozaki et al. (2001) from <i>Saccharina japonica</i>
k^{re}	0.009	d ⁻¹	endogenous respiration rate	This study
k^{P}	0.018		photorespiration rate	This study
ϵ_x	0.008		exudation rate	This study
m_x^{max}	0.001		natural mortality rate	This study
K_x^{m}	0.001	gC.d.m ⁻³	mortality half saturation constant	This study
G_x	0.00008	d ⁻¹	grazing rate over macroalgae	This study
K_x^{N}	0.0373	mg.L ⁻¹	nitrogen half-saturation constant for macroalgae	Espinoza and Chapman (1983)
K_x^{P}	0.0095		phosphorus half-saturation constant for macroalgae	Ozaki et al. (2001) from <i>Saccharina japonica</i>
rNC	0.18	-	macroalgae nitrogen/carbon ratio	Atkinson and Smith (1983)
rPC	0.024	-	macroalgae phosphorus/carbon ratio	
V_{crit}	2.0	m.s ⁻¹	Critical velocity for detachment	This study
S_{opt}	25	psu	macroalgae optimum salinity for growth	Karsten (2007)
S_{crit}	5		macroalgae critical salinity limit growth	
S_{\min}	0		macroalgae minimum salinity for growth	
S_{\max}	50		macroalgae maximum salinity for growth	

The purpose of this chapter is to find the locations where the combination of depth, light, salinity, and nutrients is the most suited to maximize the growth of *S. latissima*, for aquaculture purposes.

Admitting that the distance between the sites was minimal at the global scale, the same atmospheric irradiance conditions were calculated by the model for all stations, at a latitude and longitude inside the estuary (38.8559°N; -8.9954°W). Other surface fluxes were disabled, except for oxygen fluxes since the water temperature is imposed from the operational model results. It was also admitted that *S. latissima* units are attached to the longline at an evenly spaced distance in a manner that they don't shade each other. In Table 24 are specified the light extinction parameters for phytoplankton and sediments in these simulations.

Table 24 - Phytoplankton and cohesive sediments specific light extinction coefficients for the *Tagus* simulations.

Light extinction coefficients	Value (m ⁻¹)	Source
k _p (phytoplankton)	0.02	This study
k _s (sediments)	0.05	Wofsy (1983)

The model computed macroalgae values in gC.m⁻³ but the objective, calculating algae mass growth per meter of line, required some conversions.

The rate of change in macroalgae mass is given by:

$$\frac{dM}{dt} = \frac{M^{t+\Delta t} - M^t}{\Delta t} = Vol * \frac{\left(\frac{M}{Vol}\right)^{t+\Delta t} - \left(\frac{M}{Vol}\right)^t}{\Delta t} \quad [17]$$

The output the model computes is:

$$\left(\frac{M}{Vol}\right)^{t+\Delta t}$$

Knowing the volume of the system and two time instants, one can get the growth rate in the system, that divided by the mass gives:

$$gr = \frac{1}{M} \frac{dM}{dt} = \frac{1}{\frac{M^{t+\Delta t} + M^t}{2}} * Vol * \frac{\left(\frac{M}{Vol}\right)^{t+\Delta t} - \left(\frac{M}{Vol}\right)^t}{\Delta t} \quad [18]$$

The growth rate can then be used to compute the growth rate on a line:

$$\frac{dM_{line}}{dt} = gr * M_{line} \quad [19]$$

$$M_{line}^{t+\Delta t} = M_{line}^t + gr * M_{line}^t * dt = (1 + gr * dt)M_{line}^t \quad [19.1]$$

In sum, by calculating the growth rate of alga at every instant in the system volume and by specifying an initial mass in the longline, the mass of alga per meter of longline M_{line} could be estimated.

4.4.3 – Simulations

All results were calculated with the same initial concentration and were converted to relative growth by the method described above. Choosing an initial mass of 25 g/(m of longline) and by applying the calculated growth rates for each specific case, the results for *S. latissima* growth in biomass per meter of line for one-meter, five-meter and ten-meter depths are displayed in Figure 38, Figure 39 and Figure 40, respectively.

One-meter depth

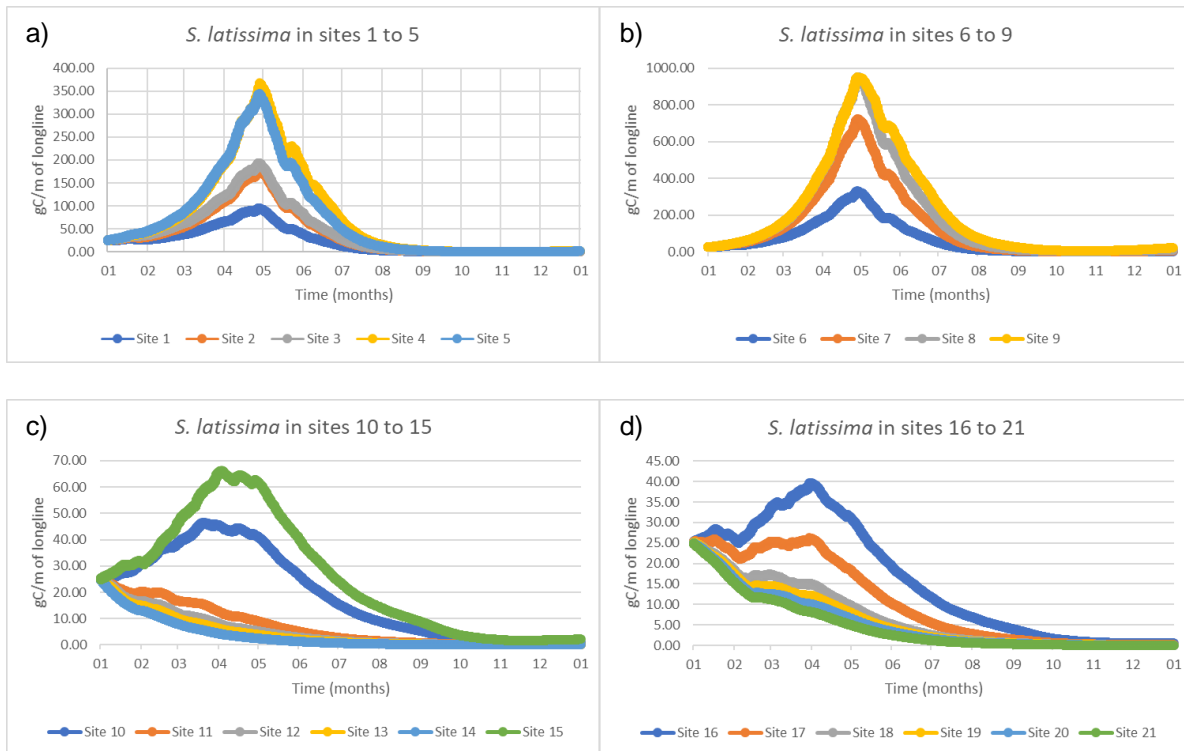


Figure 38 – *S. latissima* biomass per meter of line in sites a) 1 to 5; b) 6 to 9; c) 10 to 15 and d) 16 to 21 at a one-meter depth.

Five-meter depth

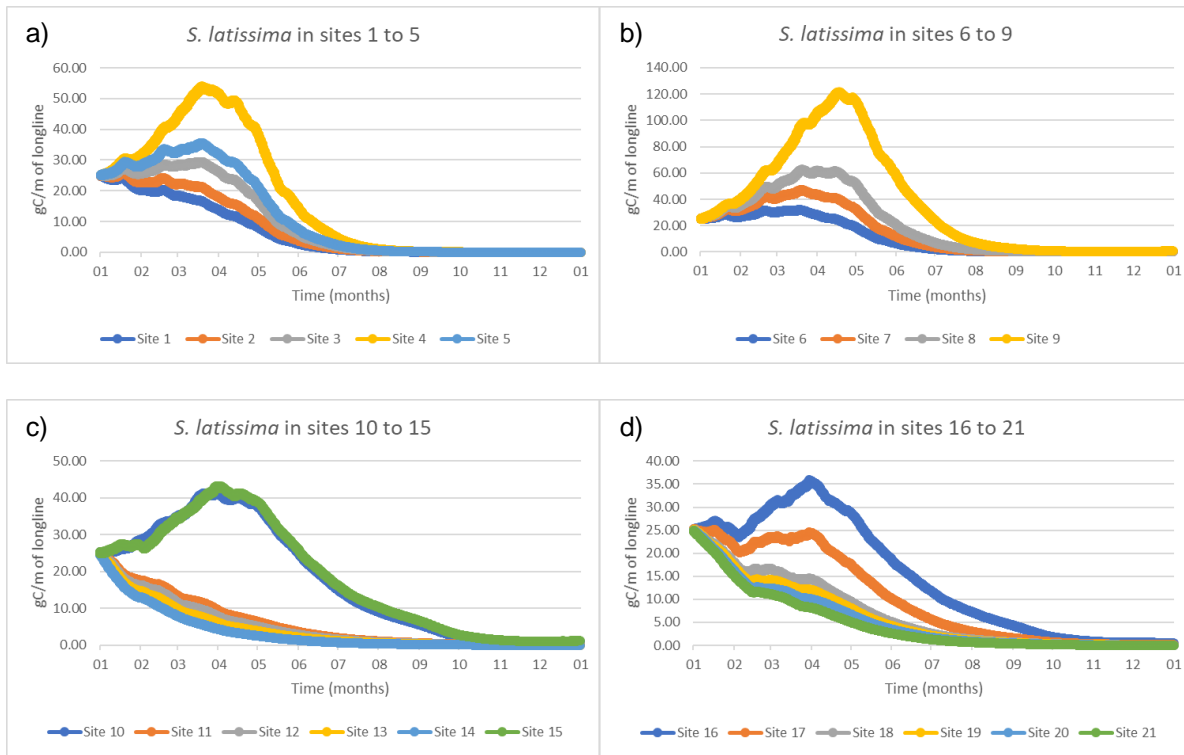


Figure 39 - *S. latissima* biomass per meter of line in sites a) 1 to 5; b) 6 to 9; c) 10 to 15 and d) 16 to 21 at a five-meter depth.

Ten-meter depth

No results were calculated for sites 1 to 10 since they were not deep enough to be able to place *S. latissima* at a 10 m depth.

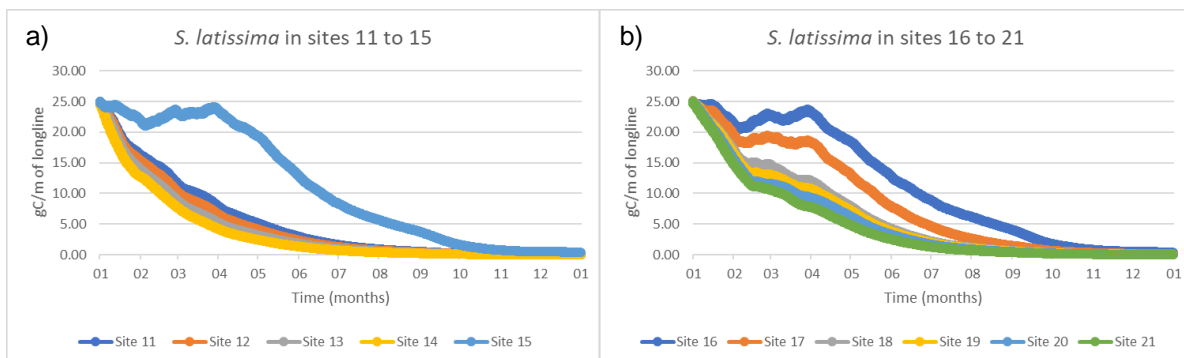


Figure 40 - *S. latissima* biomass per meter of line in sites a) 11 to 15 and b) 16 to 21 at a ten-meter depth.

4.4.4 – Analysis

A quick analysis of the results (Figure 38, Figure 39 and Figure 40) shows that the three sites that provide the best conditions for *S. latissima* growth were sites 9, 8 and 7 at a 1 meter depth (Figure 38 b)).

All peaks of maximum growth occurring between April and the beginning of May.

Among all the results, sites 11, 12, 13, 14, 18, 19, 20 and 21 displayed no growth, only decay, implying that there's at least one factor greatly limiting growth. Furthermore, for each single station, growth was apparently greater in shallower depths.

In general, *S. latissima* grew the most in the middle of the estuary, followed by the stations in the surroundings of the river discharges, then near the mouth of the estuary and finally along the coast. In the next section, it will be explained why.

To explain why growth was so different inside and outside the estuary, nutrient concentrations along the year were plotted below, for the one-meter depth. This time, the sites were separated into two groups, the sites inside the estuary and the sites outside.

Looking at Figure 41, it is evident that nitrate and inorganic phosphorus concentrations were substantially larger inside the estuary, severely limiting growth on the outside. The same shape is found for ammonia (not shown).

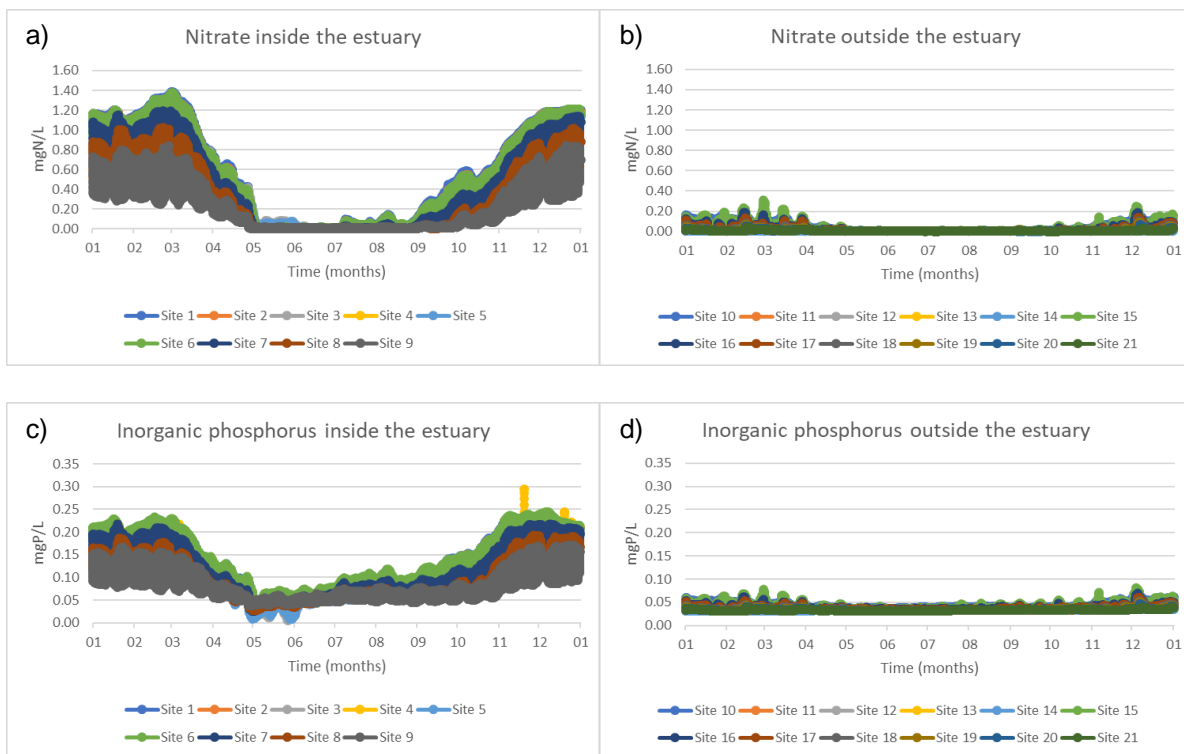


Figure 41 – Nitrate concentrations inside a) and outside b) of the estuary and phosphorus concentrations inside c) and outside d) of the estuary.

Seasonal variation of nutrients could also be evidenced by this Figure 41. In the rainy months in Portugal (from October to May of the next year), the Tagus River discharge increases, transporting a larger amount of nutrients washed from the land and leached from the soil, including the excess of nutrients from agriculture. This explains the seasonal dynamics of nutrients, with high values of nitrate and phosphorus from January until May and October to December; and the low concentration during the summer (June to September), where rain is minimal, and the Tagus flowrate and nutrient concentration are on their yearly minima.

Location Comparison

Some sites near each other exhibited similar growth behaviors in response to similar environmental conditions, so, for the purpose of comparing locations where *S. latissima* grew more than others, representative stations of sets with similar growth stations were chosen (see Table 25). Also, since the greatest verified growth was generally in the shallowest depth, this analysis was conducted for the properties of the sites at the shallowest depth.

Table 25 – Sites grouped by *S. latissima* growth and respective representative station.

Group of stations	Group designation	Representing stations
1, 2, 3, 6	“rivers end”	3
4, 5, 7, 8, 9	“middle estuary”	9
10, 15, 16	“estuary mouth”	15
17, 18, 19, 20, 21	“northern coast”	17, 18
11, 12, 13, 14	“southern coast”	12

Among these groups, growth was ranked in the following order, from greatest increase to no growth: the “middle estuary”, “rivers end”, “estuary mouth”, “northern coast” closely

Temperature

Temperature profiles showed a broader thermal amplitude in the sites inside the estuary (3 and 9, Figure 42 a) and b)) than in sites outside (Figure 42 c), d), e) and f)). Temperatures were higher in site 3 and 9 from June to September, reaching 26°C and 25°C, respectively, and lower in the remaining months, matching accordingly with the average seasonal temperature variability of Portugal. In the sites outside the estuary, water temperatures were very similar among them, but much lower than on the inside. They revealed to have small variations around 15°C throughout the year, increasing slightly in September. These

broader amplitudes in the sites inside the estuary are a result of the river discharge combined with the estuary's shallow depth. Rivers and estuaries have a much shallower depth of water when compared to the open ocean, so temperatures can be easily influenced by the solar radiation, which heats up the whole water column while in the sea, being vast and deep, dissipates heat and needs much more energy to increase its temperature. In the summer the water temperature inside the estuary is higher due to the combined effect of the river discharge temperature and heat exchange between the water and the atmosphere in the the shallow areas of the estuary increase the general temperature of the water of the estuary and the the sites inside it. From the model results, this difference in temperature is slowly attenuated by water mixing caused by the tide, attenuating even further the closer the resulting river plume penetrates into the sea.

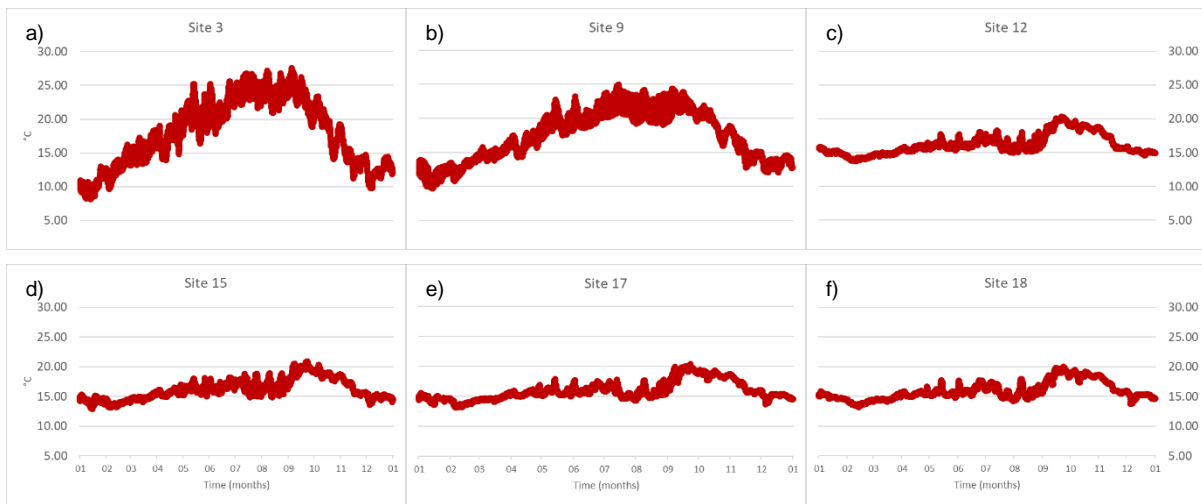


Figure 42 – Temperature variation in the selected sites a) 3; b) 9; c) 12; d) 15; e) 17 and f) 18, during a year of simulation.

S. latissima ideal range of temperatures for growing is between 10 and 15°C and it cannot growth below 0°C or above 23°C, so temperature is a limiting factor partially responsible for the algae death and mass decrease in sites 3 and 9 after May (Figure 38 a) and b)), where temperatures exceed the 23°C critical value. On the remaining sites, since temperatures oscillate around 15°C and never exceed 23°C, the conditions are somewhat near ideal, temperatures could not explain the reduced or lack of growth in those sites.

Salinity

Major differences in water salinity could also be observed between sites inside and outside the estuary. In site 3, salinity values ranged from 10 psu in January, increasing to nearly 25 psu during the summer and then decreasing back to 10 psu in the following months (Figure 43 a)). For site 9 (Figure 43 b)), salinity oscillates between 20 and 33 psu, peaking in the summer. These low salinity and yearly amplitudes are once again due to the river discharge of freshwater. Freshwater enters the estuary and mixes with the

ocean's saltwater, hence the overall low values for site 3, situated upstream where the river connects to the estuary. The amplitude between the summer and other months could be explained by the variable flowrate of the Tagus, since in the dryer events the Tagus discharges less freshwater into the estuary and the salinity from the ocean prevails. As for station 9, due to its position more downstream of the estuary, salinity is a product of further mixture from the fresh and saltwater from both sides. The great daily variation in values (maximum and minimum) is a consequence of the tides. In rising tide, the salinity of the ocean is predominant in the mixing while in ebb tide, the low river salinity predominates.

The remaining sites in the ocean side all exhibit the same behavior, apart from site 15. In those sites, salinity averages at 35 psu, the mean salinity value for the ocean, and it didn't really vary along the year, because they are already outside of the influence from the Tagus River. As for site 15, located in the coast, right outside the estuary mouth, salinity varies between 30 and 35 psu, except in the middle of the year, where it remains steadily around 35 psu.

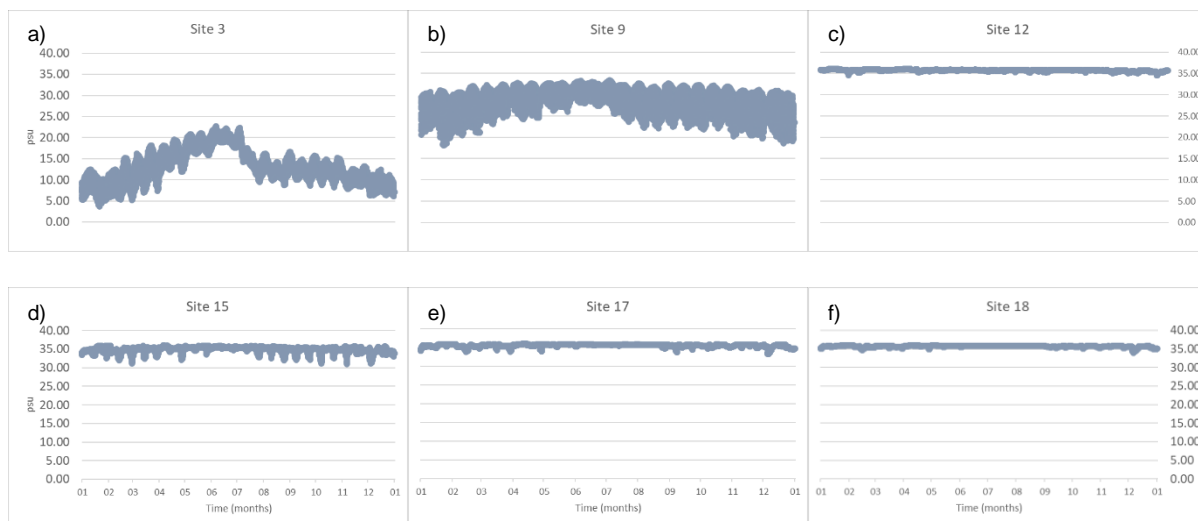


Figure 43 - Salinity variation in the selected sites a) 3; b) 9; c) 12; d) 15; e) 17 and f) 18, during a year of simulation.

Salinity preferences for *S. latissima* range from 5 psu to 50 psu (Karsten, 2007), growing faster ideally near 25 psu, so while sites 3 (mostly), 12, 15, 17 and 18 display values inside the preference range, it is site 9 that possesses salinity closer to the most preferable one, during most of the year. So, salinity is one of the factors that can explain, the highest growth verified in site 9 and the rest of the “middle estuary” group. For the other sites, salinity wasn't ideal, but it also wasn't low or high enough to completely inhibit growth, as per the salinity limitation factor (Figure 6).

Nutrients

Once again, conditions differed from inside and outside the estuary. Nutrient concentrations, especially nitrate, were much higher on the inside stations. In sites 3, 9 and 15, nutrients were relatively high until May, low during the summer and once again high from October until the end of the year (Figure 44 a), b) and d)). This dynamic happens for two reasons. Once again, due to the proximity to the river discharge and phytoplankton consumption (Figure 45 a) and b)), which increases from spring and consume nutrients, reducing the nutrients concentration in the system. Site 3 is the most upstream station and receives a fresh flow of nutrient rich water from the river, while site 9 receives moderately less nutrients due to water mixing along the estuary. The broad daily variation (visually in Figure 44 b), the “thickness” of the line) is once again the effect of the tide, where in rising tide predominates the lower concentration of nutrients from the ocean and in ebb tide predominates the high concentration from the river. The decrease of nutrients in the summer is, analogously to the salinity case before, due to the reduced river flow in the dryer summer. Site 15 still displays higher concentration of nutrients than site 12, 17 and 18 (Figure 44 c), e) and f)) because of its location in front of the mouth of the estuary.

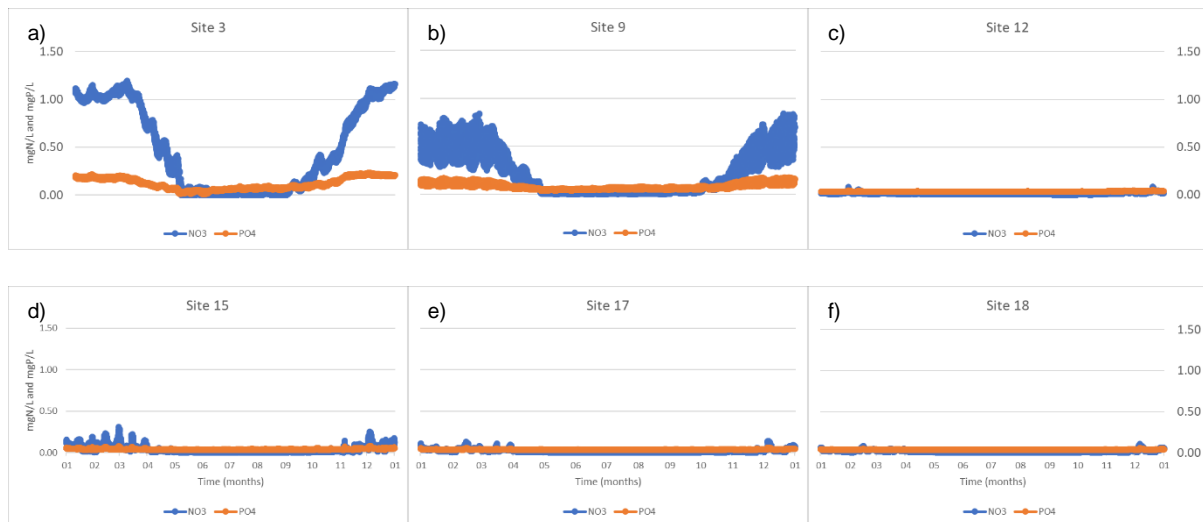


Figure 44 - Nutrient variation in the selected sites a) 3; b) 9; c) 12; d) 15; e) 17 and f) 18, during a year of simulation.

Macroalgae respond to nutrient concentrations in the environment, *S. latissima* is no exception. Nutrients are more available inside the estuary from upstream to downstream, brought in from the Tagus' discharge until they are transported and mixed with the ocean water, justifying these differences in growth between the inner and outer sites. Site 3 possessed a greater availability of nutrients but still grew less than in site 9, mainly due to other limiting factors. Outer sites grew little accordingly with the small concentration of nutrients they had available.

Phytoplankton

Phytoplankton developed the most inside the estuary (sites 3 and 9), it blooms particularly in April, persists through the summer, and declines in autumn (Figure 45 a) and b)). In site 15 can be observed once more the impact of the flow from the estuary, where phytoplankton growth is still discernible in the exact same period as the two sites discussed before, eventually attenuating by water mixing and remaining low in the other coastal stations (Figure 45 c), e) and f)). Phytoplankton blooms in spring through summer are a reaction to the increase in solar irradiance and consequential rise of temperatures.

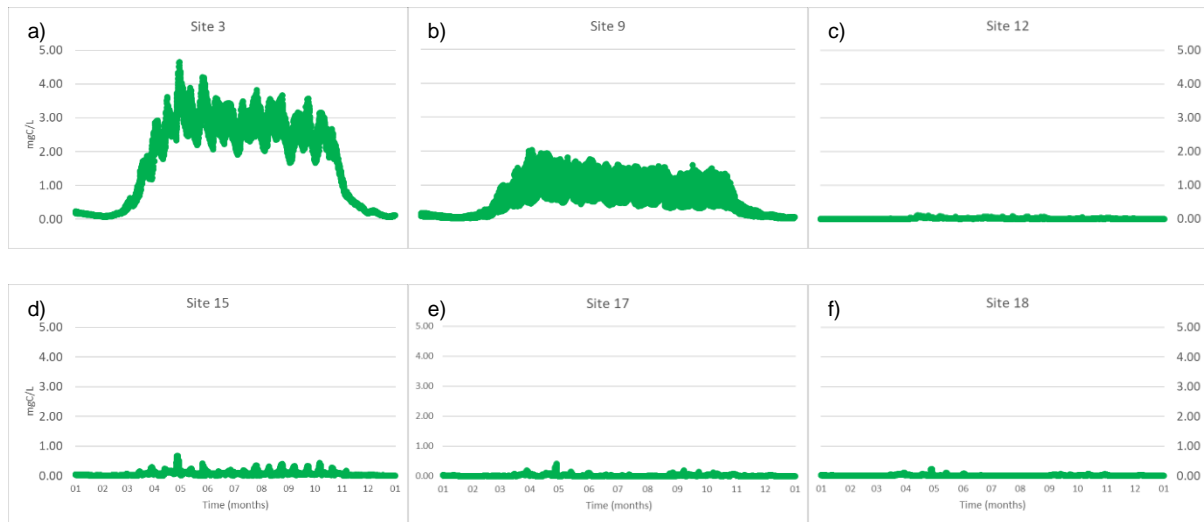


Figure 45 - Phytoplankton variation in the selected sites a) 3; b) 9; c) 12; d) 15; e) 17 and f) 18, during a year of simulation.

The tests in the former chapters confirmed that phytoplankton interferes with macroalgae growth in two aspects, nutrients, and light. Phytoplankton concentrations are low in the beginning of the period where macroalgae grow in nearly all sites. Then, phytoplankton increases and consumes nutrients from March to May and persisting until October, where they start to decrease. When they grew significantly, they started to deplete nutrients (Figure 44 a) and b)), limiting the nutrients available for macroalgae. During the summer, *S. latissima* can't grow due to nutrient depletion by phytoplankton combined with high unfavorable temperatures and excessive solar radiation that may cause photoinhibition, as evidenced before.

Cohesive sediments

Sediment concentration was higher in sites 3, then in 9 (Figure 46 a) and b) respectively) because they were dragged and transported into the estuary by the river. In site 3 overall concentrations were higher than in 9 once again because of the station being upstream, in direct contact with the river. As sediments travel

towards site 9 and then exit the estuary, they decrease because they slowly get sediment and deposit in the bottom or diffuse into the ocean. In the outside stations, sediment concentrations were very low due to no longer being influenced by the rivers flow, except for site 15, where that influence is faintly felt.

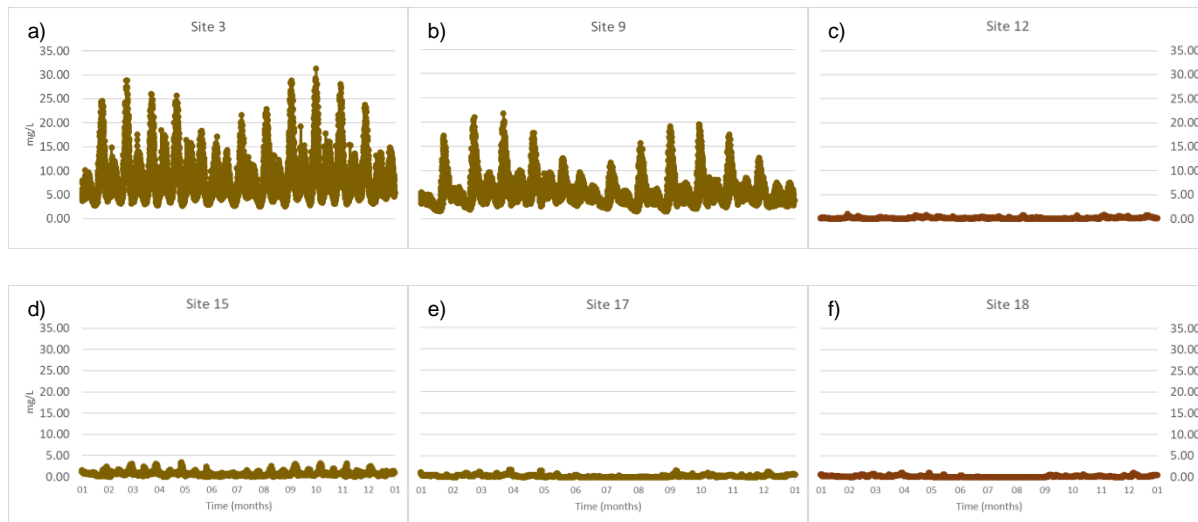


Figure 46 - Cohesive sediments variation in the selected sites a) 3; b) 9; c) 12; d) 15; e) 17 and f) 18, during a year of simulation.

Suspended sediments cloud the water and obstruct the path of light.

Since *S. latissima* was able to develop itself at a one meter depth from the surface, mostly with relatively high sediment concentrations in the estuary (sites 3 and 9, Figure 46 a) and b)), when compared to outside the estuary (sites 12, 15, 17 and 18, Figure 46 c) to f)), it can be verified that sediments, in combination with phytoplankton concentration, did not impact light availability that much, since macroalgae grew the most where the highest.

Temporal analysis

The question of “*Where to place macroalgae?*” was answered in the previous section. Now for the question “*When to place them?*”, further tests were conducted for site 9, the site with better development. For the previous tests, algae assumed to be placed in the water in January just for simplification. The next set of results were obtained in a scenario where macroalgae were placed in the water, at surface, at site 9 and left in the water for three straight years, from May of 2017 to May of 2020.

Figure 47 – a) shows that *S. latissima* growth peaked again in the month of May 2017, but on a completely different scale than in the previous experiment, where it started to grow in January 2019 (Figure 38 b)). It grew more than twice now until that peak.

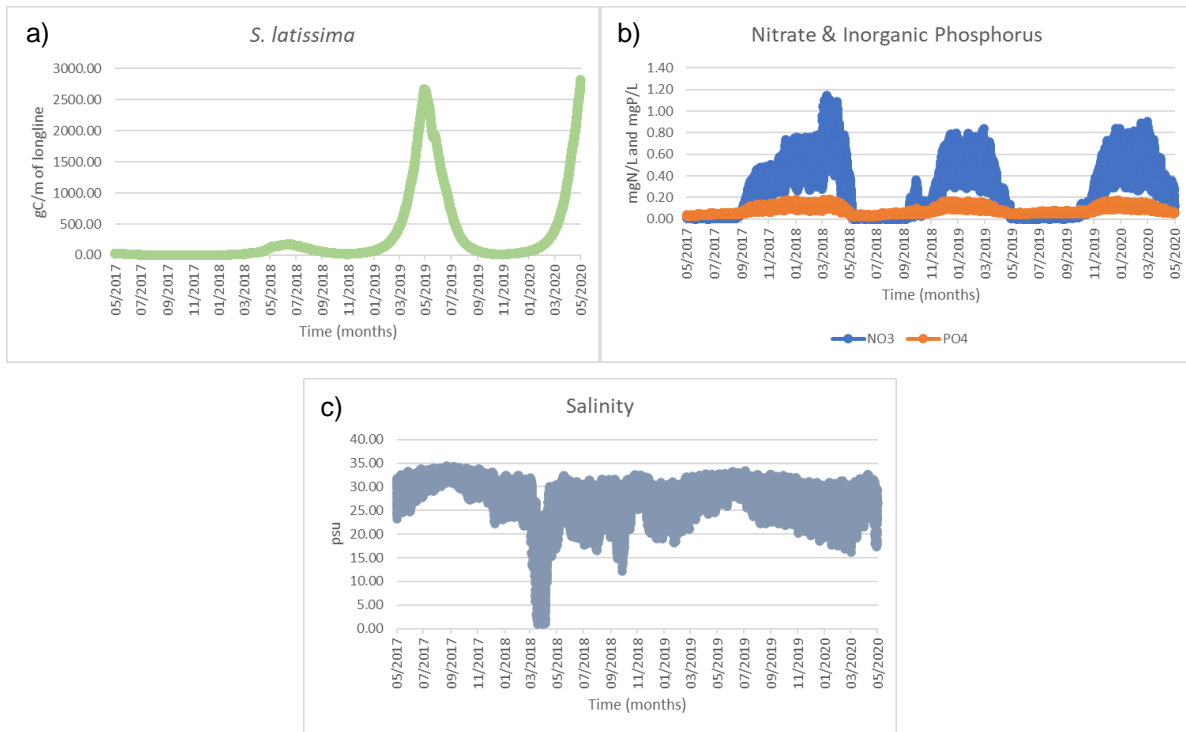


Figure 47 - a) *S. latissima* biomass, b) nitrate and inorganic phosphorus concentrations and c) salinity over the course of May 2017 to May 2020.

Figure 47 shows that although the amplitude of the peaks is different from year to year, there is a consistency in terms of its timing. Macroalgae growth starts around November, making use of the high concentration of nutrients that extends from the previous year until May of the current year. In 2018, they exceptionally did not grow as much which could be related with the anomalous decrease of salinity in March.

In sum, to maximize macroalgae growth, seeds should be planted in the water when nutrients start to increase after the summer, sometime around November, to make use of a more continuous supply of nutrients. Afterwards, harvest should happen before macroalgae reach their maximum biomass, the lines reach their maximum capacity or before conditions take a turn and they start to die. In this test and in the previous one, that moment is at the end of April or beginning of May.

Conversion from dry weight to real weight

To give a clear notion of the scale of *S. latissima* produced in site 9, from January to May 2019 (Figure 38 b)) and from November 2018 to May 2019 (Figure 47 a)), some conversions were made. Assuming that the whole dry weight of the algae is composed solely of carbon, nitrogen and phosphorus in the proportions of the Redfield Ratio (106:16:1) and that dry weight ranges from 8 to 26% of the total weight (Broch and Slagstad, 2012), the average maximum yield calculated for both cases was of 11.76 kg/m and 25.00 kg/m of longline, respectively. Nevertheless, this is a theoretical maximum value that does not consider the weight

of the yield that at this maximum could be too much for the line to hold. Based on these maximum values, it would be up to the producer to decide when to harvest in order obtain the maximum profitable conditions.

5 - Conclusions

In conclusion, *S. latissima* that was placed inside the estuary grew more than those placed on the outside. Inside the estuary, the macroalgae that developed the most were those close enough to the river to make use of the high concentrations of nutrients it provided but distanced enough not to be affected by the Tagus' fresh water. The effects of phytoplankton and sediment concentrations turned out to be negligible in the light availability to *S. latissima* since the highest growth was found in sites where those concentrations were high. Outside of the estuary, at the coast, macroalgae grew significantly less except near the estuary's mouth where some influence of nutrients from the river could still be felt. Conditions outside the estuary are generally good for growth, apart from nutrients concentrations, which are very low. Once again it proves that, despite nearly all conditions being favorable, it only takes one severely unfavorable condition to inhibit growth.

So, answering the main questions, according to this study, the best location to practice aquaculture of *Saccharina latissima* in the Tagus Estuary is in the middle of the estuary, at shallow depths of one or two meters, in the surroundings of Site 9.

The best time to plant macroalgae in order to maximize their yield is in November and harvest should occur at then the beginning of May of the following year, where their maximum biomass is achieved before they start to die.

The possibility of actually implementing macroalgae/seaweed aquaculture depends on local government authorization and other factors such as naval traffic, operational costs, pollution assessment of the estuary, capacity of the longlines and current estuary occupation, which could be combined with the results obtained in this thesis.

References

- Atkinson, M. J., Smith, S. V., (1983). C:N:P ratios of benthic marine plants. *Limnol. Oceanogr.* 28, 568 – 574.
- Benitez-Nelson, C. R. (2000). The biogeochemical cycling of phosphorus in marine systems. *Earth-Science Reviews* 51, 109–135
- Bolton, J. J., Lüning, K., (1982), Optimal Growth and Maximal Survival Temperatures of Atlantic *Laminaria* Species (Phaeophyta) in Culture. *Marine Biology* 66, 89 – 94.
- Broch, O. J., Slagstad, D., (2012). Modelling seasonal growth and composition of the kelp *Saccharina latissima*. *J Appl Phycol* 24, 759 – 776.
- Brummett, R., Yarish, C., Hansen, S., Bjerregaard, R., Valderrama, D., Sims, N., Radulovich, R., Diana, J., Capron, M., Forster, J., Goudey, C., Hopkins, K., Rust, M., McKinnie, C. (2016). Seaweed Aquaculture for Food Security, Income Generation and Environmental Health in Tropical Developing Countries.
- Chapman A. R. O., Markham J. W., Lüning, K. (1978). Effects of nitrate concentration on the growth and physiology of *Laminaria saccharina* (phaeophyta) in culture. *J Phycol* 14, 195 – 198.
- Ciais, P., Sabine C., Bala G., Bopp L., Brovkin V., Canadell J., Chhabra A., DeFries R., Galloway J., Heimann M., Jones C., Le Quéré C., Myneni R. B., Piao, S., and Thornton, P. (2013). Carbon and Other Biogeochemical Cycles. In *Climate Change 2013: The Physical Science Basis. Contribution of Working Group I to the Fifth Assessment Report of the Intergovernmental Panel on Climate Change* [Stocker, T. F., Qin D., Plattner, G. K., Tignor M., Allen, S. K., Boschung, J., Nauels, A., Xia, Y., Bex, V. and Midgley, P. M. (eds.)]. Cambridge University Press, Cambridge, United Kingdom and New York, NY, USA.
- EPA (1985). Rates, Constants and Kinetics Formulations in Surface Water Quality Modelling, 2nd ed. United States Environmental Protection Agency, Report EPA/600/3-85/040, 454 pp.
- Espinoza, J., & Chapman, A. R. O. (1983). Ecotypic differentiation of *Laminaria longicuris* in relation to seawater nitrate concentration. *Marine Biology*, 74(2), 213- 218.
- FAO (2015). World Fertilizer Trends and Outlook to 2018. Food and Agriculture Organization of the United Nations, Rome.
- FAO. Cai, J., Lovatelli, A., Aguilar-Manjarrez, J., Cornish, L., Dabbadie, L., Desrochers, A., Diffey, S., Garrido Gamarro, E., Geehan, J., Hurtado, A., Lucente, D., Mair, G., Miao, W., Potin, P., Przybyla, C., Reantaso, M., Roubach, R., Tauati, M. & Yuan, X. (2021a). Seaweeds and microalgae: an overview for unlocking their potential in global aquaculture development. *FAO Fisheries and Aquaculture Circular* No. 1229. Rome, FAO.

FAO (2021b). Fishery and Aquaculture Statistics. Global Production Statistics 1950–2019. In: FAO Fisheries Division [online]. FishStaJ – Software for Fishery and Aquaculture Statistical Time Series. Retrieved from: www.fao.org/fishery/statistics/software/fishstatj/en

Fortes M. D., Lüning, K. (1980). Growth rates of North Sea macroalgae in relation to temperature, irradiance and photoperiod. *Helgol Wiss Meeresunters* 34, 15 – 29.

Karsten, U., Research note: Salinity tolerance of Arctic kelps from Spitsbergen, (2007). *Phycological Research* 55(4), 257 – 262.

Lassaletta, L., Billen, G., Grizzetti, B., Anglade, J., & Garnier, J. (2014). 50 year trends in nitrogen use efficiency of world cropping systems: the relationship between yield and nitrogen input to cropland. *Environmental Research Letters*, 9(10), 105011.

Lopes, F. M. T. (2012). Upwelling na costa Atlântica da Península Ibérica: análise de uma simulação regional de clima. Master Thesis in Geophysical Sciences, Faculdade de Ciências da Universidade de Lisboa.

McHugh, D.J. (2003). A guide to the seaweed industry. Fisheries Technical Paper No. 441. Rome, FAO. 105 pp.

Ozaki, A., Mizuta, H., Yamamoto, H. (2001). Physiological differences between the nutrient uptakes of *Kjellmaniella crassifolia* and *Laminaria japonica* (Phaeophyceae). *Fisheries science* 67(3), 415 – 419.

de Pablo, H., Sobrinho, J., Garcia, M., Campuzano, F., Juliano, M., Neves, R. (2019). Validation of the 3D-MOHID Hydrodynamic Model for the Tagus Coastal Area. *Water*, 11, 1713.

de Pablo, H., Sobrinho, J., Garaboa-Paz, D., Fonteles, C., Neves, R., Gaspar, M. B. (2021). The influence of river flow on residence time, exposure time, and integrated water fraction for the Tagus estuary (Portugal). *Frontiers in Marine Science* (*submitted*).

Paytan, A., McLaughlin, K., (2007). The Oceanic Phosphorus Cycle. *Chem. Rev.* 2007, 107, 563 – 576.

Redfield, A. C. (1934). *On the proportions of organic derivatives in sea water and their relation to the composition of plankton* (Vol. 1). Liverpool: University Press of Liverpool.

Seitzinger, S. P., Harrison, J. A., Dumont, E., Beusen A. H. W. & Bouwman, A. F. (2005). Sources and delivery of carbon, nitrogen, and phosphorus to the coastal zone: an overview of global nutrient export from watersheds (NEWS) models and their application. *Glob. Biogeochem. Cycles* 19, 1 –11

Soares, P. M. M., Cardoso, R. M., Semedo, A., Chinita, M. J., Ranjha, R. (2014). Climatology of the Iberia coastal low-level wind jet: weather research forecasting model high-resolution results. In: *Sammelwerk Tellus A: Dynamic Meteorology and Oceanography*, Band 66/1.

Trancoso, R., Saraiva, S., Fernandes, L., Pina, P., Leitão, P., Neves, R., (2005). Modelling Macroalgae using a 3D Hydrodynamic-Ecological Model in a Shallow, Temperate Estuary. *Ecological Modelling* 187(2), 232 – 246.

Voss, M., Bange, HW., Dippner, J. W., Middelburg, J. J., Montoya J. P., Ward, B. (2013). The marine nitrogen cycle: recent discoveries, uncertainties and the potential relevance of climate change. *Phil Trans R Soc B* 368, 1621.

Wofsy, S. C. (1983). A simple model to predict extinction coefficients and phytoplankton biomass in eutrophic waters. *Limnol. Oceanogr.*, 28(6), 1144 – 1155.

Zhang, J. Z. & Huang, X. L. (2011). Effect of temperature and salinity on phosphate sorption on marine sediments. *Environ. Sci. Technol.*, 45, 6831 – 6837

Websites

Guiry, M.D., in Guiry, M.D. & Guiry, G.M. (2021). *AlgaeBase*. World-wide electronics publication, National University of Ireland, Galway. Retrieved from: <http://www.algaebase.org> Accessed on October 13th, 2021.

MARETEC, Maretec Forecast website, Instituto Superior Técnico, Universidade de Lisboa. Retrieved from: <http://forecast.maretec.org/> Accessed November 10th, 2021.

MARETEC, MOHID Technical Manuals. Instituto Superior Técnico, Universidade de Lisboa. Retrieved from [http://wiki.mohid.com/index.php?title=Mohid Bibliography](http://wiki.mohid.com/index.php?title=Mohid_Bibliography) Accessed November 3rd, 2021.

National Ocean Service NOAA – U.S. Department of Commerce, The Ekman Spiral. Retrieved from https://oceanservice.noaa.gov/education/tutorial_currents/04currents4.html Accessed December 9th, 2021

National Ocean Service NOAA – U.S. Department of Commerce, Tides and Water Levels. Retrieved from https://oceanservice.noaa.gov/education/tutorial_tides/ Accessed November 3rd, 2021

National Ocean Service NOAA Fisheries – U.S. Department of Commerce, Sugar Kelp. Retrieved from <https://www.fisheries.noaa.gov/species/sugar-kelp> Accessed November 15th, 2021

Porto Editora, Rio Tejo in Infopedia [on-line]. Porto, Porto Editora. Retrieved from: [https://www.infopedia.pt/\\$rio-tejo](https://www.infopedia.pt/$rio-tejo) Accessed November 3rd, 2021

Solar Energy Technologies Office – U.S. Department of Energy, Solar Radiation Basics Retrieved from <https://www.energy.gov/eere/solar/solar-radiation-basics> Accessed December 9th, 2021.

UN News (2020), A deep dive into Zero Hunger: the seaweed revolution, <https://news.un.org/en/story/2020/11/1077212> Accessed November 2nd, 2021.

White, N., Marshall, C. E., (2007). *Saccharina latissima* Sugar kelp. In Tyler-Walters H., Hiscock K. (eds). *Marine Life Information Network: Biology and Sensitivity Key Information Reviews*, Plymouth: Marine Biological Association of the United Kingdom. Retrieved from: <https://www.marlin.ac.uk/species/detail/1375>
Accessed November 3rd, 2021